Influence of normal stress and temperature on water content of (smectite) clays and possible implications for frictional strength of fault gouge

Msc Research Thesis

Sander M. de Jong (Student Number 0423912)

Department of Earth Sciences

Utrecht University

Table of contents

Abstract

The slip behavior of large shallow crustal faults depends mainly on the mechanical properties of fault gouge, which generally includes a number of clay phases. The frictional properties of these clay minerals indicate that they can be very weak if water is present, with friction coefficients in the order of 0.2 (e.g. for smectite, chrysotile and talc). Whereas a weakening effect is evident, going from dry to wet conditions, the mechanism by which this occurs is not. In particular, the role of smectite clay, which is able to swell due to adsorption of water in the interlayer region, in promoting fault weakness is not fully understood yet. To attack this problem, new laboratory data are reported on the *in-situ* temperature- (20-180ºC) and normal stress-induced (to 41 MPa) dehydration behaviour of two well-known montmorillonites (Ca-SAz-1 and Na-SWy-1). In this way the differential stress threshold for the onset of interlayer water expulsion is investigated. We also analyze the interaction of surface adsorbed water molecules with the mineral surface for the non-swelling phyllosilicates: muscovite, kaolinite and pyrophyllite.

The results of the present study are twofold. First, it is found that for our specific conditions (room relative humidity and temperature), a differential stress of 41MPa does not dehydrate the interlayer region of either of the montmorillonites studied. This state of stress approaches some of the thermodynamic calculations made to predict the stress threshold for the onset of dehydration. Second, we show explicitly the existence of strongly adsorbed water molecules, attached to the mineral surface, of clay minerals that cannot swell. This observation is consistent with a crustal weakening model that describes ongoing fault weakness as the result of growth of an interconnected network of weak clay minerals, characterized by surface adsorbed water films where the shear is located. Even at higher pressure and temperature, where capillary condensed water is driven-off, clay minerals can continue to be weak as a result of these more firmly attached surface adsorbed water films. The particular weakening effect of montmorillonite appears to have a *direct* and *indirect* basis. The *direct* water-assisted weakening mechanism is analogous to that seen in all charged (hydrophilic) sheet structured minerals, as a result of shear facilitated along surface adsorbed water films. The *indirect* water-assisted weakening mechanism follows from the possible expulsion of interlayer water, which results in an increase of the pore fluid pressure. We emphasize that to acquire reliable friction data on smectites, it is essential to use water-saturated or thoroughly dried (T>140ºC) conditions.

1. Introduction

Clay minerals occur as abundant phases in large-scale fault zones and their frictional properties have been suggested to put a major constrain on macroscopic fault behavior (e.g., Vrolijk, 1990; Morrow et al., 2000; Numelin et al., 2007; Ikari et al., 2009). Especially the smectite group or "swelling clay" group, a type of clay that is able to absorb water molecules in the interlayer region, allowing the solid framework to expand, has been targeted as a potential source of fault weakness (e.g., Wang et al., 1980; Bird, 1984; Saffer et al., 2001). In the literature, different correlations have been observed and reasons given for this low strength (Moore and Lockner, 2007). These include the dependence of strength on effective normal stress, temperature, and the difference between experiments performed under wet and dry conditions. In particular, there exists a discussion on the specific role of smectite interlayer water in controlling fault strength (e.g., Bird, 1984; Colten-Bradley, 1987; Ikari et al., 2007), and different fluid assisted weakening mechanisms have been put forward (e.g., Moore and Lockner, 2004).

The purpose of this current work is to investigate the particular role of interlayer water in controlling smectite and smectite bearing fault weakness. In our approach, we built up the proposed model in steps where we start with literature reviews of smectite dehydration and the interaction of water molecules with the clay structure. Smectite dehydration is then studied experimentally using two macroscopic techniques, which describe the removal of water molecules from a possible range of sorption sites. First, we use thermogravimetric analysis (TGA) to characterize the dehydration effect of two particular montmorillonites, the most common type of smectite. Then, we combine this knowledge with a series of *in-situ* temperature-driven and normal stress-driven dehydration experiments for the same materials, to examine the structure and location of water as a function of temperature and normal stress. Stress-driven dehydration is investigated qualitatively using Fourier Transform Infrared Spectroscopy (FTIR), which has proven to be a useful tool in the past (e.g., Russell and Farmer, 1964; Madejova, 2003). In our approach, it was necessary to formulate a new view on the dehydration character of two source clays, because of discrepancies occurring in the literature (e.g. due to differences in heating rate/clay type/relative humidity/resolution etc.).

We go on with an interpretation of how the stress-driven dehydration effect may be related to the frictional strength of clay gouge. As we do not conduct friction experiments in this study, we have to rely on available experimental data. We propose a model that is based

on earlier work (Collettini et al., 2009a), but addresses specifically the role of water (interlayer vs. external surface adsorbed) in controlling the frictional strength of clay gouge.

2. Fault gouge and clay minerals – crystallography

2.1 Fault gouge

The term "gouge" in fault rock nomenclature refers to a non-cohesive of fine-grained structureless rock which is a result of low-temperature deformation processes, occurring in faults in the shallow part of the crust (e.g., Sibson, 1977; Scholz, 1990). More specifically the term gouge is often used in perspective of clay-rich fault material that is characterized by its very small grainsize. While the occurrence of clay minerals is often abundant in fault zones, in the following the use of the term gouge will be directly associated with fault rock containing clay minerals, unless otherwise stated. Examples of major clay-rich fault zones would include for instance continental transform faults like the San Andreas Fault (Solum et al., 2006; Schleicher et al., 2009a; Schleicher et al., 2009b) and subduction zone megathrusts (e.g., Vrolijk, 1990; Underwood, 2007), even so clays have reported to be abundant in (low angle) normal fault systems (Numelin et al., 2007).

Regarding the origin of clays in fault gouge, three factors often play a major role: 1. the availability of clays in the protolith, for example the influx rate of detrital clay derived from low temperature alterations of volcanic ash, 2. mechanical processes such as cataclasis and physical incorporation of clay particles into faults from adjacent wall rock, such as via clay smearing (Lehner and Pilaar, 1997) and 3. chemical processes such as the growth of clays through alteration of fault rocks (Wintsch et al., 1995), physical and chemical weathering of adjacent protolith, and mineral reactions taking place at elevated temperatures and pressures (Vrolijk and van der Pluijm, 1999). The last two factors can also be considered to be part of a more integrated process of mineral reactions leading to gouge formation and are ongoing as fault movement continues.

From several studies on the mineralogical content of natural fault gouge (e.g., Vrolijk, 1990; Numelin et al., 2007), it can be inferred that gouge zones are intrinsically heterogeneous. The total percentage of clays can vary by as much as ~50 vol% of the rock within several meters of the fault zone (Numelin et al., 2007). In addition, the total content of smectites or "swelling clays", a clay group that is able to absorb water in the interlayer region of the clay structure, in a single fault depends on the site and may vary in addition close to

~50% (Vrolijk and van der Pluijm, 1999; Solum et al., 2006). From the group of expandable clays, the mineral montmorillonite is reported to be the most common represented in natural fault zones (Wu et al., 1975; Liechti and Zoback, 1979; Vrolijk and van der Pluijm, 1999). As a case-study example, extensive effort has been put recently into the mineralogical characterization and assessment of the frictional properties of the San Andreas fault during the SAFOD project (Solum et al., 2006; Schleicher et al., 2009a; Schleicher et al., 2009b). It was concluded that the fault zones encountered during drilling contain a variety of mineral assemblages. In particular the ratio of clay phases to non clay material, most commonly minerals such as quartz/feldspars and minor amounts of calcite, has been found to be rather variable and in the range of $1 \leq wt\% \leq 69$ (Solum et al., 2006).

2.2 Structure of clays

Clay minerals have unique chemical and physical properties amongst the phyllosilicates. Being derived from the weathering of volcanic and sedimentary rocks, they make up an important constituent of the Earth's crust. Beside fault gouge, clays are common minerals in fine grained sedimentary rocks such as mudstone, siltstone, shale and in low grade metamorphic rocks like slate. Compared to other Earth materials, their fine grainsize and distinct hydrological properties, such as low permeability and high intrinsic porosity values, makes clays distinctive from any other silicate.

While the number of different clay groups is fairly small, examples include: kaolin, smectite, illite and chlorite, the diversity in composition is enormous. This aspect can be largely ascribed to the occurrence of a broad range of solid solutions, and the fact that clays easily form polyphased networks of individual stacking layers. Clay crystals might be composed of several layers which often exhibits a polycrystalline composition. This is the reason why it remains a challenge to compare experimental results of different clay studies; there is a need for invariant source material. By definition, layered silicates are referred to as clays when their grainsize is smaller than 2µm. Mineral sciences had made vast progress during the development of modern probing techniques such as x-ray diffraction, IR spectrometry and NMR/ESR spectrometry. These methods allow a structural investigation of the molecular structure of clay particles to be made. In the following, a brief overview will be provided on the basic arrangement of the clay crystal structure and the hydration properties of smectites. The clay structure characteristics we mention are derived from both XRD studies (e.g., Brindley and Brown, 1980; Moore and Reynolds, 1989) and spectroscopic

determinative methods (e.g., Wilson, 1994). For an extensive discussion on clay crystal structures the reader is referred to Meunier (2005).

Both micas and clays belong to the group of layered silicates, whereby crystals are built of alternating tetrahedral and octahedral Si-O sheets (fig. 1). At first the perfect structures will be described here, i.e. where no solid solutions have taken place. In the tetrahedral configuration four oxygen anions are positioned around a central silica cation. Linkage occurs by shearing three of the four vertices, leading to a formula of SiO_4^{4-} per tetrahedra. The remaining apical oxygen anion is used for connection with an octahedral sheet. This sheet is composed of aluminum or magnesium cations in sixfold coordination with oxygen anions and hydroxyl groups, i.e. for aluminum as the interstitial cation the formula per octahedra is $AlO_4(OH)_2^{7-}$. The sheet is linked to a tetrahedral sheet by sharing six vertices, which can be done in two different ways. Three cations are bonded to each anion in the trioctahedral type and two bond to each anion in the dioctahedral type. While the unit cell dimensions among tetrahedral and tri- or dioctahedral sheets deviate significantly, connection through the free apical oxygens incorporates elastic deformation of the structure. The nature of the bending defines the symmetry group. Two major configurations are possible in clay minerals, depending on the way the individual sheets are built. Basic stacking units of 1:1 clays consist of one tetrahedral sheet that is bonded to one octahedral sheet, 2:1 clays consists of an octahedral sheet that is captured between two tetrahedral sheets (fig. 1). Connection between two separate stacking units in a 1:1 configuration occurs through hydrogen bonding of the octahedra hydroxyl groups with tetrahedra apical oxygen anions. The same type of bonds cannot be formed in the 2:1 structure as both the lower and upper sheet only consist of tetrahedra. In this case the layers are fixed in a clay crystallite by weaker van der Waals forces. This distinction has important effects on the chemical and physical properties of 2:1 clays.

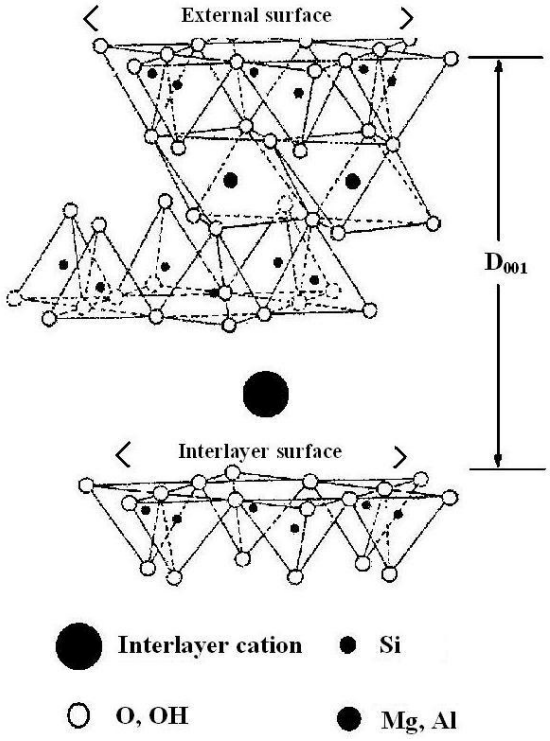

Figure 1: Typical structure of a perfect 2:1 clay mineral (pyrophyllite or talc). In the case of smectites, where solid substitutions have occurred, the crystallite is charged and counter-ions are attracted on external surfaces and in the interlayer regions. As a result, a number of possible water sorption sites are being identified, in the interlayer (interlayer surface/interlayer cation) and along the external surface. The basal spacing is defined as the d001 distance and increases with higher hydration states.

Clay minerals include the following groups (table 1), where the division is made on the basis of structure and hydration properties. The ability of certain 2:1 clays to incorporate water molecules in the crystal structure, causing the interlayer region to swell, will be discussed extensively in a later stage. Some mineralogists also include the mica mineral groups in this classification due to structural similarities (Bailey, 1980).

Group name	*Structure*	*Examples*
Kaolin group	1:1	Dioctahedral: kaolinite, dickite Trioctahedral: serpentine (e.g. antigorite/lizardite)
Smectite group	2:1 'swelling' clays	Dioctahedral: montmorillonite, nontronite Trioctahedral: saponite
Illite group	2:1 'non-swelling' clays	illite
Brittle mica (Chlorite group)	2:1 'non-swelling' micas	Dioctahedral: margarite Trioctahedral: chlorite, clintonite
True mica	2:1 'non-swelling' micas	Dioctahedral: paragonite, muscovite Trioctahedral: biotite

Table 1: group definitions of clay minerals

Clay minerals are further defined in subgroups based on the purity and configuration of the sheets. Relatively perfect di and tri- octahedral 1:1 clays for instance are kaolinite and lizardite. In the 2:1 arrangement, the equivalent minerals are referred to as pyrophyllite and talc. Although the latter duo formally belongs to the smectite group, consisting of minerals that are able to incorporate water molecules inside their crystal structure, they provide an exception to this classification as both do not possess hydration properties.

To this point, mineral structures are described as having a small extent of impurities. Clays however tend to form a broad range of solid solutions with cations of similar size and lower charge. Most common substitutions are Al^{3+} for Si^{4+} in the tetrahedral sheet and Mg^{2+} or $Fe^{2+/3+}$ for Al^{3+} in the octahedral sheet. These imperfections lead to a net negative charge deficiency in the crystallite of the interlayer and outer surface region. Other sites which are believed to be important for the charge deficiency nature are broken bonds around crystal edges and exposed hydrogen atoms of hydroxyl groups at the surface of 1:1 clays. The latter site causes a negative charge by means of proton exchange with a fluid phase at the crystallite surface (Grim, 1968). In order to maintain neutrality, positive counter- ions are attracted in those regions. The number of exchangeable cations required depends on the valence and total negative charge, defining the cation-exchange-capacity (CEC) as the total number of counter-ions a structure attracts at a certain pH. In this study, the definition of exchangeable cation is used slightly differently by also referring to interlayer cations, which sit in the interlayer space. Note that this convention is applicable to smectites, as they represent the clay group containing interlayer water. It is believed that for smectite, part of the CEC is of independent of pH. However as the ions are assumed to be the same, at first it is not relevant in what proportion can be spoken of interlayer- or outer surface cations. Both are present in smectites and to make clear, the term exchangeable cation could refer to ions located in interlayer space, but also on external surfaces, unless otherwise stated. Another interesting parameter is the location of charge deficiency in 2:1 clays, i.e. whether the substitutions solely occur in octahedral sheets or are distributed along tetrahedral sheets as well. The classification of minerals belonging to the smectite group in table 1 is further refined using the characteristics as just described (nature/amount of charge deficiency and size/valence of exchangeable cation).

2.3 Swelling of clay minerals

The smectite group is able to adsorb water molecules in the interlayer region and the external surface. Positive counter-ions (interlayer and exchangeable) attract polar molecules (water) on both these sides and the structure swells as the interlayer region increases in volume due to water uptake (fig. 1). The addition of water molecules to a (clay) structure is called *hydration* and contains two basic mechanisms. The first is 'adsorption' and can be used to describe water adsorption directly to hydrophyllic sites (exchangeable cation/inter and external surface) and to describe the adsorption of water molecules in the first few multilayers of charged surfaces (diffuse layer). 'Capillary condensation' (or dispersive adhesion of water molecules) in (meso)pores of crystallites is the second hydration mechanism that operates and causes remaining pore space to become filled with water. In some studies, the distinction between both these hydration processes (adsorption vs. capillary condensation) is rather weak. The term *adsorption* will be used here primarily in the perspective of water bonded directly to exchangeable cations or surface hydrophilic sites (equivalent to monolayer adsorption as a result of surface hydrogen bonded water molecules), and secondarily by referring explicitly to a multilayer surface water film which is held together by double-layer attraction. The more general definition of *sorption* is used here as being equivalent to *adsorption*. The second hydration process (capillary condensation) is regarded as a distinct mechanism that fills remaining pore space at high water activity (see also Prost et al., 1998).

Upon hydration, smectite clays swell and it is generally accepted that this takes place stepwise (e.g., Norrish, 1954; Harward and Brindley, 1965). The term *hydration state* refers specifically to the number of water molecules or layers that are present in the interlayer region of smectites. In a similar way, *hydration water* can only refer to the interlayer water content of smectites. The expansion is controlled by a balance of attraction and repulsion forces between the clay platelets. Attraction arises as a result of Coulomb and van der Waals forces, and repulsion follows from the hydration energy of the interlayer region, both around interlayer cations and along surface sites. The explanation why smectite clays have swelling properties, whilst other clays only adsorb water molecules on the external crystal surface, and even others are considered to be hydrophobic, follows from small differences in the crystal structure. In a totally perfect clay crystal structure, there are no available water sorption sites. This is the reason why certain 2:1 clay minerals such as pyrophyllite and talc do not swell. The lack of an interlayer charge does not require the presence of interlayer cations, which serve as the primary form of attraction for water molecules. A similar argument causes the

(internal/external) surface to be neutral. This means that no hydrogen bonds between water molecules and surface siloxane groups are possible (secondary form of attraction), making both surfaces hydrophilic.

In case of solid substitutions in the structure (e.g. Mg^{2+} for Fe^{3+}), a negatively charged interlayer and surface arises that attracts exchangeable cations, which in turn can attract water molecules. Two additional conditions are required for clay minerals to swell, thus to expand the d_{001} spacing as defined in figure 1: 1. the average interlayer charge needs to be low ($\leq$ -0.8*e* per unit cell) and 2. the stacking configuration needs to be 2:1. The first argument can be understood as a high charge makes the interlayer cations to function as locks, adding to the attraction force and allowing no expansion due to water adsorption between the clay platelets. Micas for example have a high interlayer charge of $\geq$-1.0*e* (Meunier, 2005) and water sorption does not occur. Illite has an interlayer charge of ~ -0.9*e* (Meunier, 2005) and is also not believed to be hydrous. The second argument follows from the opposition of two octahedral sheets in 2:1 structured clay minerals. In contrast, a tetrahedral sheet is directly opposed by an octahedral sheet in the 1:1 configuration, allowing strong hydrogen bonds between the platelets to be made. These bonds prevent the clay sheets to expand and therefore minerals like kaolinite and serpentine possess no swelling properties. As the interlayer region of 2:1 clays is faced on both sides by octahedral sheets, this type of hydrogen bonding does not occur and the platelet attraction primary consists of van der Waals forces, with a minor electrostatic component. To conclude, the sorption properties of smectite clays are attributed to the combined effect of a low interlayer charge ($\leq$ -0.8*e* per unit cell) and existence of a 2:1 crystal structure.

Montmorillonite is an abundant natural occurring dioctahedral smectite that has been extensively studied in the past for its sorption properties from a theoretical, experimental and computational point of view (e.g., Fripiat et al., 1960; Harward and Brindley, 1965; Farmer, 1978; van Olphen and Fripiat, 1979; Sposito and Prost, 1982; Colten and Bradley, 1987; Moore and Reynolds, 1989; Johnston et al., 1992; Skipper et al., 1995; de Pablo et al., 2004; Ferrage et al., 2007a). Water interaction with synthetic montmorillonite has also received interest and allows comparisons to be made with natural clays (Harward and Brindley, 1965/Tamura et al., 2000/da Silva, 2002/2003). Its crystal structure is similar to figure 1, with solid substitutions possible in either both sheets or just one. An apparent charge deficiency between -0.20 and -0.60*e* is compensated by the attraction of counter-ions like Ca^{2+}/Na^{+}/Li^{+} and K^{+}. The interlayer water content of montmorillonite can be probed by techniques such as x-ray and neutron diffraction (Harward and Brindley, 1965; Cebula et al., 1979; Hawkins and

Egelstaff, 1980; Sato et al., 1992; da Silva et al., 2002). These methods measure the basal spacing (d_{001}) as defined in fig. 1, which can provide information on its evolution as a function of different controls (e.g. relative humidity/temperature/pressure). It has been shown that the basal spacing of smectites changes stepwise as a function of the hydration state. This vector is often described as an integral number of water layers separating the interlamellar space. A way to control the state is by imposing a relative humidity gradient. Beside environment, the swelling properties of smectite clays like montmorillonite have been shown to be a function of several other factors. Crystallographic controls include the size, nature and valence of interlayer cations, amount and distribution of charge deficiency and extent of hydratable surface area of the crystallite (Harward and Brindley, 1965; Norrish, 1954; Sposito and Prost, 1982; Sato, 1992; Prost 1998; Laird, 1999). Additional environment parameters are variables such as temperature, pressure and salinity (Poinsignon et al., 1982; Koster van Groos and Guggenheim, 1984; Colten-Bradley, 1987; Bray et al., 1998). In section 3, a literature review will be presented on available dehydration studies of smectite-water systems, based on a number of experimental, computation and thermodynamic studies. Particular interest at this point will be allocated to the dehydration behavior of montmorillonite and structure of the remaining water molecules.

2.4 Surface adsorbed water films

Clay minerals with high interlayer charge (>-0.9*e*), or a 1:1 crystal structure do not adsorb water in their interlamellar space. Yet some of them still have the capacity of adsorbing water molecules on the external crystallite surfaces. It has been shown experimentally that water is attracted to the surface of negatively charged sheet structure minerals and forms films that contain an integral number of molecules (Rutter, 1983; Ormerod and Newman, 1983; Israelachvili et al., 1988; Renard and Ortoleva, 1997). Primary sorption sites arise due to the attraction of water molecules by exchangeable cations, or as a result of surface attraction (van der Waals/H-bond). In addition, H_2O molecules can be adsorbed as surface films (multilayers) in interstitial pores, along the edges of the sheets (Sposito and Prost, 1982) and in mesopores between the platelet stacks (Knudsen et al., 2003). Remind that capillary condensation is regarded as a separate hydration mechanism to attract water molecules (Prost et al., 1998).

The adsorption process, a result of surface energy reduction, is a complex function of charge deficiency, type of attracted counter-ion, surface area and various environmental parameters. An important aspect is the work of adhesion between the water molecules and the

crystallite. Basically this hydration force can be described along two theories that explain the electrostatic adhesion: the cation – dipole attraction between the compensating counter-ions along the surface and the water molecules in the pore space and hydrogen bonding between the siloxane planes and water molecules. The hydrophilic character of the siloxane surface is governed by the ability to create hydrogen bonds, a minor contribution arises from van der Waals attraction. This strength is dependent on charge deficiency location and thus the type of clay structure. The external sorption properties of clays with substitutions in the tetrahedral sheets will be different from the octahedral equivalent, allowing stronger hydrogen bonds to be made in the first case (Güven, 1992; Sposito, 1984). Some studies even consider the surface of clays with substitutions solely in octahedral sheets as almost hydrophobic (Prost et al., 1998; Laird, 1999), letting the sorption properties completely rely on the existence of exchangeable cations on external surfaces. In the absence of positive counter-ions, the negative charge is delocalized around the siloxane surface and water molecules will form proton bonds with the charge partition. An interesting point in such (monolayer) adsorbed water films is the distinction between the (de)localized charge surfaces, with respect to their sorption properties. Both sites are similar in location but have different electrostatic potentials (Bleam, 1990). Experimentally it has been shown that the extent of surface wetting, determined from measuring contact angles of water on 2:1 clay minerals, is a function of the degree of tetrahedral substitution (see Schrader and Yariv, 1990). In this study, the angle decreased with higher states of tetrahedral substitution, pointing toward an increase of the hydrogen bond strength between water and the siloxane plane.

The nature of the structure can be important as well. Cleaving a 2:1 clay mineral in the d_{001} direction exposes a tetrahedral sheet on both sides, allowing only oxygen anions to be in direct contact with the pore space. On the other hand, the 1:1 structure exposes an octahedral sheet to the surface that can interact physically with an aqueous solution in the pores. It has been argued that beside isomorphic substitution, charge on the sheets may arise due to protonation of exposed hydroxyl groups (Grim, 1968). The low CEC nature ($<15 cmol_c\ kg^{-1}$) of relative 'perfect' kaolinite is believed to arise specifically from exposed OH planes rather than from substitutions (Sposito, 1984; Ma and Eggleton, 1999). In the latter study, the amount of negative charge appears to be clearly dependent on particle size, pH and ion concentration. High pH leads to higher charge and higher CEC. There is however some disagreement on whether the sheets of kaolinite contain isomorphic substitutions at all. According to the constant basal surface charge model of Zhou and Gunter (1992), most of the negative surface charge arises from the substitution of Al^{3+} for Si^{4+} in the tetrahedral sheet.

Despite the fact that possibly some of these sheets could indeed be charged, experimental evidence supports that the CEC nature of kaolinite is strongly dependant on pH (Kim et al., 1996; Ma and Eggleton, 1999). This implies that the dominant mechanism is the result of protonation of exposed hydroxyl groups. It has been shown that the hydration energy of kaolinite surfaces is considerably high (Rutter, 1983) and distinctive from relative perfect 2:1 clays like talc and pyrophyllite, being hydrophobic. Note that other 1:1 clay minerals such as dickite or nacrite generally do contain several types of solid substitutions. As a result, the CEC nature of those minerals will become more a function of this mechanism.

Hence, the adhesion work of surface adsorbed water is a complex function of the bonding type that occurs between the water molecules and the platy surfaces. In the experimental section 5, an attempt will be made to differentiate between the various types of (smectite) clay water interactions and in particular to the location of possible sorption sites, interlayer(surface) vs. external surface.

2.5 Introduction to clay gouge frictional strength

Deformation of the Earth's shallow crust is often characterized by intense strain localization mechanisms that typically give rise to the development of faults. The rock lithology and amount of (total) displacement determine to a large extent whether the fault zone is characterized by formation of single fault planes or the creation of fault gouge. This involves a scale problem, on the outcrop view. What appears to be a single fault is more than often comprised as a zone of strong deformation. On a smaller scale, microstructural evidence is found for processes such as wear, fracture and rolling, i.e. for brittle frictional processes (Paterson, 1978). Deeper in the crust, the fault zone grows wider with above processes prevailing up to the temperature/pressure conditions where crystal plasticity becomes the most favorable deformation mechanism. As was described earlier, the term fault gouge is used to describe the type of fine-grained fault rock, which results from these (low-temperature) deformational processes. It is not exclusively that this rock contains clay minerals by definition, although numerous studies have indicated their presence (e.g., Vrolijk, 1990; Underwood, 2007). For that reason, gouge lithology is identified with these phases here.

To describe fault gouge frictional strength, an important material property is the coefficient of friction (μ), which is classified as the ratio of shear stress (τ), to normal stress (σ_n), acting on the fault plane. Presence of pore-fluid pressure invokes mechanical effects that change the above relation. A term referred to as the effective normal stress $\sigma_n^e = (\sigma_n - P_p)$ is

introduced, where P_p is the water pressure occurring in the pore space (e.g., Biot, 1956; Rice and Cleary, 1976). In a typical continental crust, consisting of feldspar/quartz rock-forming minerals, Byerlee (1978) found that the maximum coefficient of friction has a value in the order of ≈ 0.85. This "law" assumes that the material cohesive strength is zero, which is a reasonable statement in case of fault reactivation on existing slip zones. A small dependency on normal stress was found, suggesting that the friction coefficient slightly reduces to 0.7, at (effective) normal stresses exceeding 200MPa. For values below this stress state, no relation between μ and σ_n^e was observed.

Whereas Byerlee's "law" (Byerlee (1978) holds for many rock forming minerals, several studies have indicated that the sheet silicate group is a major exception to this law (e.g., Morrow et al., 2000). The phyllosilicates, including micas and clay minerals, have been shown to vary in strength at constant (effective) normal stress, with friction coefficients in the range of 0.2-0.7. This spread of values reflects to a large extent the level of water saturation used in the friction experiments (e.g., Bird, 1984; Morrow et al, 2000; Moore and Lockner, 2004a; Ikari et al., 2009). It is believed that such weak phases can have major effect on fault slip and induced seismicity, and could be crucial to understanding the strength of crustal faults (e.g., Wang and Mao, 1980). The smectites are the only phyllosilicates group that is able to swell due to water adsorption of the interlayer region. Friction experiments on montmorillonite have shown that it can be a low-strength mineral, with μ ranging from 0.06 to 0.78, depending on effective normal stress and hydration state (Moore and Lockner, 2007). The large spread within these results is believed to be a function of some water-induced weakening mechanism, for example μ could characterize the work necessary to shear through the interlayer region (Bird, 1984). However, this may not only be appropriate to smectites, but to sheet-structure minerals in general (Morrow et al., 2000). The hydration properties of smectites are even proposed to be irrelevant to its frictional strength, compared to other phyllosilicates (Moore and Lockner, 2004a).

Whereas a weakening trend of clay minerals is evident (incl. smectite), the associated mechanism is not. Understanding of what controls the strength of clay gouge in detail is crucial to make predictions of crustal strength at seismogenic depths. In the following, an overview is provided of results on friction experiments of smectites (montmorillonite) and other phyllosilicates, structured by the way the corresponding study was performed (dry vs. wet) and influence of clay type. Specific interest is allocated to different frictional processes that cause the dry- and wet strength to change considerably. Note that this serves only as an introduction to the low strength of phyllosilicates in general, and smectite in particular.

2.6 Influence of fabric

In friction experiments on clay gouge minerals, the development of a shear-related fabric is commonly observed (e.g., Saffer et al., 2001; Moore and Lockner, 2004b; Solum and van der Pluijm, 2009). Structural features such as alignment of clay minerals (preferred grain orientation) along shear bands (Riedel shear bands/Boundary shears) are characteristic. This is proposed to have important implications for the weakening effect of clays (e.g., Saffer et al., 2001). In a typical clay gouge friction experiment, an initial observed peak and subsequent frictional strength decrease is attributed to this alignment. The early strength increase is explained by the rotation of minerals into a preferred direction, once the alignment is attained, the gouge shear strength drops (Moore and Lockner, 2007).

Textural evidence for shearing on the 001 plane of sheet-structure minerals has been reported in the friction experiments of Moore and Lockner (2004a). It was shown that the minerals rotate until their shear plane is sub-parallel to the foliation plane, from which Riedel shears start to develop. It was argued that ongoing shear then gets localized along the interlayer plane and not specifically between two separate grains. This is based on estimations of adhesive forces occurring between the grains, which are believed to be comparable to the values for interlayer bonds and therefore the shear can be concentrated in the 001 plane (Moore and Lockner, 2004a). In experiments on the frictional properties of natural fault gouge from a Low-Angle-Normal-Fault (LANF), it was concluded that the alignment of clay minerals was held responsible for shear localization and foliation development (Numelin et al., 2007). Similar arguments were made by Collettini et al., (2009b). In the latter study, the weakening effect of a particular continental low-angle normal fault is explained by the growth of interconnected talc networks. It was reasoned that large amounts of talc can develop along the fault plane which has major implications for the fault mechanics.

The particular role of fabric was investigated recently by Collettini et al. (2009a). A general argument is made here that the formation of a lattice preferred orientation in fault gouge contributes to the weakening effect. Growth of an interconnected phyllosilicate-rich network is a mechanism that may be operative along many faults within the upper crust. In friction experiments of Moore and Lockner (2007) on thoroughly dried (~22 hours/125ºC) and water-saturated montmorillonite, an important difference was found for the type of texture under shearing of both conditions. Whereas water-saturated gouge showed clearly the development of crystal foliation and shear surfaces, the dry gouge sample showed only the formation of a preferred orientation on a much smaller scale. These results provide textural

evidence that frictional processes are influenced by the availability of water. Shearing of dry montmorillonite resulted in hardly any foliation development, which implies that here strain was more likely accommodated by typical brittle processes. A similar trend was found for texture development in other phyllosilicates, under dry and wet conditions (Moore and Lockner, 2004a).

2.7 Dry friction

Frictional deformation processes, such as fracturing and abrasion, occur in most common rock-forming minerals during experiments at 'dry' conditions (Paterson, 1978). Dry is cited here in quotation marks because the term is not equally defined for all minerals. As introduced, clay minerals (and micas) may contain interlayer or surface water, even at elevated pressure and temperature conditions. Giese (1978) calculated the change in surface energy along the 001 plane of several sheet-structure minerals in kcal/mol. This term is interpreted as a reasonable estimate for the interlayer bond energy (Giese, 1975). From these calculations, it was found that the strongest bonds are present in micas and 1:1 structure minerals, since in the first case the minerals have the highest layer charge. The interlayer cations serve as locks, bonding the platelets together. In case of divalent ions, this attraction force is even higher. In the second group, strong bonds arise as between the sheets hydrogen bonds are allowed to be made. Weaker interlayer bonds are present in perfect 2:1 clays (pyrophyllite and talc), because the according structures are neutral. Here, the platelet attraction only exists as a result of van der Waals forces. The exact interlayer bond strength of non-perfect 2:1 clays (smectites), for instance montmorillonite, has not been determined yet. This is because of the lack of crystallographic structural information. It was concluded though that dioctahedral smectites are always stronger than the trioctahedral version (Giese, 1978)

In a study by Morrow et al., 2000, the mechanical properties at room temperature of 15 oven-dried (to 180ºC) gouge minerals were investigated for dry strength. It was found that a range of frictional behavior exists, which is suggested to be directly correlated to the type of interlayer bond. In figure 2, the observed (dry) frictional strength of the minerals is related to their interlayer bond separation energy, as was calculated by Giese (1978). The shown friction data represent results of a run at constant effective normal stress (100MPa) and room temperature. Evaluation of the data displays clearly the existence of a connection; weak bonds correspond to low coefficients of friction, while the stronger bonds approach the typical range as observed for other crystalline rocks ($\mu \approx 0.8$). The minerals kaolinite and lizardite

(serpentine group), held together by hydrogen bonding, are rather strong and conform to Byerlee's law. Also the expected dry strength of chrysotile, whose friction is found to be ~0.7 at 100MPa effective normal stress (Moore and Lockner, 2004b), agrees with the predictions based on its crystal structure. The result for graphite is included in this graph to notice the link with a structure of which the d_{001} plane is bound purely through van der Waals forces. The reason why no data is incorporated for montmorillonite is due to the lack of information related to the interlayer bond strength. From the figure it is concluded that when the separation energy equals ~70kcal/mol or higher, the interlayer bond strength corresponds to values that are typical for Byerlee's law. This implies that for phyllosilicates, typical brittle processes like microcrack growth occur when this energy is at least ~70kcal/mol. Below this amount, it becomes easier to accommodate the strain by breaking through interlayer bonds (Morrow et al., 2000/Moore and Lockner, 2004a).

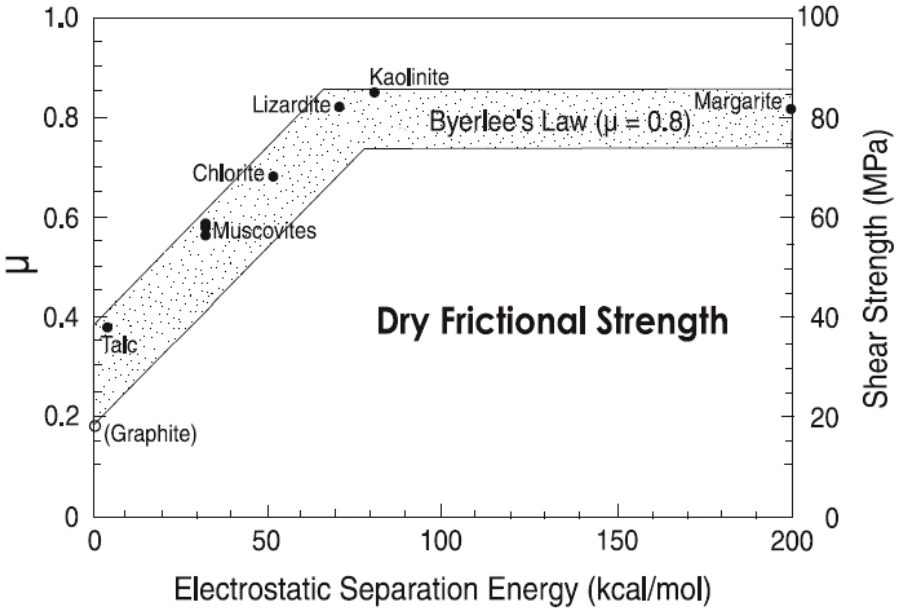

Figure 2: Maximum values of μ (dry) at room temperature for several phyllosilicates (measured at constant effective normal stress of 100MPa) as function of the calculated electrostatic separation energy (Giese, 1978). The results of pyrophyllite are left out of the graph due the large variation concerning its strength (modified after Moore and Lockner, 2004a).

Since the discovery of weak phases such as montmorillonite (Byerlee, 1978), the smectite group has received great attention in determination of its frictional properties at room-temperature (e.g., Wang et al., 1980; Bird, 1984; Saffer et al., 2001). A great number of these results are contradictory with respect to each other as the reported friction coefficient values vary extensively. The differentiation reflects the usage of various source material (different structure), initial hydration state, (effective) normal stress and sliding velocity. Depending on temperature, the shear strength of 'dry' montmorillonite is found to be quite high relative to what would be expected if the predictions of Giese (1978) are extrapolated. As the mineral structure has a low charge compared to micas, the interlayer bond energy is

expected to be less. It appeared however that in experiments of Moore and Lockner (2007), the friction coefficient of oven-dried (125ºC) 100% montmorillonite at 100MPa normal stress was found to be ≥0.7. Bird (1984) reported on friction coefficients in the order of 0.50-0.70, depending on the exchangeable cation (Na vs. Ca) with calcium giving the highest value. The 'dry' experiments of Ikari et al. (2007), performed on 100% montmorillonite (unknown type) at 100MPa normal stress (heated at105ºC), resulted in a shear strength that is slightly lower (~0.45). This discrepancy may reflect a different initial hydration state, although it was argued by the latter study that further dehydration up to 260ºC resulted in only 1wt% additional weight-loss.

These results from above may be not easily compared, because of variable source material for instance. It appears however that montmorillonite is stronger than would be expected solely on the basis of (expected) interlayer bond separation energy. Different arguments have been proposed to explain this discrepancy. The fact that montmorillonite has a very fine grainsize (even smaller than other clay phases) may contribute to this high strength (Güven, 1992). Shear strength results of (dry/wet) pyrophyllite and dry montmorillonite are expected to be similar, due to structural similarity. The basic difference is that pyrophyllite is not charged and therefore does not attract water firmly. Uncertainties about the dry strength of this mineral however impede making a proper comparison (Moore and Lockner, 2004a).

2.8 Wet friction

Textural evidence shows that a different deformation mechanism is operative when phyllosilicates are sheared under 'wet' conditions (Moore and Lockner, 2004a). Again the hydration term is cited in quotation marks, because this state is not equally defined for all minerals. The major difference is the fact that smectites can contain interlayer water (or hydration water). In table 2, an overview is presented of the mechanical properties for several phyllosilicates (excluding montmorillonite) under 'dry' (pre-heated ≥ 120ºC) and wet (water-saturated) conditions. The collected data were determined using triaxial/double-direct shearing or ring-shear friction experiments. Because different experimental configurations were used among the analyses, it is hard to directly compare the results. However it is assumed here that such irregularity is less relevant for the scope of this work, which is to show the principal weakening trends. All experiments in table 2 were performed at room temperature using an applied effective normal stress of 100MPa. The sliding velocity in the

shearing-type experiments can vary among the studies. For simplicity, literature results of smectite shear strength (wet) are discussed afterward.

Clay mineral/mica	μ (dry)	μ (wet)	Source
Chrysotile	0.70	0.2	Moore and Lockner (2004b)
Chrysotile	0.4-0.5	0.2	Morrow et al. (2000)
Talc	<0.1	0.2	Moore and Lockner (2008)
Talc	0.25	0.2	Morrow et al. (2000)
Kaolinite	0.85	0.55	Morrow et al. (2000)
Muscovite	0.60	0.45	Morrow et al. (2000)
Chlorite	0.65	0.35	Morrow et al. (2000)
Graphite	0.15	0.15	Morrow et al. (2000)
Quartz	0.70	0.70	Morrow et al. (2000)
Pyrophyllite	?	0.28	Moore and Lockner (2004a)
Margarite	0.80	0.68	Moore and Lockner (2004a)

Table 2: Mechanical properties of various phyllosilicates under dry (pre-heated ≥ 120ºC) and wet (water-saturated) conditions measured at 100MPa applied effective normal stress and room temperature. Note that all dry vs. wet experimental results from Morrow et al. (2000) were basically replicated by Moore and Lockner (2004a).

The introduction of water has no effect on the coefficient of friction for quartz and graphite. This is an expected result while both minerals are considered to be hydrophobic. Shearing under wet conditions does have a pronounced consequence for the frictional strength of clay minerals and micas. The value for μ decreases by addition of water for nearly all sheet-structure minerals, depending principally on the way the platelets are stacked (1:1 vs. 2:1). It appears that the 1:1 configuration is more influenced by 'wetting', i.e. resulting in a decrease of μ from 0.85 to 0.55 for kaolinite. According to Morrow (2000), the serpentine mineral group (e.g. chrysotile, a trioctahedral 1:1 clay) displays the largest strength drop when sheared wet. The 2:1 clay minerals show i.e. a decrease from 0.80 to 0.68 for margarite. The role of water could reduce the frictional resistance between the minerals (Morrow et al., 2000), but this 'wetting' effect is not equally defined for each crystallographic group.

Friction experiments on smectite clays are hardly novel since its recognition as a weak phase by Byerlee (1978). Numerous studies have investigated the effects of hydration state, normal stress and shear velocity on the mechanical properties of montmorillonite (e.g. Wang et al., 1980; Ikari et al., 2007). The first control is rather poorly defined as the mineral usually

contains bound water both inside and outside the structure, which is primarily a function of relative humidity (e.g., Bird, 1984). Experiments performed at room-temperature are not dry in a similar way as is the case for quartz. Instead, the water content fluctuates depending on local climate conditions. This is one of the main reasons why there exists an enormous discrepancy between published values of friction coefficients (see also Bird, 1984). In an overview by Moore and Lockner (2007), it was illustrated that the strength of montmorillonite varies from $\mu = 0.06$ to 0.78, between 100 and 150 MPa effective normal stress. We already pointed out that the upper limit represents shearing under 'real dry' conditions. This implies that the crystal structure is considered to be totally free of water (no hydration or surface adsorbed water). The amount of absolute weakening depends at first on the chosen reference of its (real) dry strength, which lies near 0.8, if the material is heated to sufficient temperature (Moore and Lockner, 2007). Upon introducing water, the shear strength drops and different relations to normal stress dependency are observed (e.g., Morrow et al., 1992; Saffer et al., 2001; Ikari et al., 2007).

In the experiments of Saffer et al. (2001), who were the first in investigating the frictional properties of montmorillonite over a range of normal stresses and sliding velocities, it was found that the mineral can be very weak with μ ranging from 0.30 to 0.14 measured at 5MPa and 50MPa normal stress respectively. The experiments were performed at room humidity and temperature. This implies that in unloaded state, the water content in the pores of the clay is under- or partially saturated. Such experiments can potentially lead to incorrect results because no control is invoked for the possible change in pore-fluid pressure. This hypothesis was firstly introduced by Wang et al. (1980). If normal stresses are high enough to mechanically expel water from the interlayer, in the duration of the experiment, the pore pressure might built up. Given that clay gouge in general has low (anisotropic) permeability and that compaction contributes to void reduction in the structure, the pores can become locally fully saturated at sufficient normal stress, causing P_f to rise. This process gets enhanced with ongoing shear, as the development of fabric and associated anisotropy is suggested to decrease the permeability dramatically (Ikari et al., 2009). Undetected high P_f could lead to friction coefficients that are taken too low as the measured applied effective normal stress is higher than the true effective normal stress. This problem can be avoided by conducting future friction experiments of smectites only under water-saturated conditions. In that case, if the sample is thin enough, the fluid-pressure can be constrained in a systematic way and remain equilibrated with a set value using computer-controlled adjustments to the fluid or confining pressure. The scenario as describe here could have been the case for the

experiments of Saffer et al. (2001), although the imposed normal stresses were still fairly low. The theory and background of pressure induced smectite dehydration is extensively described in section 3.

Other experiments performed under partially saturated conditions have provided comparable values for the coefficient of friction measured at ~100MPa normal stress. For instance, Saffer and Marone (2003) reported a value in the order of $\mu \sim 0.1$ for pure smectite (Ca-montmorillonite) and $\mu = 0.2$ for a gouge mixture composed of 50:50 quartz and Ca-montmorillonite. These results are in agreement with a study Ikari et al. (2007), who investigated in detail the effects of hydration state on the frictional properties of smectite. Here it was found that a three-layer state 100% montmorillonite sample (= maximum hydration state) at 100MPa normal stress had a friction coefficient of ≤ 0.1. Mixtures of 50:50 smectite/quartz at equivalent hydration conditions showed that $\mu = 0.21$. In general, the authors observed that the strength of the gouge decreases with higher hydration state and clay content.

As argued, the usage of partially saturated conditions in friction experiments of smectite can be problematic. However, despite the possibility that in these particular studies excessive fluid pressure developed, montmorillonite has been reported to be weak under water-saturated conditions as well. In the studies of Morrow et al. (2000) and Moore and Lockner (2007), it was found that its coefficient of friction is near ~0.2 at 100MPa effective normal stress. Ikari et al., (2009) observed coefficients in the order of $\mu = 0.19 – 0.23$, in the range of 10 to 60MPa effective normal stress, for a gouge composed of a 50:50% mixture of quartz and montmorillonite.

In this section, various terminologies are introduced on clay water interactions. Important to recognize is the fact that only smectite clays are able to adsorb water molecules in the interlayer region. Other clay minerals may still be able to adsorb water films on external crystal surfaces. Moreover, the hydration of both groups (smectite and all other clay minerals) involves two different processes (adsorption and capillary condensation); however this can only lead to hydration (or interlayer) water in the case of smectite. Other terms that are worth repeating are the conditions ‘dry’ and ‘wet’ in frictional experiments on clays. From earlier, the condition ‘dry’ is not equally defined for all minerals, i.e. smectites may still contain interlayer water if the samples were not sufficiently pre-heated. In case of ‘wet’ experiments there is an important distinction between under- and fully saturated conditions. We have also indicated that montmorillonite is mechanically weak under saturated and non- saturated conditions. Then we argued that the strength of other clay and sheet-structured groups can be

affected too by the introduction of water. In the discussion, a section is devoted to possible weakening mechanism(s), partly based on experimental results obtained in this work.

3. (Smectite) clay-water interactions - a literature review

In this section, an attempt is made to provide the reader with a comprehensive overview of results from earlier studies, concerning the structure of water in smectite clays upon dehydration. The content is organized with respect to the technique utilized and the method of dehydration, examples include: thermogravimetric analysis (TGA), X-ray diffraction (XRD) and infrared spectroscopy (FTIR). Beside the experimental approach, smectite clay-water systems and dehydration can be studied using computational modeling techniques and thermodynamics, a number of these relevant studies are evaluated in the second part. In the last section, a conceptual model is provided of the structure of adsorbed and capillary condensed water, aiming to differentiate between various sorption sites. Particular interest in the review is assigned to the equivalent methods and materials used in this work.

As pointed out by Sposito (1982), the information provided by the experimental approach is distinguished according to the timescale at which the structure is probed. For instance: IR-spectroscopy, XRD and thermodynamic modeling have different timescales on which the technique is applicable, providing information of different nature. Following the theory of Sposito (1982), infrared studies can be used to study the vibrationally averaged structure (V-structure). This is the arrangement that arises due to the vibration motions of water molecules. Infrared cannot probe the diffusionally averaged structure (D-structure) as the timescale on which the molecules diffuse is longer than the time it takes for the molecules to adsorb energy from infrared light. The D-structure entails effects of vibration and translation (diffusion) of water molecules and can be probed using XRD and TGA. Additional experimental methods such as nuclear magnetic resonance (NMR) and electron spin resonance (ESR) spectroscopy probe the molecular structure at intermediate timescales. The information they present is quite complex and describes the structure of water molecules going from the V- to a D-structure. Alongside the discussion of the different techniques, it is important to realize that the structure of water in smectite is dynamic. It depends on the technique involved which aspect of the dynamic state is being probed.

3.1 TGA

A classical way to study clay-water interactions follows from the dehydration of clay upon heating. One of the most common techniques used is thermogravimetric analyses (TGA) or related methods, e.g. differential thermal analysis (DTA). From TGA, it is possible to extract temperature(s) of water removal and to gain insight into the amount of water lost. This dehydration takes place on a macroscopic scale and affects all possible sorption sites in a crystal structure. For this reason, the method cannot easily differentiate water that is bound in different ways, unless the relative adsorption strength is identified. Due to the fact that the technique is a dynamic method, the data does not correspond to equilibrium states and the information provided is therefore complex.

In the analyses, a fixed amount of sample is heated and the according weight-loss due to evaporation is continuously being monitored. The rise of a peak in the according derivative function is defined by the onset of a dehydration period, related to a dewatering reaction in the sample. Superposition of an additional peak at near equal temperatures causes the signal of both reactions to represent a sum, expressed as the appearance of a shoulder. The reaction rate should therefore be interpreted as the total sum of several individual reactions. The method does not allow differentiating between separate contributions, if they occur at the same peak temperature. It has been argued that the data of thermal analysis is sensitive to a number of experimental and environmental variables that influencing the reaction rate. Dehydration includes both water desorption from sorption sites (V-structure) and diffusion (D-structure) of the desorbed molecules into the gas phase. This manifests itself in a variability of results for experiments done at different heating rates

In the same sense, the rate (and peak position of the derivative) has to be read with care as kinetic problems could occur during desorption, preventing reactions occurring at higher temperatures than would be expected. For instance it has been shown experimentally that sample size and preparation method both have pronounced affects on the position of peaks and shoulders. In a study by Schilling (1990), the increase in peak temperatures with sample size are attributed to the effects of thermal lag. Structures with tight packing hinder diffusion rates across the material, thereby causing a shift and broadening of peaks. In general the results suggested that for a given material, both parameters need to be considered when evaluating data. For a summary on the possible factors that influence the temperatures of dehydration, see Guggenheim and Van Groos (2001). Despite these problems, TGA analysis

provides a distinction to be made among different energetically bound water molecules in a crystal structure.

Smectite dehydration has been investigated in abundance using TGA (e.g., Hendricks et al. 1940). These studies provide evidence that the process occurs in discrete thermal events. This led to the suggestion that water molecules inside the structure vary in bond strength with respect to its sorption site. General agreement between two major weight-loss episodes is commonly obtained, at low temperatures between 40-70°C and at higher temperatures of 120-150°C (e.g., Poinsignon et al., 1982; Zabat and van Damme, 2000; Bish and Duffy, 1990). In Table 3 an overview is given of several dehydration peak temperatures for montmorillonites as published in the literature. To describe the spread of available data, a distinction was made solely between the two major events. For the moment, the detection of additional shoulders is not considered. If the exchangeable cation is cited in brackets, it occurs as the dominant ion. In the column 'comments' is cited if the sample consisted of homo-ionic (only one type of exchangeable cation) source material and under which special conditions the analysis was performed, in case of multiple experiments on the same samples. Note that other variables such as: heating rate/sample size/packing and humidity surrounding the sample are not constant among individual studies. The spread in the results reflects to a large extent the variability of experimental conditions. The two DTA studies of Koster van Groos and Guggenheim (1984; 1986) report only the results of high temperature dehydration events. In a study of Takahashi et al., 2007, no report was made of a low temperature dehydration peak, or the type of montmorillonite used in the analysis. A detailed overview of TGA analyses of the widely used clay mineral society source clays (e.g. Wyoming 'SWy' and Arizona 'SAz' montmorillonite, see section 4.1 for specific clay properties) is given in Guggenheim and Van Groos (2001). A comparison of results with equivalent experiments conducted in this study is included in the discussion (section 6).

Sample	T_{max1} (°C)	T_{max2} (°C)	T_{max3} (°C)	Comments
Na^{+}- SWy-1[1]	62	-	-	Homo-ionic
Cs^{+}- SWy-1[1]	61	-	-	Homo-ionic
Li^{+} - SWy-1[1]	64	112	-	Homo-ionic
Mg^{2+}- SWy-1[1]	72	146	-	Homo-ionic
Ca^{2+}- SWy-1[1]	70	128	-	Homo-ionic
Ba^{2+} - SWy-1[1]	65	104	-	Homo-ionic
Al^{3+} - SWy-1[1]	59	86	-	Homo-ionic
La^{3+} - SWy-1[1]	72	139	-	Homo-ionic
STx-1[2]	70	130	-	Mixed interlayer cations/10mg powder
(Na^{+}) SWy-1[3]	57	192	-	Mixed interlayer cations
Na-MMT [4]	not reported	105	-	?
(Na^{+}) SWy-1[5]	not reported	140	210	DTA/Mixed interlayer cations/1bar
K^{+} - SWy-1[6]	not reported	150	200	DTA/Homo-ionic/1bar
(Ca^{2+}) SAz[7]	65	144	-	Mixed interlayer cations/no purge
(Na^{+}) SWy-2[7]	51	139	-	Same composition as SWy-1/no purge

Table 3: overview of several dehydration peak temperatures for montmorillonites as published in the literature
1. Zabat and Van Damme (2000)
2. Schilling (1990)
3. Bish and Duffy (1990)
4. Takahashi et al. (2007)
5. Koster Van Groos and Guggenheim (1984)
6. Koster Van Groos and Guggenheim (1986)
7.Guggenheim and Koster Van Groos (2001)

According to the findings, water molecules in smectite clays can be classified into at least two types (1) free water derived from capillary condensation and (2) water which is adsorbed and electrostatically bound to positively charged cations. Some studies (Koster van Groos and Guggenheim, 1984; 1986; Guindy et al., 1985) support the existence of additional shoulders at temperatures higher than 200°C, which is clearly a different observation from the bulk data. Specific effects of ionic radius and type have been investigated by Guindy et al., (1985). In their analysis a number of homo-ionic montmorillonites samples were prepared by cation exchange procedures. It was shown that the total weight-loss decreases upon increasing the radius. The temperature of the last dehydration step, corresponding to the removal of strongly bonded water, is more elevated for ions with higher hydration energies (see fig. 2 in Guindy et al., 1985). These relationships were confirmed in a TGA study by Zabat and van Damme (2000). From Table 2, it is found that the position of the first water-loss peak is less a function of the cation type. This is in agreement with the interpretation of being attracted by capillary forces and multilayer adsorption. The water interacts only weakly with the clay

surface and the exchangeable cations. Effects of surface sites and charge location have not been taken into account by most authors. Most of these experiments have been performed at high heating rates exceeding 10°C/min. In this study, a comprehensive analysis is performed of montmorillonite dehydration in the low temperature region at low rates (0.4°C/min).

In a study by Koster van Groos and Guggenheim (1984), the effects of an imposed hydrostatic pressure, on the dehydration reactions temperatures, for a specific source clay (Na-SWy-1) was investigated. Using high pressure differential thermal analysis (HP-DTA) up to 1.5kbar, it was found that mean stress increases both peak temperatures, which were located at 140°C and 210°C under 1 bar. It was observed that both peak temperatures showed a large jump with only a small pressure increase (<100 bars). For example, an increase of 1 bar confining pressure raised the primary peak by 40°C to 180°C. At higher pressures (>400 bars), the pressure dependence became rather small. The DTA signal at 1.345 kbar is practically equal to the signal at 448 bars. Increasing dehydration temperatures at elevated confining pressures are expected; mean stress hinders the expulsion of interlayer water. It is suggested that differential stresses, caused by tectonics or the compaction of sediments, will tend to squeeze out the interlayer water at lower temperatures than if the process would be exclusively thermally induced (e.g., Colten-Bradley, 1987).

So far, we have explained that despite the imprecision and range of results associated with TGA analyses on montmorillonites, it appears that there are at least two different types of water molecules present in the crystal structure. General agreement is found between two major weight-loss episodes, at low temperatures between 40-70°C and at higher temperatures of 120-150°C. The first event is interpreted as the weight-loss resulting from free water (derived from capillary condensation) and the second event is due to the loss of more strongly adsorbed and electrostatically bound water molecules. The detection of additional shoulders suggests that other sorption sites, beside around the exchangeable cation, play a role in the crystal structure as well. It was also experimentally proved that the imposition of confining pressure hinders both major dehydration reactions, requiring higher temperatures to initiate the reaction.

3.2 XRD

A classical way to study the swelling behavior of smectites is to use x-ray diffraction (XRD). Experiments on montmorillonite powders, especially as a function of relative humidity, have been extensively carried out in the past (e.g., Mooney et al., 1952). The principle relies on

measuring the change in basal spacing reflections as a function of hydration state. XRD analyses can only provide information on the processes occurring at the micro-structural level, at the level of interlayer water. The method does not allow measuring the contributions to the total water content of H_2O located in pores or water being adsorbed on external surfaces. There are a number of ways to impose the hydration state. One of the most important techniques is the usage of vapor pressure changes. The results showed that the basal spacing transforms in steps as a function of relative humidity, which is in correspondence to the existence of several layers H_2O molecules in the interlayer space (fig. 3). It is concluded that the d_{001} spacing of smectites changes sharply from ~10Å to ~19Å, corresponding to 0,1,2 or 3 mono-layers of H_2O at particular vapor pressure boundaries (Norrish, 1954).

The hydration state transition zone boundaries have shown to be a function of several parameters including amount of charge deficiency, exchangeable cation (type, valence and hydration energy) and location of charge (Bird, 1984; Sato et al., 1992). In the study by Bird (1984), two hydration-phase diagrams as function of vapor pressure were constructed for the homo-ionic source clays SWy-1 and SAz-1 at room conditions. From their results and according thermodynamic calculations, regarding the coordination state of H_2O, a definition of proposed phases was presented. For a relative humidity of 40% at equilibrium, Na-SWy-1 and Ca-SAz-1 (meaning Na^+ and Ca^{2+} are the only exchangeable cations resp.) occur in a 1- and 2-layer state respectively. Sato et al., (1992) investigated more extensively the separate effects of layer charge and charge location on a series of ten homo-ionic smectites using relative humidity induced dehydration experiments. It was found that basal spacings were larger when the charge deficiency is derived from the octahedral sheets. This is in agreement with the existence of a weaker attraction force between the clay platelets.

Fewer studies have been performed on the effects of temperature by measuring basal spacing changes under *in-situ* conditions. Bray et al. (1998) conducted a series *in-situ* synchrotron XRD thermal dehydration experiments to investigate the time-temperature dependence of structural modifications in Ca-exchanged montmorillonite. The heating rate was varied from 10 to 99°C/min up to the onset of dehydroxylation. Results successfully reproduced the basal spacing set of 10.3, 11.7 and 15Å (see fig. 2 Bray et al. 1998). It was found that for all runs, following the initial rapid drop in spacing from ~15Å to ~12.3Å (from a 2-layer to a 1-layer state), the reaction rate decreased which reflects a change in rate determining step. As proposed by Bray et al. (1998), a change into a diffusion rate controlled reaction mechanism occurs at the final stages of dehydration. It was also obtained that the first

water layer does not dehydrate before 100°C is reached, from which it was concluded that the two-layer state seemed to be bounded relatively loosely.

In a study by da Silva et al., (2003), *in-situ* XRD thermal dehydration experiments up to 125°C were performed on a synthetic Na-fluorohectorite. Although their results cannot be compared directly to natural montmorillonites, some interesting features were shown. It was found that at intermediate temperatures, broad line shapes of the Bragg peaks and the occurrence of more than two peaks indicated the coexistence of various hydration states. For instance, the one-layer state peak of ~12.5Å showed continuous intensity over the entire investigated temperature range. The 'dry' peak of ~10Å started to appear at temperatures of 40°C, although its relative intensity remained low until 70-80°C was reached. It was also found that changing the temperature resulted in a direct change to one of the d_{001} spacings where a particular hydration state would be favored. These observations are in agreement with the experiments of Bray et al., (1998).

Recently, the thermal dehydration kinetics of homo-ionic Ca-montmorillonite was studied under isothermal conditions using *in-situ* XRD analysis (Ferrage et al., 2007). Experiments were performed in the 30-125°C temperature range and the relative proportions of defined hydration states were investigated. The results show that in temperature-time space, some domains exist with a fairly homogeneous hydration state, whilst others were completely heterogeneous. At 30°C, the vast majority of the layers occur in a two-layer state. Between 35 and 50°C a nearly complete transition to a one-layer state occurred, although the two-layer peak prevailed up to 85°C. The remaining water layer started to be removed at temperatures higher than 85°C, even though near 125°C, the reaction was still ongoing. These results are in qualitative agreement with Bray et al., (1998), although their transition from 1-layer to a 'dry' structure did not occur prior to 100°C. The results of Ferrage et al. (2007) are also in agreement with the suggestion that the second layer is not strongly coordinated to the interlayer cation (see also Ormerod and Newman, 1983). Furthermore, the heterogeneous occurrence of multiple hydration states agrees well with da Silva et al., (2003) and earlier XRD relative humidity dehydration experiments of Ferrage et al., (2005).

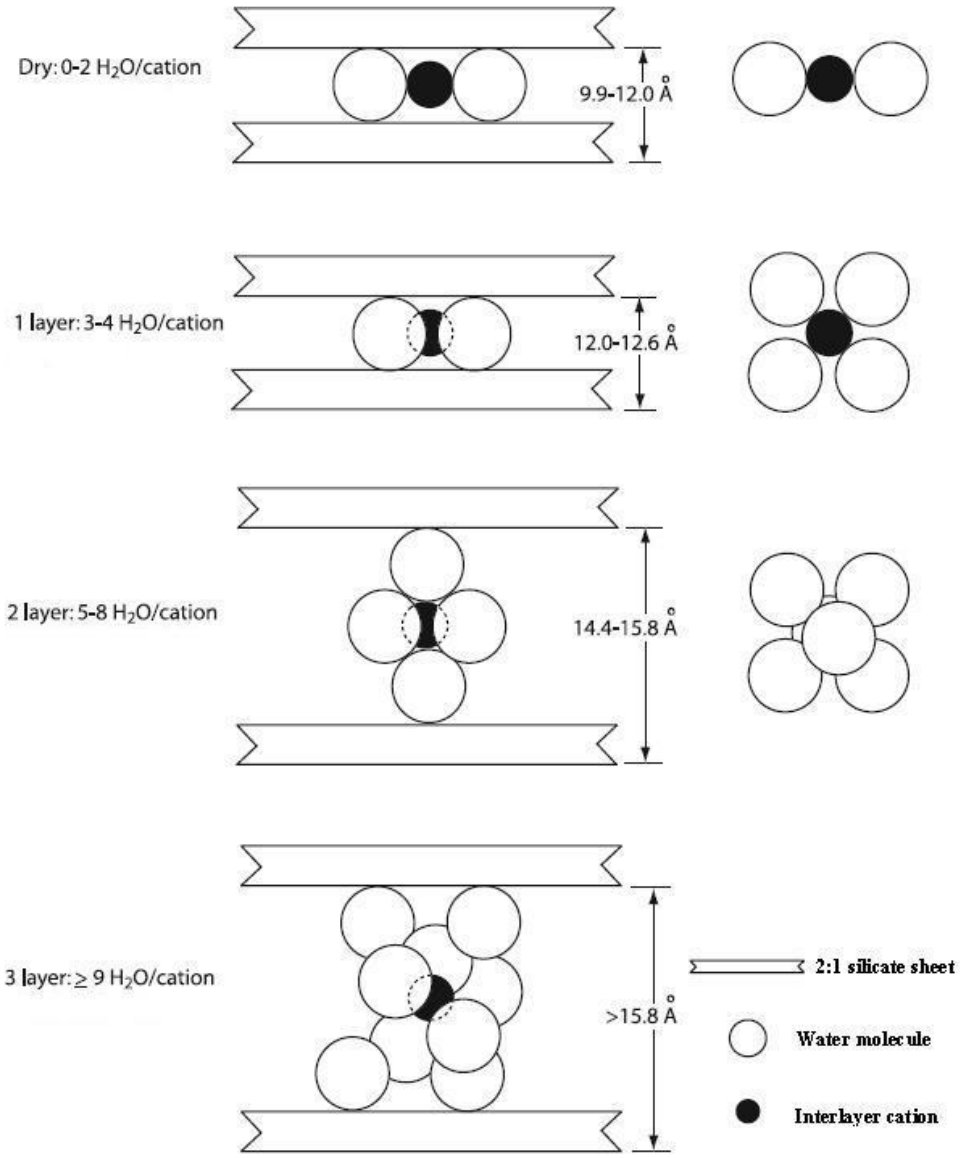

Figure 3: Schematic representation of the basal spacing configuration in a typical Ca-montmorillonite showing clay swelling/shrinkage upon a change in the hydration state. Predictions on the amount of water molecules per cation are based on calculations of Sposito and Prost (1982), for a specific crystal structure. Modified from the work of Ikari et al. (2007) and Colten-Bradley (1987).

The (total) confining pressure dependence of montmorillonite dehydration temperatures has been studied using *in-situ* XRD analysis by Huang et al. (1994), and more extensively by Wu et al. (1997). In the first study, it is found that a three-layer hydrate of homo-ionic Na-SWy-1 is stable up to temperatures of 340°C with confining pressures of ~2kbar. At 483°C and ~4.4kbar, the structure dehydrates to a one-layer hydrate. The conclusion was made that such a hydrate would be stable at P-T conditions encountered in shallow sedimentary basins, without the existence of differential stresses. The results indicate that dehydration temperatures increase with mean stress, which was the same conclusions of

Koster Van Groos and Guggenheim, (1984). Huang et al. (1994) argues that this is consistent with the idea that interlayer H_2O density must be higher than free H_2O in pore space. In the study by Wu et al. (1997), comparable dehydration experiments were performed on homo-ionic Mg- and Ca-SWy-1 up to pressures of ~10kbar. Their results provide additional proof that a three-layer hydrate is stable at 200-385°C under elevated hydrostatic pressures along the geotherm. In addition, this study supported the coexistence of multiple hydration states at equal temperatures, in terms of a broad character of the d_{001} peak. This indicates the interstratifications of various hydration states.

The technique of XRD is in particular useful to study the evolution of the d_{001}-spacings, and so the interlayer water content of smectites. It does not give information on the water content associated with externally adsorbed water films for other clay minerals. Clay swelling appears to occur stepwise in discrete layers of molecules, is heterogeneous (occurrence of multiple hydration states at the same conditions), occurs at rates in the order of minutes and is strongly a function of specific crystallographic controls (interlayer cation/amount and location of charge deficiency). Dehydration of the third and second water layer appears to take place more easily than removal of the final layer, of which generally temperatures above 100°C are required.

3.3 Infrared spectroscopy

IR-spectroscopy permits to study the structure of specimens on a timescale that corresponds to the vibration of molecules. It probes the molecular V-structure through the absorption of normal mode frequencies and rotations. If the energy of a specific frequency matches the energy required to activate a normal vibration, the molecule absorbs that wavelength and the detector observes a net energy change. In order for a molecule to be infrared 'active', the vibrations (or rotations) have to cause a net change in the dipole moment. For instance, no absorptions emerge from nitrogen gas because of its coinciding charge centre. Functional groups such as O-H, CO_2 or CH_2 give rise to absorption bands in well-localized regions in the spectra. As a rule, the number of possible normal modes for polyatomic polar groups can be calculated with: 3N-6, where N is the quantity of atomic compounds. However, due to symmetry effects, fewer bands are typically being observed. Selection rules forbid the activation of some bands, while others appear more intense. This is not the case for water molecules and three normal vibrations can be observed on the mid-IR scale. The rise of Fourier transform infrared instruments significantly improved the signal to noise ratio and

spectra quality. FTIR spectrometers also allow the gathering of spectra over an entire frequency range to be collected simultaneously. The result is a spectrogram, revealing a number of specific wavelengths that were absorbed from the light. Different reflection and transmission techniques can be used to probe the necessary type of information. An overview of various methods is given by Madejova (2003). Compared to reflection techniques, transmission IR-spectroscopy allows both qualitative (mineral identification) and quantitative (concentration measurement) studies to be conducted on smectites.

Infrared spectroscopy has proven to be a useful tool for studying the structure of adsorbed water molecules on smectites (e.g., Farmer, 1978; Sposito and Prost, 1982). In addition, effects of water sorption have shown to induce changes in the molecular vibrations of structural OH groups located in the octahedral sheet (Bishop et al., 1994; Xu et al., 2000). The effects of dehydration on the band positions of adsorbed water molecules has been studied extensively (e.g., Russel and Famer, 1964), relative peak position and intensity contain important implications concerning the structure of remaining water molecules and/or cations (e.g., Prost et al., 1998; Bishop et al., 1994).

Water molecules have three fundamental vibrations: a symmetric and asymmetric OH stretch (υ_1 & υ_3), and the H-O-H (υ_2) bending mode. The spectral results show that sorbed water gives rise to absorptions in the OH stretching region (3000-3700cm^{-1}) and H-O-H bending region (1600-1650cm^{-1}). Absorbance in the latter region can be directly related to the total amount of sorbed H_2O by smectite, for all sorption sites. This directly follows from the Bouguer-Beer-Lambert law, where absorbance is proportional to concentration of the specific molecule group. A sharp peak at ~3620cm^{-1} observed for all montmorillonites is assigned to the OH stretching mode of structural hydroxyl groups located in the octahedral sheet (Madejova, 2003). Structural OH bending gives rise to several absorptions near ~900cm^{-1}, strongly depending on the extent and type of substituting cation. The wide band near 3400 cm^{-1} is comprised of both OH stretching modes that partially overlap, of which ν_1 has the strongest intensity. Another reason for peak broadening is attributed to effects of hydrogen bonding. Note that IR spectroscopy acts on a macroscopic scale; all interfaces in the crystal structure are “sampled” resulting in spectra where a range of adsorbed molecules is detectable.

According to groundwork laid by Eisenberg and Kauzman (1969), bulk liquid water has the following normal OH stretching vibrations: υ_1 ~ 3439 cm^{-1} and υ_3 ~ 3600 cm^{-1}. In the same spectral region, a bending overtone ($2\upsilon_2$) can be observed near ~3200 cm^{-1}. In the bending region, the absorption of bulk liquid H_2O occurs near ~1643.5 cm^{-1} (Venyaminov et

al., 1997). Different models have been proposed to explain the physical state of adsorbed water molecules. An important constrain arises from the study of band evolution upon dehydration. Band positions and intensity have demonstrated to be clearly a function of the hydration state. This method allows to differentiate between various water types in a clay structure, at high water contents the spectra is comprised of a mixture of all signals. At low water content, the signal primary represents water molecules that are associated with the strongest sorption site, which is the attraction arising through to the exchangeable cations. It was argued that direct dipole-cation attractions are the strongest and require the highest amount of work to be broken. In most FTIR dehydration studies the assembly of *in-situ* conditions is performed using relative vapor pressure as the dehydration mechanism. This invokes two possible techniques, vacuum methods or a flowing-gas manifold (Johnston, 1992). Both act on clay films in specially designed environmental cells to control relative humidity in the sample chamber.

Earlier studies suggest a complex clay-water system in montmorillonites. It has been argued that multiple water sorption sites can be recognized in spectrograms, including water bound to exchangeable cations, water bound to surface sites (internal and external) and water occurring in multilayers and pores (Russell and Farmer, 1964; Sposito and Prost, 1982; Johnston et al., 1992; Bishop et al., 1994; Xu et al., 2000). Dehydration and rehydration experiments on Na-montmorillonite led to the conclusion that the υ_1 & υ_3 peak shifts to lower frequencies as the water content increases. However, it would never become equal to the values for bulk H_2O (Sposito and Prost, 1982). This shift to lower energies suggests that the amount of hydrogen bonding increases with higher water content, or the other way around, water coordinated directly to cations is less hydrogen bonded and therefore the OH stretching bands shift to higher energies. This description is in agreement with results obtained by Madejova (2003) and Bishop et al. (1994). The structural OH band intensity at ~3620cm^{-1} has shown to decrease upon dehydration as well. This can be explained by the broad character of the OH stretching region and partially overlap of the υ_3 band. The structural peak is made up partially of absorption due to H_2O.

Johnston et al. (1992) used IR transmission spectroscopy to investigate the effect of exchangeable cations (Na^+, K^+, Co^{2+} and Cu^{2+}) on the band position of the υ_2 vibration upon dehydration. Using a specially designed FTIR/gravimetric cell, it was possible to obtain simultaneous spectroscopic and gravimetric data from ion-exchanged SAz-1 and SWy-1. The results show that for all cations at fairly dry conditions (<6 water molecules per cation), the band shifts to lower frequencies. This is an opposite relation to the drift seen for OH

stretching modes (see also fig. 6 Johnston et al., 1992), and in agreement with analyses of Russell and Farmer (1964). The opposed position trends are consistent with the idea that effects of hydrogen bonding are reduced at dehydrated conditions. Different cations give rise to slightly different position shifts. The most obvious shift is seen for Cu^{2+} exchanged SAz-1, where at ~3 H_2O/cation the absorption occurs near ~1620cm^{-1}. In addition to spectroscopy, Johnston et al. (1992) measured the basal spacing evolution upon dehydration using three different methods: interference fringes, powder XRD and film thickness calculations. The author argued that the discrepancy seen amongst these results presents evidence of water layer adsorption on external surfaces, consisting of H_2O molecules which are coordinated to exchangeable cations.

Using a similar experimental set-up, Xu et al. (2000) investigated the dehydration effects on homo-ionic SAz-1 and SWy-1 for all mid-infrared H_2O absorptions, including the OH-stretching region. Results show that the υ_2 positions upon dehydration are in good correspondence with Johnston (1992), with reported values of 1625cm^{-1} and 1629^{-1} for Na-SWy-1 and Na-SAz-1 resp. at ~2 H_2O/cation. Xu et al. (2000) also found that structural OH-bending absorptions are a function of the total H_2O content and exchangeable cation, influenced by the way water molecules are coordinated around surface sites. This is explained as at low water content, the basal spacing decreases and interlayer cations move into ditrigonal cavities of the siloxane plane, thereby increasing the interaction between the two molecule groups.

IR-spectroscopy studies of smectite-water systems primary entail the analysis of reduced hydrogen bonding upon dehydration. Earlier experimentation suggested that properties of H_2O molecules surrounding exchangeable cations, at the external surface and interlayer region, are distinct from those of bulk water and strongly influenced by the cation type. Desorption (or dehydration) initially removes water located in the pore space and on multilayers of 'free surfaces', attracted by both adsorption and the mechanism of capillary condensation (Prost et al., 1998). According spectroscopic evidence upon removal consists of a decrease in band absorption intensity. Up to here peak shifting is believed to play to a relative unimportant role. Those water molecules are relative easy to remove, but the method does not show a distinction between the sites (multilayers vs. pores), where in both cases the attraction primary arises from van der Waals forces. The remaining water molecules require more work to be removed due to the large hydration energy of the exchangeable cations and surface sites. The band positions of those remaining H_2O molecules correspond to higher OH-stretching and lower HOH-bending frequencies, with respect bulk water properties. A

consequence that is allocated to reduced effects of hydrogen bonding at lower hydration states.

In contrast to results from XRD studies, the dehydration process does not seem to occur stepwise on the macroscopic scale. This difference is supported by the idea that for particular hydration states, a mixture of basal spacing's exists (e.g., da Silva et al., 2003). On a larger scale, such effects produce an 'average' absorption pattern. Influences of the remaining sorption site, the crystallite internal and external surfaces, on effects on spectra shifting have not been reported explicitly. Although it is expected that at low water contents (<6H_2O/cation), both the siloxane surfaces and the exchangeable cations influence the structure of remaining water molecules. At high water contents corresponding to a three-layer state (>10H_2O/cation) in montmorillonites, from IR-spectroscopy no significant additional evidence is presented of that particular state (e.g. peak shifting to bulk water properties). In other words, the method does not allow making a clear distinction between to two- and three-layer state, except for the relative absorption intensity which is higher in the latter case (Xu et al., 2000). Spectroscopic properties start to get influenced at lower water content (≤10 H_2O/cation).

To summarize, all infrared spectroscopy dehydration studies on smectites show that the characteristic water absorption bands shift in frequency upon water removal. Because the individual absorption peaks represent contributions of all water molecules in the crystal structure (macroscopic), upon dehydration these shifts thus indicate the new absorption wavelengths of the remaining water molecules, which can be associated with the hydration sphere of the exchangeable cation. It is also concluded that this method cannot distinguish between a two- and three-layer state. This is due to the fact that in both cases, the larger part of the signal is caused by absorptions of water molecules outside the exchangeable cation hydration shell.

3.4 Other experimental techniques

The methods neutron scattering, nuclear magnetic resonance (NMR) and electric spin resonance spectroscopy (ESR) probe the molecular structure at timescales of the transition region between the V- and D-structure. The scale of the measurement (micro vs. macro) depends on the technique, both interlayer structure and external region data are accessible.

On the basis of NMR, it was found that depending on hydration state and charge location, the cation can be located in two different sites (Prost et al., 1998). Both situations

exist of ions close to the siloxane surface and near the mid-plane in the interlamellar space (see fig. 4).

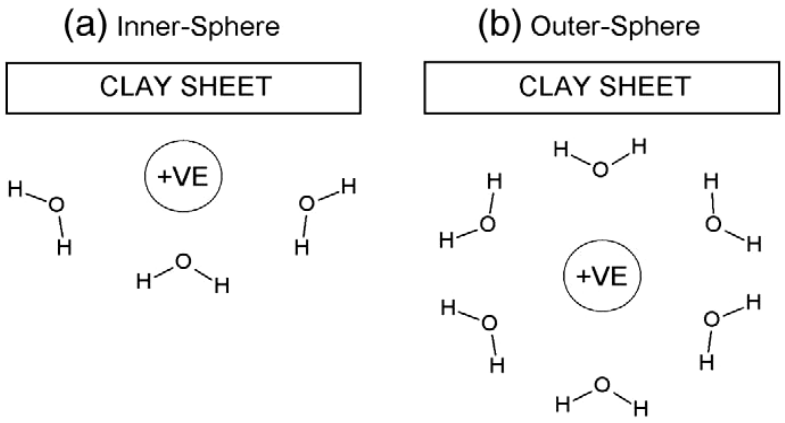

Figure 4: Schematic figure showing two possible cations coordination states in the interlayer region of smectites (*after* Anderson et al., 2010)

When the charge deficiency arises from the tetrahedral sheet, at low water content the cations are located as close as possible to the isomorphic substitutions forming *inner sphere complexes* (no water molecules occur between clay surface and cation). This involves movement of the ions into ditrigonal cavities of the siloxane surface. On the external surface, it was inferred that water is configured in pillars of hydrated cations instead of monolayers, at equivalent water contents (Prost et al., 1998). At higher water activity, the molecules start to hydrate the surface forming multilayers. In case of charge delocalization (without ion-substitutions of the tetrahedral sheet), the cations are be located in a plane parallel to the plane of the structure, in the mid-interlayer (Sposito and Prost, 1982). Such a configuration is referred to as an *outer sphere complex* (cations are entirely surrounded by H_2O). In this case, the external surface sorption properties will largely be governed by the availability of exchangeable cations. Upon dehydration of smectite structures, where the charge is derived from the tetrahedral sheet, Prost et al. (1998) argued that surface hydrogen bonded water is preferentially removed over cation bonded water. This theory is consistent with the idea that the first site restrains lower hydration energy than the polar attraction arising from exchangeable cations

Recently the geometry and dynamics of interlayer water was studied of homo-ionic synthetic Na-fluorohectorite using NMR spectroscopy (Tenório et al., 2008). Here, an earlier argument made concerning the structure of interlayer water at low hydration states is reinforced. We already saw for a 1-layer state there are two different sorption sites, depending on the charge location of the silicate structure. In this study, evidence is presented of water molecules occurring outside the hydration shell of the interlayer cation, both for the two- and

one-layer state. This water does not necessarily need to be associated with a surface sorption site. It can be bonded to a water molecule of the hydration shell through a proton exchange mechanism (Tenório et al., 2008). The ratio of this additional 'state' to cation hydration water still needs to be determined, but was proposed by the authors to be considerable.

To this point, the focus of the adsorbed water structure has been laid in the interlayer region. However a significant number of studies have provided experimental evidence of water sorption on external surfaces. Most of these facts come from simultaneous experiments on basal spacing and gravimetric changes along a sorption isotherm (which gives for a certain temperature the amount of water retained by the sample as a function of relative vapor pressure). For instance, Ormerod and Newman (1983) investigated this method using Ca-montmorillonite. It was suggested that a relative large amount of water is located on external surfaces. Calculations based on water sorption isotherms and XRD basal spacing measurements indicated that over a range of relative humidity, the larger part of the total water content is located outside the interlayer cation hydration sphere.

A similar conclusion was made in a study that used external area calculations and XRD experiments performed on a number of different smectites (Laird, 1999). In here, the results indicate that hydration equally occurs on external surfaces and that the amount of H_2O involved is proportional to the number of sorption sites (surface/exchangeable cation). The external sorption showed to be even more enhanced at vapor pressures that go beyond a two-layer state (typically >40% for Ca-montmorillonite, Bird, 1984), where multilayer adsorption can occur on 'free surfaces'. At even higher water activity, the amount of water retained by capillary condensation increases, filling the pore space between the clay aggregates. This idea is in qualitative agreement with recent XRD experiments of Warr and Berger (2007), who showed that relative uptake of H_2O in bentonite (impure clay of ~ 92% montmorillonite) is divided into a ~50:50 ratio, with half located in the interlayer and half on external surfaces or in pore space. The spatial distribution of this externally sorbed water at low water content is believed to be similar to a pillar structure (Prost et al., 1998). H_2O is localized around exchangeable cations and/or surface sites forming complexes (pillars) rather than mono-layers (Laird, 1999).

It is argued by Prost et al., (1998) that both hydration mechanisms on external surfaces are a function of the surface area. This study also provides experimental evidence of multilayer water absorption on external surfaces. Smectite clays contain a large amount of rather weakly bonded water located on these external sites. This concept is supported by a study of Knudsen et al., (2003). Here, using small-angle neutron scattering on synthetic Na-

fluorohectorite, it was demonstrated that water absorption occurs partially in mesopores between platelet stacks.

Currently, with evidence from remaining experimental techniques, we made clear that there exists a range of sorption sites in smectites for water molecules, both between the clay platelets and on the external surface. We argued before that the distinction, between water molecules directly bounded to exchangeable cations/surface sites and molecules derived from multilayer adsorption or capillary condensation, can be made using IR-spectroscopy dehydration experiments. This is because it probes the molecular structure at the macroscopic scale, thereby effectively 'sampling' both the interlayer and the external areas. In this section, we also denoted that different theories exist of the coordinated water structure around external sites, however it is widely accepted that the same distinction of sorption site type as to the interlayer region exists (cation vs. surface). Once hydration has completely surrounded the cations and wetted the charged surfaces of smectites, multilayer adsorption occurs on remaining free surfaces and capillary condensation fills the remaining pore space (Prost et al., 1998).

3.5 Evidence from simulation studies

Molecular simulations have proven to be a powerful instrument to gain more insight in the swelling phenomenon of smectites. Such studies on the swelling of clay minerals are hardly novel. In the early days when computer power just started to develop, a great number of publications showed up in the literature using Monte Carlo molecular dynamics (e.g., Skipper et al., 1995). The main focus of these studies is laid in the interlayer region, trying to reproduce the experimentally determined basal spacing evolution as function of hydration state. In this way, predictions can be made concerning the structure of interlayer water and the influence of various crystallographic controls. Numerous studies confirm that swelling properties are a function of the interlayer cation type and extent of isomorphic substitutions (e.g., Chang et al., 1998). This part focuses on a number of relevant results obtained from simulation work

Simulation studies support the formation of discrete hydration states, corresponding to one-, two- and three-layer hydrates, e.g., see Tambach (2005). In this work, the distinction between inner- and outer sphere complexes (made by Prost et al., 1998) is verified with simulations of Wyoming and Arizona montmorillonite. Whereas Wyoming montmorillonite shows both types of structures present for all hydration states, Arizona montmorillonite shows

only outer-sphere complexes, where the interlayer cations are located in the diffuse layer between the clay platelets. These predictions are consistent with conclusions of Sposito and Prost (1982). As Arizona montmorillonite has substitutions in the octahedral sheet only, the charge is delocalized along the surface resulting in a weaker attraction to the cation. Tambach (2005) also indicated that at low relative humidity, the water molecules are sorbed primary to interlayer cations.

The occurrence of water molecules outside the hydration shell of interlayer cations was experimentally inferred from the study of Tenório et al. (2008). Molecular simulations of montmorillonites (Li-, Na-, and K-SAz-1) have confirmed this presence. A considerable amount of molecules are positioned not directly next to the cation but sit in the diffuse layer (Tambach et al., 2006). This was shown to occur for both 1- and 2-layer hydrates. In the same work, simulation evidence is presented of the stability of a hydration state in between two layers. This 'new' state has more water molecules coordinated than the 1-layer but less than the 2-layer. Depending on the size of the interlayer cation, clay swelling is less enhanced in case of K^+ but shows higher degrees of sorption for Li^+. As naturally occurring smectites have a poly-ionic nature, this provides an explanation for the simultaneous occurrence of different hydration states at similar conditions

Molecular simulations of smectite (de)hydration are successfully in reproducing the experimentally observed basal spacing measurements. It was also confirmed that the water content of the interlayer region is comprised of the cation hydration sphere and water molecules that occur outside this sphere. Simulations were also successful in reproducing the inner- and outer-sphere complex configurations as is illustrated in fig. 4.

3.6 Stress-induced smectite dehydration – predictions from thermodynamics

The properties of smectite-water systems can be described by thermodynamics, e.g. to predict temperatures and pressures at which smectite dehydrates under typical geological conditions. While temperature effects on dehydration reactions have been investigated extensively in experiments, due to experimental limitations the effect of different pressure conditions has received less attention. We explained from the studies of Koster Van Groos and Guggenheim, (1984), Huang et al. (1994) and Wu et al. (1997) that hydrostatic pressure tends to promote the stability of hydrates at elevated temperatures. Those results showed that imposition of a confining pressure hinders the expulsion of interlayer water, requiring higher temperatures to initiate dehydration reactions. To compare with, as far as the author is aware of, no direct

experimental evidence has been published to date of dehydration resulting from differential stress conditions, i.e. when one of the principal stress magnitudes is higher than the other two. To clarify, in a pressure system with *solely* confining pressure or effective confining pressure, no differential stresses can exist. Pore fluid pressure lowers the existing confining pressure, which leads to an effective confining pressure. This effective confining pressure is still an equal-sided pressure condition ($\sigma_{11} = \sigma_{22} = \sigma_{33}$), which cannot lead to differential stresses on its own (i.e. to $\sigma_{11} > \sigma_{22} = \sigma_{33}$). For example in experiments, differential stress conditions are imposed by using uniaxial compression. In the literature, differential stress-induced smectite dehydration has been studied with thermodynamics, resulting in a number of predictions on stresses required to induce hydration state changes.

Dehydration experiments on smectites at differential pressure conditions are very rare. In a study by Fitts and Brown (1999), the effects of a normal load on the dehydration reaction of smectites at room temperature has been investigated by measuring concentration differences of chloride, under water-saturated conditions. This provides an indirect method to express the expulsion of interlayer water as having effects on saline pore fluids freshening. Beside these concentration measurements, the basal spacing evolution had been verified with *ex-situ* XRD analysis. This invoked sample movement from the load set-up to the XRD. The analysis had been carried out for SWy-1 and smectite-rich sediment (55-70 wt% smectite). In both samples, the initial hydration state corresponded to three-layer states, imposed by using saturated conditions and verified with XRD measurements of the basal spacing. The results (see fig. 4 and 5 in Fitts and Brown, 1999) showed a clear chloride concentration reduction at effective normal stress (or differential stress because the horizontal stress component is zero) of ~1.35MPa and ~1.70MPa, for the sediments and SWy-1 resp. The authors concluded that water expulsion, resulting from dehydration of the three-layer state into a two-layer state, would have caused the pore-fluid freshening. In particular for SWy-1 (fig. 3b. in Fitts and Brown, 1999), the according results are in agreement with dehydration of the three-layer (18.1Å) to a two-layer (15.4Å) state. However because the XRD analyses were performed within 10-15min subsequent to load removal, it remains unclear if a direct effect is seen here of normal stress induced dehydration. Despite the uncertainty, we believe that this study has provided indirect experimental data that smectites can dehydrate from a three-layer to a two-layer state at low differential stresses (~1.50MPA).

Bird (1984) investigated the effects of what is mentioned in this work as ‘effective confining pressure’ on the hydration states of homo-ionic Na-SWy-1 and Ca-SAz-1. By describing the swelling of montmorillonite as a series of hydration phase changes, the

generalized Clapeyron law was used to predict the stability of these states. Although the author referred to his applied pressure condition as being an 'effective confining pressure', the calculations correspond to the stability of hydrates at differential pressure conditions. The results of Bird (1984) are included in fig. 5, where P_s has to be read as the effective normal stress exerted on the clay platelets. This effective normal stress represents a differential stress because the horizontal stress component is assumed to be negligible (eq. 2 on page 245 in Bird, 1984).

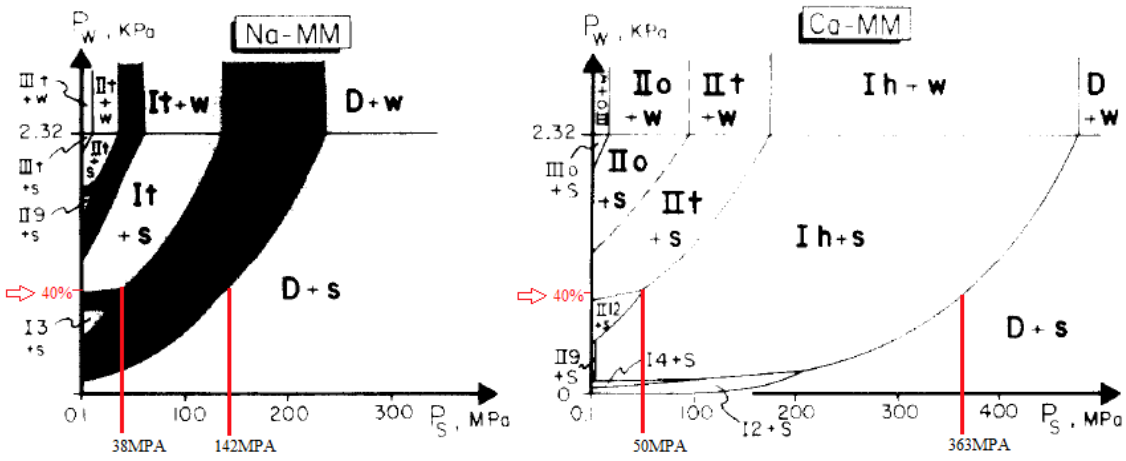

Figure 5: Hydration phase diagrams for homo-ionic Na-SWy-1 and Ca-SAz-1 at T=20°C, as a function of normal effective stress (or differential stress because normal stress in the other direction is taken as zero) P_s, and relative vapor pressure Pw. The shaded regions indicate the stability of mixed-phases. At P_w = 2.32KPa, the saturation point is reached which indicates the point of 100% relative humidity. The average vapor pressure in our laboratory is indicated with a red arrow (~40%). For additional terms and symbol definitions, see Bird (1984). *Modified* after Bird (1984).

The diagrams of fig. 5 can now be analyzed. At room temperature and 40% relative humidity (our laboratory conditions), for Na-SWy-1 the transition zone from a 1-layer hydrate to dehydrated conditions would start at an effective normal stress of 38MPa and is completed at 142MPa. For Ca-SAz-1, to go from 2- to 1-layer requires at least 50MPa effective normal stress and the last water layer is removed at stresses around 363MPa. The predictions show that at higher (initial) relative humidity, more effective normal stress is needed to remove interlayer water. It also shows that the hydration energy of calcium ions is larger than for sodium, while it requires less work to dehydrate Na-SWy-1. The calculations of Bird (1984) suggest furthermore that effective normal stresses of <5MPa are needed for both samples to expel the three-layer state out of the clay structure.

A similar type of calculation was performed by Colten-Bradley (1987), trying to assess the influence of different pressure conditions on the dehydration reactions of smectite

at room temperature. The increasing stability of the reactions at elevated (effective) confining pressure was successfully predicted and agrees with the experiments of Koster Van Groos and Guggenheim (1984), Huang et al. (1994) and Wu et al. (1997). On the other hand, differential pressure conditions show an opposite relation (see fig. 7 Colten-Bradley, 1987). In general, the results show that the differential stresses required are slightly higher than the calculations of Bird (1984). According to Colten-Bradley (1987), Na-smectite (unknown structural type) would dehydrate respectively at 60, 100 and 500MPa, for going from an initial three-layer state to a full dehydrated state (for an interlayer water density of $1.04 gcm^{-3}$). The results are strongly depending on interlayer water density, if $\rho_{interlayer}$ is slightly higher around $1.15 gcm^{-3}$, then these calculations are more in agreement with fig. 5. In that case, to go from the three-layer state to a two-layer state requires a differential stress of ~16MPa. Evidence for realistic values of interlayer water density is restrained by current available thermodynamic data. Depending on hydration state and total charge in the clay structure, the density is found to be greater than $1.0 g/cm^3$ (Colten-Bradley, 1987) if the basal spacing corresponds to a three-layer state or less. These predictions are in agreement with conclusions of Huang et al. (1994). However, more work has to be done in order to constrain the boundaries of this parameter in a systematic way

It was experimentally confirmed that solely the effect of an imposed (effective) confining pressure raises the temperatures of dehydration reactions (e.g., Huang et al., 1994), thus increasing the stability of interlayer water. So far, no direct evidence exists of analogous experiments based on differential stress-induced smectite dehydration. In this section, we mentioned some order of magnitudes of differential stress-induced smectite dehydration at room conditions, derived from thermodynamic calculations. From the predictions it appears that the third water layer is easily removed, requiring only a few MPa differential stress (Fitts and Brown, 1999; Colten-Bradley, 1987; Bird, 1984). The second water layer needs conditions in the order of 38-60 MPa differential stress to dehydrate (Bird, 1984; Colten-Bradley, 1987). The remaining water layer would be removed at very high differential stresses in order of 142-500 MPa (Bird, 1984; Colten-Bradley, 1987). We note at this stage that the presented overview is only indicative of what magnitude orders are to be expected. This is because numerous factors (crystallographic and environmental) will influence the exact differential stress magnitudes needed for each single smectite structure.

3.7 Sorption site overview

Until now we have seen that the separate contributions of layer charge, distribution and type of counter-ion all have influence on the hydration properties of smectites. The mutual effects of crystallography and environment determine the extent of smectite swelling and surface wetting. Based on the content of this chapter, in figure 6 an overview is shown of what experimental and simulation work has found for the water molecule configurations, with respect to possible sorption sites and definitions of adsorbed molecules. Note that this structure is pure hypothetical. Note also that the coordination states of the sorption sites are only schematically. Effects of the second hydration mechanism (capillary condensation) are *not* shown here. This mechanism fills the remaining pore space at sufficient water activity.

The top T-O-T complex contains tetrahedral substitutions and may contain octahedral substitutions as well. Clearly a distinction is made between two possible surface sorption sites as the charge deficiency is localized; some water molecules are hydrogen bonded directly to the siloxane surface, others are attracted to interlayer cations that are located in hexagonal holes of the outer sheet. Both these sites occur also on the external surface, giving rise to water adsorption in monolayers. It was explained that in this configuration, outer sphere complexes can be formed in the interlayer, resulting in higher coordination states of the interlayer cation. On the external surface, water molecules are attracted in equal way as in the interlayer region, with respect to surface sites. The according structure can either be the formation of monolayers or pillar structures. An osmotic pressure sets up between the surface and the pores holding the molecules in the same position when hydrating the ions. Multilayer adsorption occurs on resulting ‘free surfaces’ where the layers are held together by double-layer forces and relative weak van der Waals attractions.

In the lower T-O-T complex, only the octahedral sites have to be charge compensated which results in an internal/external surface that has more a hydrophobic character. The charge deficiency is delocalized along the surface allowing no hydrogen bonds to be made. The hydrophilic nature almost completely arises from the hydration properties of exchangeable cations, giving rise to the formation of outer sphere complexes in the interlayers. On the external surface, the ions are hydrated and configured mainly in pillar structures, neutralizing the charge. Multilayer adsorption occurs again on ‘free surfaces’ and in pore space.

In the interlayer region, water molecules outside the hydration sphere of the cations exist (indicated by ‘outer cation hydration water’ in figure 6). This water is weakly attracted

to the clay platelets and to other H_2O molecules from the direct hydration sphere. In the experimental section, no clear distinction was found between the physical characteristics of these molecules in relation to H_2O that is attracted by double-layer forces on 'free surfaces'. Also, the properties of the third water layer state are believed to be in agreement with this description, as it is rather easily being removed upon dehydration. The second layer state requires more work upon removal, this is where the ions commence to show more influence. Although a distinction is made between the cation inner- and outer sphere, with respect to structure, no particular evidence was found for a difference in sorption strength.

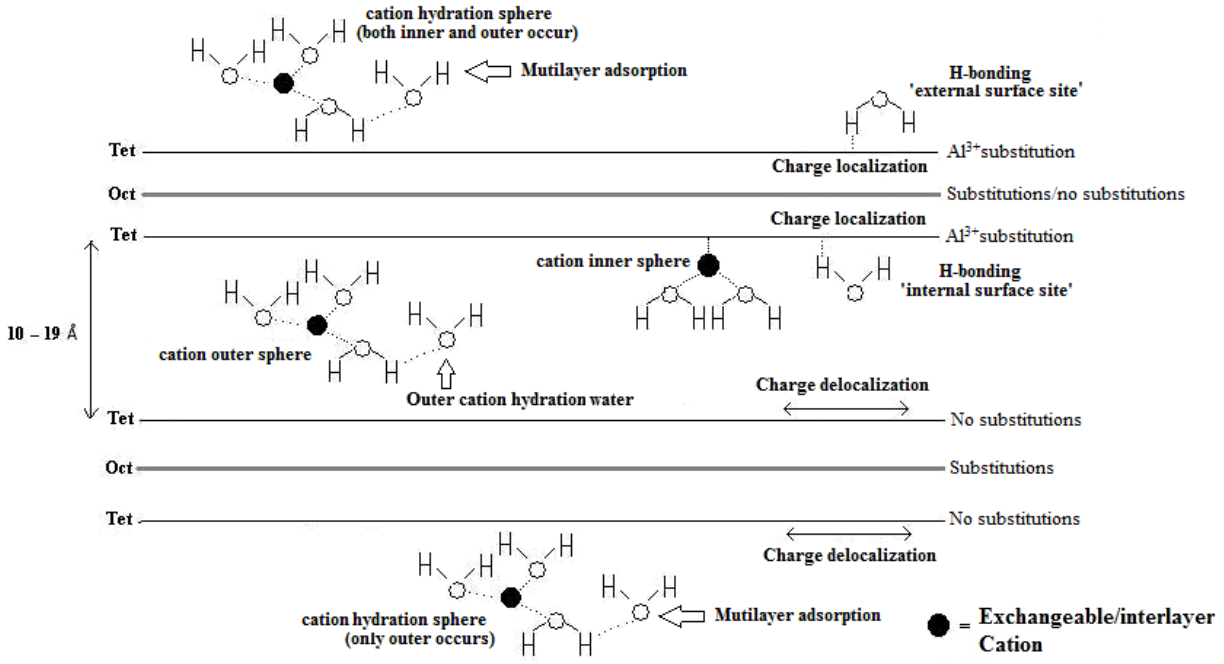

Figure 6: Sorption site model for two different smectites structures. Strictly, there is a distinction between the terminologies of both cations (exchangeable vs. interlayer), but this is constrained by location and not by differences in physical state; in the interlayer region, interlayer cations occur while on external surfaces, they are generally referred to as exchangeable cations.

4. Experimental materials and methods

In this work, *in-situ* temperature- and normal stress-induced dehydration experiments were carried out on montmorillonites (naturally occurring and synthetic) using TGA and FTIR-spectroscopy. In addition, FTIR-spectroscopy experiments were performed on non-swelling clay minerals and quartz. An overview of the different experiments performed and the materials used is presented in table 4.

Material	*Experiment(s)*
Ca-SAz-1 (naturally occurring montmorillonite)	1. TGA 2. Temperature- (using EIR cell) and normal stress- (using HPIR app.) induced dehydration (both with FTIR-spectroscopy on a SSF of clay) + FTIR-spectroscopy (KBr-method)
Na-SWy-1 (naturally occurring montmorillonite)	1. TGA 2. Temperature- (using EIR cell) and normal stress- (using HPIR app.) induced dehydration (both with FTIR-spectroscopy on a SSF of clay) + FTIR-spectroscopy (KBr-method)
K-10 (synthetic montmorillonite)	TGA
Muscovite	FTIR-spectroscopy (KBr-method)
Kaolinite	FTIR-spectroscopy (KBr-method)
Pyrophyllite	FTIR-spectroscopy (KBr-method)
Quartz	FTIR-spectroscopy (KBr-method)

Table 4: Materials used and experiments performed in this study. The material properties are described in detail in section 4.1. The experimental techniques are explained in sections 4.2 and 4.3. The two optical cells (EIR and HPIR app) are described in detail in 4.4 and 4.5 resp. SSF refers to a Self-Supporting-Film, which can be found in section 4.6.

The aim of the normal stress-induced dehydration experiments is to constrain the differential stresses needed for the removal of interlayer water. The TGA analyses and temperature-induced dehydration experiments serve as benchmark studies to define the specific dehydration signal in terms of infrared spectroscopy absorptions of water molecules. Once this dehydration 'pattern' is recognized with temperature-induced infrared spectroscopy, the

results are compared with the spectrograms of normal stress-induced dehydration, to determine changes of the hydration state upon applying a normal stress. Additional FTIR spectroscopy experiments on non-swelling clay minerals are performed to verify the nature of adsorbed water molecules in these particular materials.

4.1 Materials

Two of the studied smectite samples are the naturally occurring Ca-SAz-1 (Arizona) and Na-SWy-1 (Wyoming) montmorillonites, obtained from the Source Clays Repository of The Clay Minerals Society (extensively characterized by van Olphen and Fripiat, 1979). According to the data of Olphen and Fripiat (1979), the interlayer cation of Arizona montmorillonite is predominately calcium, only negligible amounts of potassium and sodium ions have been detected too. Wyoming montmorillonite is largely charge balanced by sodium, however herein a significant quantity of calcium ions has also been found. SAz-1 is a high charge montmorillonite (CEC=120cmol$_c$ kg^{-1}), with solid substitutions occurring solely in the tetrahedral sheet. SWy-1 is a low charge montmorillonite (CEC=80cmol$_c$ kg^{-1}) with substitutions in both the tetra- and octahedral sheet. According to Bird (1984) and Sato et al., (1992), at the vapor pressure of the steady initial stage used in this study (40±5%), the hydration states of Ca-SAz-1and Na-SWy-1 correspond to a 2 and 1-layer state respectively. The remaining studied smectite sample was synthetic K-10 montmorillonite, commercially obtained from Sigma-Aldrich Co. The specifications of K-10 show that it has a very low charge (CEC=30 cmol$_c$ kg^{-1}). No additional information was provided regarding the charge distribution among the sheets. A SEM analysis was carried out to determine the nature of the interlayer cation. It was found that the material is rather inhomogeneous and contains a mixture of K^+/Na^+/Ca^{2+} and Fe^{2+} ions, the first two being the most occurring. Pure muscovite was obtained from Aspanger Bergbau und Mineralwerke GmbH & Co. The mineral has a 2:1 crystal structure, but does not have the ability to swell while the interlayer charge is too high (-1.0*e* per unit cell). Pure kaolinite was obtained from Sigma-Aldrich Co.; this clay mineral has a relatively perfect 1:1 structure with hardly any solid substitutions (Meunier, 2005). The low CEC nature of kaolinite is believed to arise solely from protonation of the surface hydroxyl groups, in contact with an aqueous solution (Ma and Eggleton, 1999). Pyrophyllite was obtained from Robbins, North Carolina (API Sample H-49) and has a perfect 2:1 crystal structure. No clay swelling is observed due to the lack of an interlayer charge. Pure quartz was obtained from Fluka Chemika. In this work, we did not remove the impurities by cation

exchange procedures to make a complete homo-ionic clay structure. All materials were used as received in powder form, without any mechanical treatment such as size fractionation prior to testing.

4.2 TGA

Thermogravimetric analysis was performed using a V5.1A DuPont 2000 instrument. All samples were stored at room conditions (T=22°C/Φ=40%) prior to taking each measurement, no purge was used. The first set of experiments was conducted on the naturally occurring SAz-1, SWy-1 and synthetic montmorillonite K-10 over the range 20°C to 1000°C, using a heating rate of 5°C/min. The loosely packed powder samples had a slightly variable size (from 20.6 to 24.1mg) and were placed in a small Al basket in the apparatus. A programmable controller in the analyzer automatically lowered the heating rate at stages of pronounced weight-loss. To verify the character and position of peaks, a set of duplicate experiments was performed at a constant heating rate of 0.4°C/min up to 200°C. This temperature was observed as the highest temperature of interest in the dehydration region. The sample size was doubled in the duplicate set to ~42mg, which significantly improved the quality of the signal. The second set of experiments was performed solely on SAz-1 and SWy-1. K-10 montmorillonite was excluded because it only showed an 'expected' trend during the first run. The according results did not need further refinement. All collected data of both sets was analyzed using a spreadsheet program and the TGA signals were fit to a moving average trendline.

4.3 Fourier Transform Infrared (FTIR) spectroscopy

In this study, thermal- and normal stress-induced dehydration experiments were performed using a Jasco infrared (Jasco IRT-30 microscope + Fourier Transform-IR470) spectrometer, with a signal- to-noise ratio of 5000:1 and a mercury cadmium telluride (MCT) detector. Our method is based on the fact that water molecule band positions can shift upon dehydration and/or decrease in absorbance intensity. Note that only a qualitative analysis can be performed as no accurate information is available on clay film thickness, which is explained in section 4.6. In all runs a resolution of 2 cm^{-1} was handled and the microscope aperture size had been set to 625 x 625µm, unless otherwise stated. Each measurement was signal averaged with several scans for noise reduction. The number of scans varied between the different types

of experiments and is specified in the according sections. Single beam background spectra of a clean calcium fluoride window were taken prior to each run. All lenses were washed with ethanol and water after each run. Spectrograms were analyzed using Spectra Analysis software from Jasco for windows 95/NT. All data was processed with a means movement fitting function, no baseline correction was handled. On occasion, due to changes of the atmosphere in the lab, it was required to intensify the level of data processing and curve smoothing. The technical set-up of each experiment will be described in the following sections.

In addition to infrared micro-spectroscopy, the KBr pressed disc technique was used to visualize the band positions of possible adsorbed water molecules on the external crystal areas of muscovite, pyrophyllite, kaolinite and quartz. Also, the water band positions of Wyoming and Arizona montmorillonite were studied at room conditions with this method. Pellets were made using 0.5 to 1 mg sample, grinded into a matrix of 500mg KBr and compressed into a disc. Infrared spectra were obtained using a Jasco FTIR470 instrument (TGS detector, ceramic IR source and KBr beam splitter). The resolutions of the spectra are 4.0cm^{-1} and 50 scans are signal averaged. A blank spectrum of pure KBr was measured prior to the analysis of each pellet.

4.4 Environmental Infrared (EIR) cell

Temperature-induced dehydration experiments on Na-SWy-1 and Ca-SAz-1 have been carried out *in-situ* using an environmental infrared (EIR) cell (see table 4), originally designed for solubility measurements of CO_2 (Kramers, 2006). The EIR cell is shown in figure 7 and allows FTIR transmission spectra of material in powder form to be collected directly at elevated temperatures or different relative humidity. The steel cell contains two calcium fluoride lenses (ø=5mm/width=5mm), glued into steel mushroom shaped holders, which are placed on top of each other. The volume of the chamber between the lenses is estimated to be $1.96x10^{-5}cm^3$. To create a controlled environment, the chamber where the SSF of clay (see section 4.6) was applied is sealed with Viton O-rings. The total light pathlength in the cell is 1cm. In order to avoid energy scattering of the incident beam, the shape of the screw cap and celleron cover is adjusted to coincide with the incidence angle of infrared light.

Temperature-induced dehydration experiments have been performed up to temperatures of 180°C. A SSF of clay was applied to one of the calcium fluoride windows by the method as described in section 4.6. X-ray analyses of comparable heating experiments on

montmorillonite and other clays up to temperatures of 180°C showed that the according crystal structures are not affected by mineral transformations upon heating (Morrow et al., 2000). The initial conditions in the sample chamber are assumed to be equal to room conditions (Φ=40% and 1 bar atmospheric pressure). The number of averaged scans for each measurement was kept constant at a hundred times. Temperature inside the cell was regulated with a precision of 1°C by two metal heater-bars (see fig. 7), which are connected to a DIN Autotune PID temperature controller – CAL990. The thermocouple was positioned in close vicinity of the sample chamber.

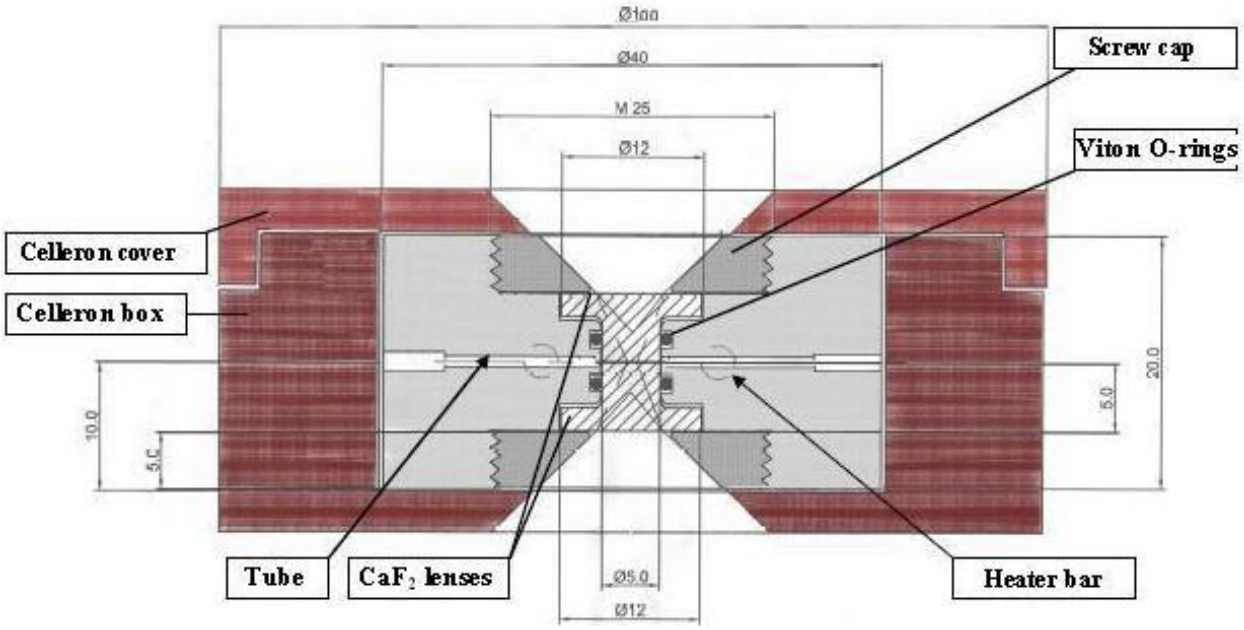

Figure 7: Schematic drawing of the EIR cell used for *in-situ* FTIR temperature-induced dehydration experiments, indicated dimensions all are given in mm. The CaF_2 lenses were exchangeable and the celleron cover as showed here was applied during experimentation at elevated temperatures to protect the spectrometer from heat. The location of the heater bars is indicated in the figure. A thermocouple was placed adjacent to the sample chamber passing through a small tunnel (not shown). The cover can be removed in case of vapor pressure-induced dehydration experiments; in that case one of the tubes is connected to a flowing-gas manifold. The set-up was mounted on an adjustable stage under the spectrometer. (*Modified* after Kramer, 2006).

4.5 High-Pressure Infrared (HPIR) apparatus

Normal stress-induced dehydration experiments on natural montmorillonites (see table 4) have been performed with a specially designed high-pressure infrared apparatus (fig. 8). The HPIR app. allows FTIR transmission spectra of material to be collected that is directly subjected to a uniaxial load (or differential stress as the horizontal stress component is zero). The application of a spring (paper binder clip) as indicated in the figure exerts a force on the edge of the steel limbs which is multiplied with factor four at the sample location (the anvil lens). This holds while the moment sum at the hinge is zero. In theory, the force can be

regarded as a point load to where it is being applied (at point A in fig. 8). However it cannot be excluded that this spring type affects the load support position to be slightly offset. This could lead to imbalanced loading at the contact. We found that the effect is limited and occurs on a small scale. Interlimb spacings at both ends, at various states of normal stress, varied just about a few tens of micrometers. It is therefore assumed here that the SSF of clay was symmetrically loaded at all times.

To quantify the magnitude of the force at the contact point (the sapphire anvil lens), all springs had been pre-calibrated by applying an equal amount of weight on one of the steel grips until the opening displayed a gap of exactly 12.5 mm. This distance was measured in the unloaded state and is equal to the thickness of the total set-up including a clay film applied on the lower CaF_2 crystal (see fig. 8). Note that this method, by which the exerted force was measured, is subjected to a number of uncertainties. Duplicate calibration experiments show that the amount of weight needed varies by as much as 10% for each single spring. In part this is explained by imprecision of measuring the gap distance, but also by the extent of spring nonlinearity. As a result of these problems, an error bar of 15% is included in the quantification of the normal stress at the contact point. The hinge is spot welded and did not show any displacement or twisting, even at the highest stresses.

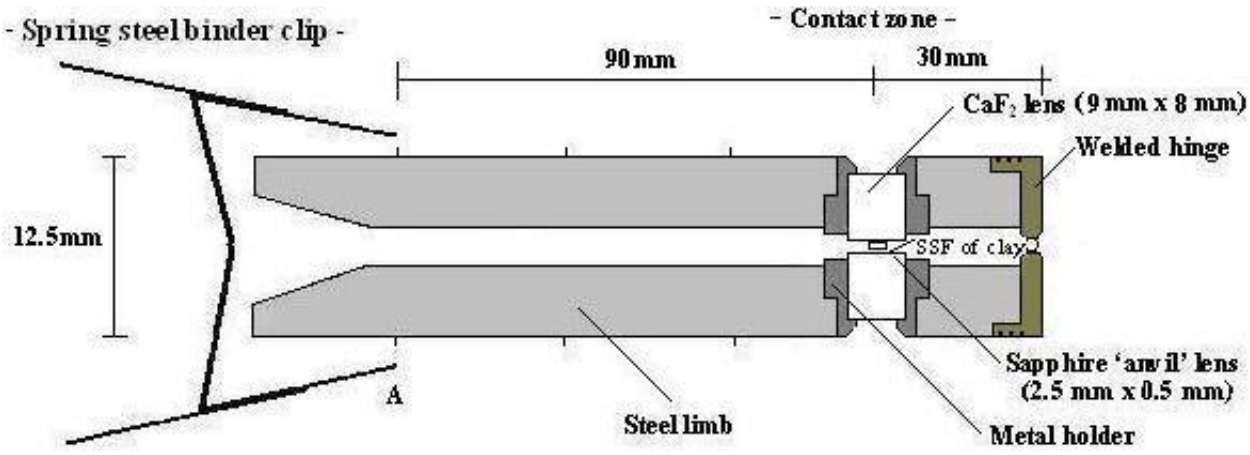

Figure 8: Schematic drawing of the designed HPIR app. used for in-situ FTIR normal stress-induced dehydration experiments. Note that given dimensions are not to scale. In order to avoid energy scattering of the incident beam, the shape of metal holder was adjusted to fit with the incidence angle of infrared light. The metal holders are exchangeable, allowing the placement of a SSF on one of the faces (see section 4.6). In the unloaded state, the interlimb space is measured at 12.5mm and the force ratio between A and the contact zone is 4:1.This set-up was mounted on an adjustable stage under the spectrometer.

The CaF_2 lenses are mounted into steel mushroom shaped holders to increase the strength by supporting the load partially on metal instead of glass. In this way, no more than

an opening of 4.5mm is permitted for infrared light to pass. The total pathlength through the set of lenses is 19.5mm. A smaller sapphire anvil lens is used to transmit the force, in this way the normal stress at the contact point increases significantly due to the quadratic radius dependence of stress. For the type of anvil lens, tests indicated that any other infrared transparent material at the mid-IR scale showed to be either too weak (CaF_2) or would simply dissolve with atmospheric water (halite) under a load, the latter probably also due to amounts of water that became released. For the least amount of energy scattering at the interfaces between the crystals, one would argue the use of a set-up with single CaF_2 or sapphire crystals instead of a combination. Yet this appeared to be not practical as mentioned, for the reason that a small CaF_2 lens could not endure the stress state and would simply fracture. For each spring the according normal stress at the contact zone is calculated using the formula given below.

$$\sigma_n(\text{MPa}) = \frac{4\text{mg}}{(1.25*10^{-3})^2\pi} \quad (1)$$

Here, m is the equivalent mass in kg needed to open the spring a distance of 12.5mm and g is gravitational acceleration constant ($9.81 ms^{-2}$).

Normal stress-induced dehydration experiments have been performed on Na-SWy-1 and Ca-SAz-1 up to a value of 41MPa. A SSF of clay was applied to one of the calcium fluoride windows by the method described in section 4.6. The number of averaged scans for each stress step varied between fifty and a hundred times, but was kept constant for a single run. In all runs, a relative humidity of 40% and 1 bar atmospheric pressure correspond to the initial conditions in the unloaded state. Temperature under the infrared microscope was assumed to be constant at all times, equal to room conditions (20ºC). The atmospheric vapor pressure is also assumed to have been reasonably constant throughout the experiment. This is based on the existence of a well-designed ventilation system in the laboratory. The atmosphere around the microscope is continuously flushed with a constant stream of air, keeping the vapor pressure at the same level (±5%), not taking into account influences of changing climate conditions.

4.6 Preparation of self-supporting thin clay films

In the set-up of the EIR cell (fig. 7) and the specially designed HPIR apparatus (fig. 8), a self-supporting film (SSF) of clay was prepared by applying a small amount of powder (~0.5mg) on top of a calcium fluoride window (ø=5mm/width=5mm for the EIR cell and ø=8mm/width=9mm for the HPIR apparatus), in both set-ups glued into steel holders. A second equally sized window was placed on top and both crystals were sheared manually by rotating the holders in opposite directions. Shearing continued until a self-supporting clay film of desired thickness was at hand on one of the crystal faces. This would become the bottom crystal in the set-up. Other techniques such as making clay suspensions in various solvents (see e.g., Johnston, 1992) led to film concentrations that were too high, therefore it was required to develop this new technique.

The film thickness could be controlled by varying the amount of pressure between the holders. It was found that usually the powder stuck to the window surface and acquired a flaky texture. The transmission method in FTIR requires a specific sample thickness that still allows sufficient energy to be collected by the detector. In this study, a number of handled criterions were used to make a distinction between fitting and non-fitting films (e.g., those that appeared to be too concentrated). High accuracy data were obtained by controlling the following two constraints: 1. the amount of energy that got transmitted through the specimen and 2. the intensity of according absorption bands. It was found that relatively thick films of >100µm gave spectra in which most of the bands are close to the saturation point of the detector. This causes infrared absorptions of the normal modes, from the functional group regime, which are too strong, making the spectrograms incomprehensible. Tests confirmed that thinner films of <75 µm allow the collection of infrared spectra of sufficient precision. However once found that a film appeared be of acceptable size, it was not possible to measure its exact thickness. Small variations of clay film thicknesses between the different runs existed and therefore the initial absorption intensities are not uniform. This is not a problem as no thickness variations during a single run existed, implying that here an infrared absorption change shows just the effect of concentration changes, in our case due to dehydration processes.

5. Experimental results and analyses

5.1 Thermogravimetric analysis

The results from our TGA experiments (see table 4) are shown in the figures 9 to 11. Clearly a distinction is evident between two major weight-loss events. The figures 12 and 13 present the TGA results obtained for the natural clays (Arizona and Wyoming montmorillonite) during a second run carried out at slower constant heating rate in the dehydration region. At low temperatures (<200°C), thermal dehydration takes place associated with the removal of water molecules from various sorption sites in the clay structure (e.g., Guindy et al., 1985). At higher temperatures (>400°C), all materials display weight-loss as a result of dehydroxylation reactions, involving the breakdown of structural hydroxyl groups (e.g., Schilling, 1990). The similarity between the onset of structural collapse is put in contrast with variable positions of dehydration reactions. This is a direct consequence of differences in structural parameters, affecting clay water interactions in many ways. Recall that thermal analysis describes on a macroscopic scale the removal of all water molecules present in the structure. Therefore in these experiments, the weight-loss could be attributed to dehydration of water molecules adsorbed around exchangeable cations, adsorbed to internal and external surfaces, or condensed in pore space.

Figures 9, 10 and 11 show the TGA results over a wide temperature range (20-1000°C) for Na-SWy-1, Ca-SAz-1 and synthetic K-10 montmorillonite. At first heating rates were kept "constant" over the duration of the experiment at 5°C/min. Note that once the analyzer recorded a significant weight-loss episode, the rate automatically decreased to denote the position of shoulders or peaks. This rate-adapting character is visualized by the sigmoidal shape of the blue line in figures 9 to 11. The red line records the weight-loss as a function of temperature; its derivative function is symbolized by a black line. The latter is interpreted as a signal that describes the rate of various weight-loss reactions. Figure 9 displays the according curves for Na-SWy-1. It can be clearly observed that the removal of water molecules occurs in steps. At fairly low temperatures (~40°C), the main episode of dehydration occurs, at higher temperatures (139°C) a second peak is apparent although it corresponds to a much smaller weight-loss step. The crimped shape of the derivative curve in between those extremes may be accompanied by smaller events. In particular around 100°C, the signal appears to describe an increased rate. Near 300°C, a small and wide rebound is detected, note however that the total weight-loss from temperatures exceeding 200°C to the

onset of dehydroxylation is less then ~1wt%.

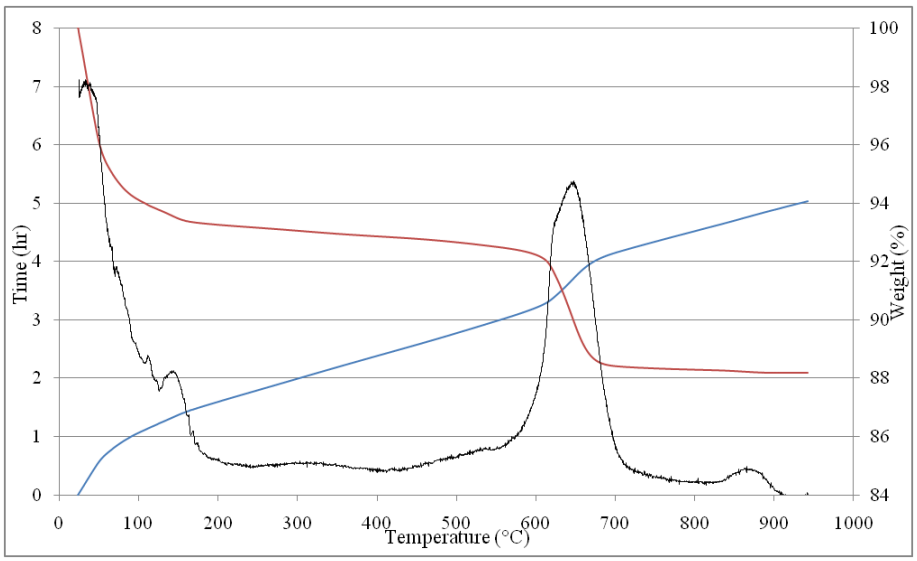

Figure 9: TGA (red line) and derivative TGA curve (black line) for montmorillonite Na-SWy-1. In the experiments, the heating rate is not exceeding 5°C/min (blue line) and was automatically lowered at stages of increased weight-loss.

Figure 10 presents the set of curves for Ca-SAz-1, again a distinction can be made between a low (<200°C) and high (>500°C) temperature interval. At low temperatures (~45°C) most of the weight-loss arises with a clear shoulder around 70°C. At higher temperatures (near 140°C), a second peak is observed that corresponds to a step of ~3wt%-loss. Note that at temperatures exceeding 200°C, no explicit weight-loss period can be distinguished. Yet until the onset of dehydroxylation at 500°C, the material still looses approximately 2wt%.

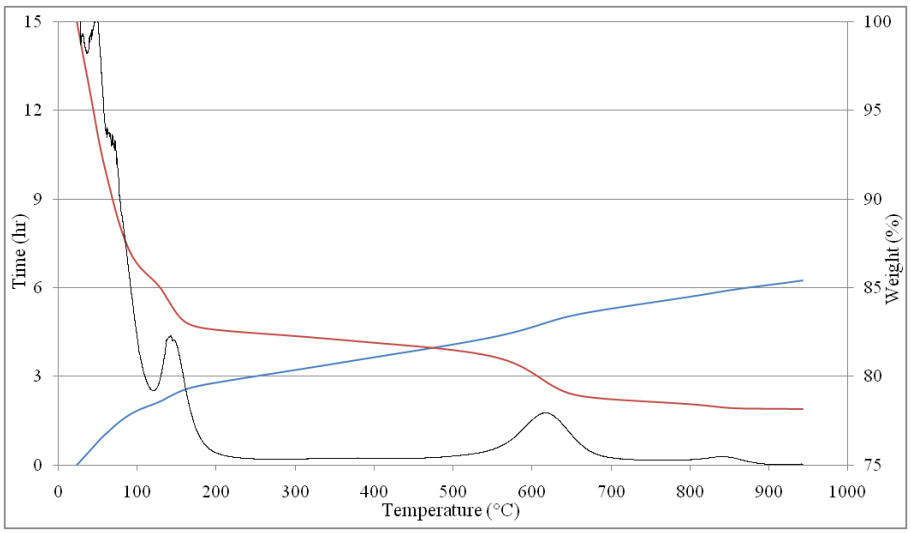

Figure 10: TGA (red line) and derivative TGA curve (black line) for montmorillonite Ca-SAz-1. In the experiments, the heating rate is not exceeding 5°C/min (blue line) and was automatically lowered at stages of increased weight-loss.

The positions of the first and second major dehydration events are practically identical for both Na-SWy-1 and Ca-SAz-1, at this particular heating rate. However in contrast to Na-SWy-1, both weight-loss steps for Ca-SAz-1 are significantly larger. This reflects higher total water content in the latter case. Both materials record, for instance near 140°C, a particular weight drop of ~1wt% and ~3wt%, respectively for Wyoming and Arizona montmorillonite. An inverse relation is seen for the dehydroxylation stage, where the according steps are 4 and 3wt%. The distribution of smaller dehydration peaks shows to be clearly dependent on the type of clay structure, reflecting the existence of different sorption site hydration energies.

Figure 11 shows the TGA results of synthetic montmorillonite K-10. It shows that the dehydroxylation phase is subdivided into two stages of which the first initiates at lower temperatures than for the natural clays. The dehydration region is initially characterized by a sharp peak at ~40°C, and then shows a relative constant rate decline up to 200°C. The absence of a second dehydration peak (near 140°C) is noteworthy. Instead the derivative curve displays an irregular form that in part is explained by unexpected movement of the sample pen. The spikes at 120°C, 130°C and the 'violent' descent between 160-180°C is explained in similar way. This is considered as noise that is not related to particular dehydration events. In contrast with the natural clays, showing a major rate decline following the first peak, the dehydration rate of K-10 remains fairly high until the material becomes more stable around 200°C.

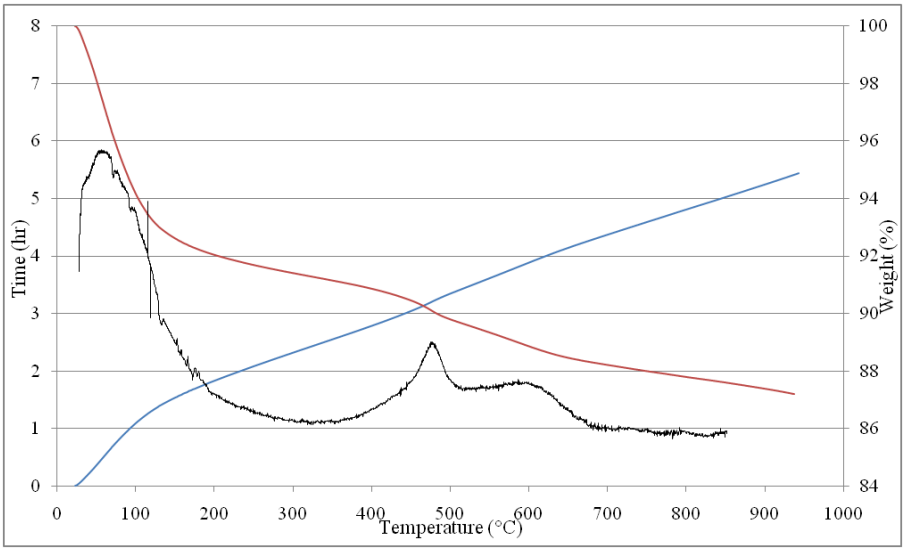

Figure 11: TGA (red line) and derivative TGA curve (black line) for synthetic montmorillonite K-10. In the experiments, the heating rate is not exceeding 5°C/min (blue line) and was automatically lowered at stages of increased weight-loss.

It is concluded from the above that the major temperature interval of interest is in the range of 20 to 200°C. To acquire more detail in this region, a set of duplicate experiments is performed at a slower constant heating rate of 0.4°C/min. Figures 12 and 13 present the results of the according analyses for the natural clays Na-SWy-1 and Ca-SAz-1. In this set of graphs, the left vertical axis displays the weight-loss rate in wt%/hr.

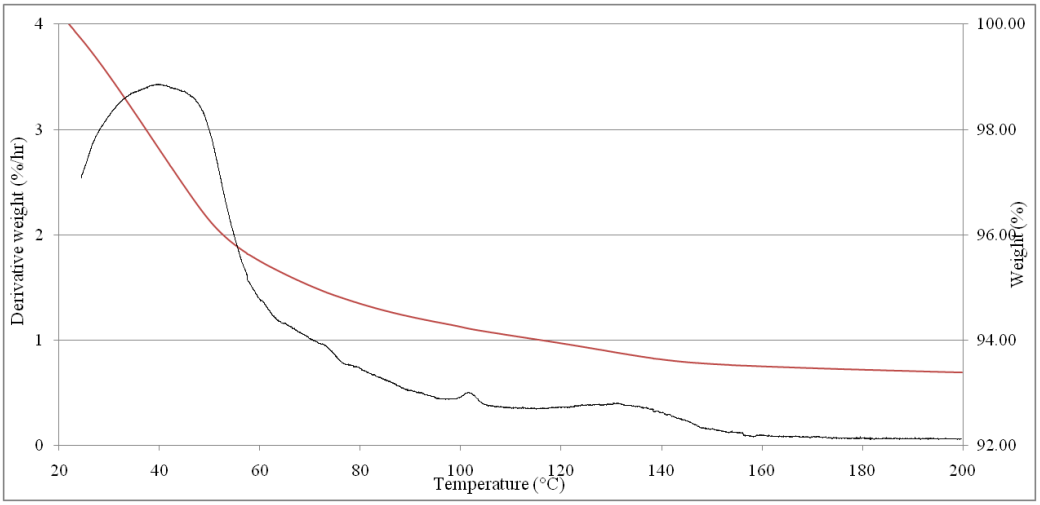

Figure 12: TGA (red line) and derivative TGA curve (black line) for montmorillonite Na-SWy-1. In this experiment, the heating rate is held constant at 0.4°C/min.

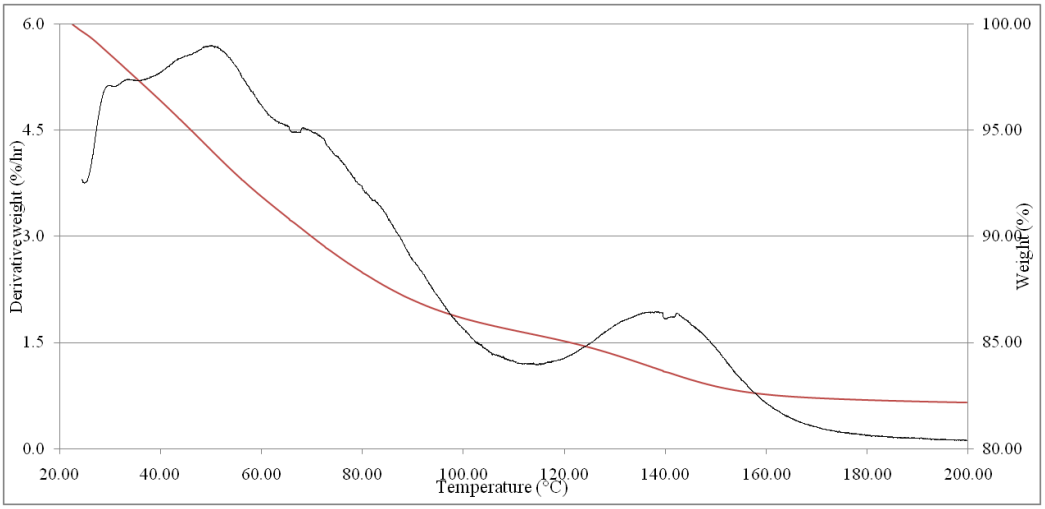

Figure 13: TGA (red line) and derivative TGA curve (black line) for montmorillonite Ca-SAz-1. In this experiment, the heating rate is held constant at 0.4°C/min.

It is found from both graphs that for this heating rate, the main observations between temperature and the two major dehydration events <200°C still persist. For Na-SWy-1 the first peak arises at 40°C and the second at 130°C, for Ca-SAz-1 these positions correspond to slightly higher temperatures of 50°C and 138°C respectively. The character of the first weight-loss step is different for both montmorillonites: Wyoming type shows a rather

symmetric parabola, whereas the peak of Arizona type is best interpreted as made of several crests. The latter shows a major broad and minor shoulder at 70°C and 82°C respectively. As observed in figure 9, a sharp peak is detected near 100°C for Wyoming montmorillonite, however the according weight-loss step is too small to quantify. In addition, the irregular decline between 60 and 80°C for Na-SWy-1 might indicate the existence of another shoulder, however this could also be related to inaccuracy in the measurement. The earlier observed total weight-loss difference in figure 11 and 12, of the two major dehydration events, is clearly displayed in the figures 13 and 14; i.e. all dehydration events of Arizona montmorillonite correspond to considerable more weight-loss.

In both sets experiments at different heating rates (figures 9 and 10 vs. 12 and 13), the removal of water molecules occurs in distinct steps. The TGA signals of the three montmorillonites studied differ mainly in the dehydration region (30-200°C), their dehydroxylation peaks show less variation. As pointed out in section 3, the dehydration peak position reflects the bond strength between the adsorbed water molecules and their sorption sites, and gives an indication on the amount of water that is released. One of the main parameters involved is the type of exchangeable cation; higher cation hydration energies correspond to higher temperatures of release. The occurrence of two major dehydration events at temperatures below 200°C is recognized in earlier TGA signals of Na and Ca-montmorillonites (e.g., Van Olphen and Fripiat, 1979; Bish and Duffy, 1990; Zabat and Van Damme, 2000, see also table 3). It is generally accepted that both dehydration peaks for Ca-montmorillonites occur at higher temperatures than for Na-montmorillonites (Guindy et al., 1985; Zabat and Van Damme, 2000), which is in agreement with the results obtained here. An explanation why this absolute difference of our results is only minor (8-10°C) could be attributed to the poly-ionic nature of the exchangeable cation in both our specimens, in particular for Wyoming montmorillonite. The inferred weight-loss difference between Na-SWy-1 and Ca-SAz-1 suggests that Arizona montmorillonite has less total water than Arizona montmorillonite, yet on the basis of layer charge one would expect an opposite trend as decreased water sorption is generally observed with high charge. This observation implies that charge location plays an additional role in the balance of attractive and repulsive forces, controlling the amount of interlayer expansion (or swelling) upon (de)hydration.

According to earlier TGA studies (e.g., Guindy et al., 1985), water molecules in the smectite clay structure can be classified into at least two types: 1. free water derived from capillary condensation that is dehydrated at ~50°C and 2. water that is adsorbed and electrostatically bound to the positively charged cations, requiring higher temperatures to be

released (>100°C). Consequently in the present experiments, the primary peak represents the dehydration of weakly bonded free water that occurs in the pore space (capillary condensation) and along neutral surfaces of grains and particles (multilayer adsorption). The secondary peak results from the removal of the more strongly bonded water. This could represent the last remaining water layer in the interlayer, in particular in the case of Wyoming montmorillonite. This is because for Na-SWy-1 in the initial stage, the hydration state consists of just one-layer (Bird, 1984; Sato et al., 1992). Arizona montmorillonite has a two- layer state at the start, of which removal of the second could explain the broad shoulder near 70ºC (see fig. 13). The last layer of Ca-SAz-1 is removed at higher temperatures exceeding 100ºC. The additional shoulders detected in the TGA signals of both samples suggest that other sorption sites also have influence on the dehydration pattern. More specifically, the structural type of montmorillonite appears to be important as well. Previous TGA research (e.g., Guindy et al., 1985) has been performed at relatively high heating rates exceeding 5°C/min, in contrast with 0.4°C/min used in this study, allowing a more comprehensive description of montmorillonite dehydration events to be made in the dehydration region. The reader is referred to section 6.1 for a detailed interpretation of our studied TGA signals.

The absence of a second dehydration peak for synthetic montmorillonite K-10 (fig. 11) is most-likely a consequence of the strong poly-ionic nature of exchangeable cations. SEM analyses show that these ions consist of K^{+}/Na^{+}/Ca^{2+} and Fe^{2+}, with both potassium and sodium being the dominant species in the framework. Since every ion has its own hydration energy, the second dehydration step corresponding to the removal of strongly bonded water, is delocalized. This argument is in agreement with the lack of major shoulders and the fact that the weight-loss rate remains relatively high after the first peak. The existence of a mixture of exchangeable cations is thus directly coupled to the fact that each cation has its own energy barrier to overcome upon releasing its adsorbed water.

5.2 Infrared spectroscopy

Temperature-induced dehydration (EIR cell)

IR spectra of Na-SWy-1 and Ca-SAz-1 were obtained *in-situ* (see table 4) under constant pressure and relative humidity, along a number of isotherms, where the dehydration process was allowed to equilibrate with temperature, thereby reaching a 'stable' state. This generally occurred fast, within several minutes, from which no further change of absorption spectra was being observed (on the minute scale). However the scope of this work is not to investigate in a systematical way the coupled time-temperature dependency of the dehydration reactions, but rather to investigate their effect on the infrared absorptions of water molecules. Both montmorillonites rehydrated to their initial hydration states within several minutes after the heating system was switched off. From section 3 it is known that the infrared spectral regions of interest are the OH-stretching region and HOH-bending region. The according absorption bands of interest are the position of the ν_1 and ν_2 normal mode wavelengths (see also section 3.3). Possible influences of dehydration on the structural OH-bending region (800-1000cm^{-1}) cannot be probed as CaF_2 is not infrared transparent at wavelengths higher than ~1000cm^{-1}.

In figure 14, spectrograms are presented in the OH-stretching (14a) and HOH-bending (14b) region of temperature-induced dehydration up to 140ºC for Ca-SAz-1. We argued from figure 13 that at this temperature, the crystal structure is about to release its last remaining interlayer water, i.e. molecules that are adsorbed to the exchangeable cation. Figure 15 shows the results of continued dehydration at higher temperatures, up to 180ºC. As a result of resolution loss on the duration of the analysis, it was necessary to apply a new clay film for the spectrograms representing dehydration from 140 to 180ºC. This is the reason why the baseline position of fig. 15 is offset. Hence, the linkage of both temperature intervals is solely coupled to the positions of absorption peaks.

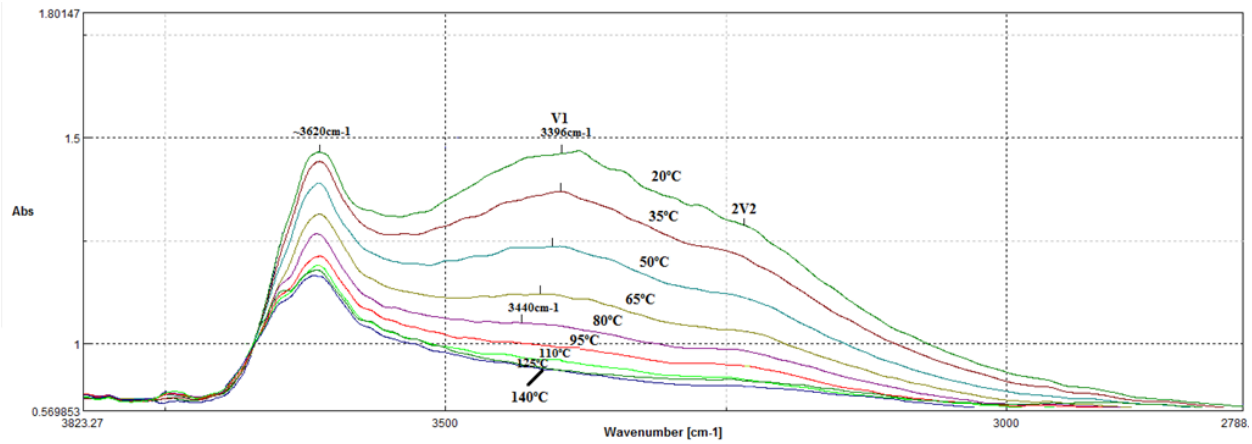

Figure 14a: Spectrograms in the OH-stretching region of Ca-SAz-1 thermal dehydration up to 140ºC. The set of curves shows discrete temperature steps of 15ºC, starting at 20ºC, where the strongest ν_1 mode absorption occurs (top green curve). The crimped shape of the 20ºC, 35ºC and 50ºC curves (i.e. the top three curves) is related to influences of atmospheric water vapor. The bottom curve is taken at 140ºC. The position of the ν_1 peak is approximated for the first three curves, from which it could be measured, until it started to disappear at the last obvious observation (80ºC curve, ν_1= 3440cm^{-1}).

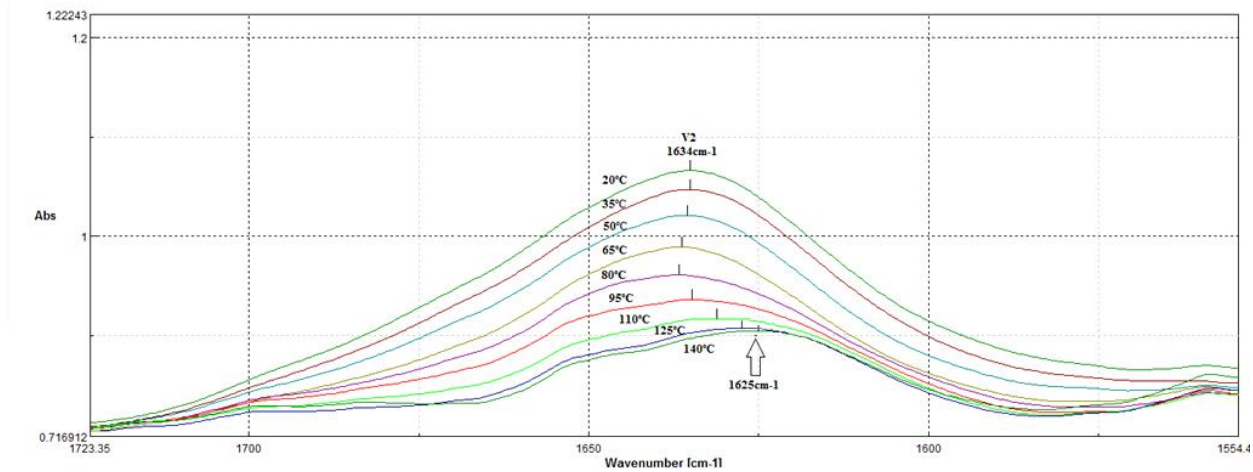

Figure 14b: Spectrograms in the HOH-bending region of Ca-SAz-1 thermal dehydration up to 140ºC. The set of curves shows discrete temperature steps of 15ºC, starting at 20ºC, where the strongest ν_2 mode absorption occurs (top green curve). The position of the ν_2 mode absorption is continuously measured at temperature steps of 15 ºC. At the highest temperature (140ºC), the peak is located at 1625cm^{-1}. The shoulder arising at ~1650cm^{-1} is regarded as noise, related to influences of atmospheric water and the result of subsequent curve smoothing.

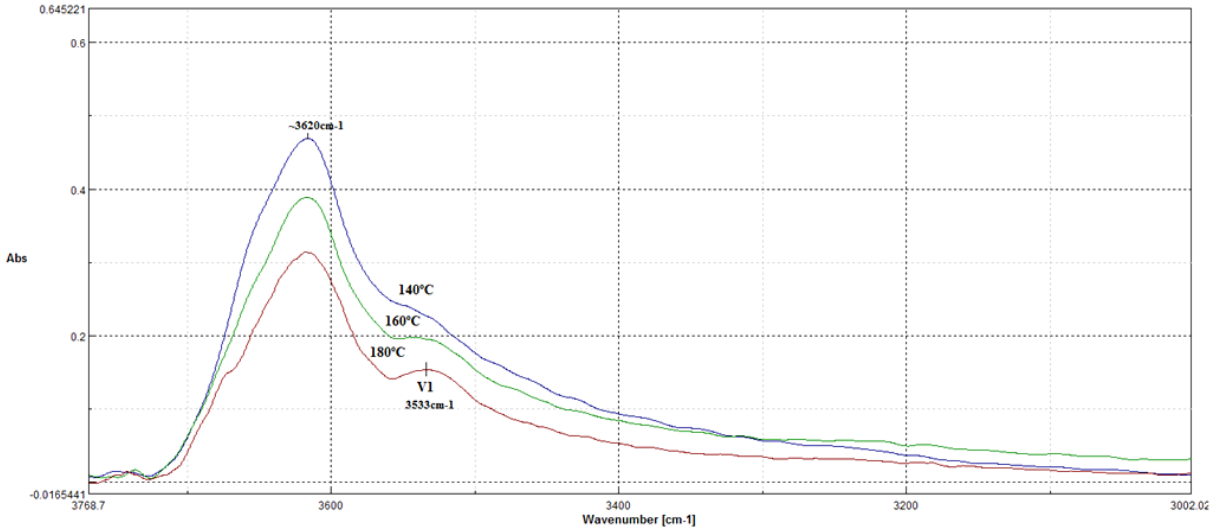

Figure 15a: Spectrograms in the OH-stretching region of Ca-SAz-1 thermal dehydration from 140ºC up to 180ºC. The set of curves shows discrete temperature steps of 20ºC, starting at 140ºC.

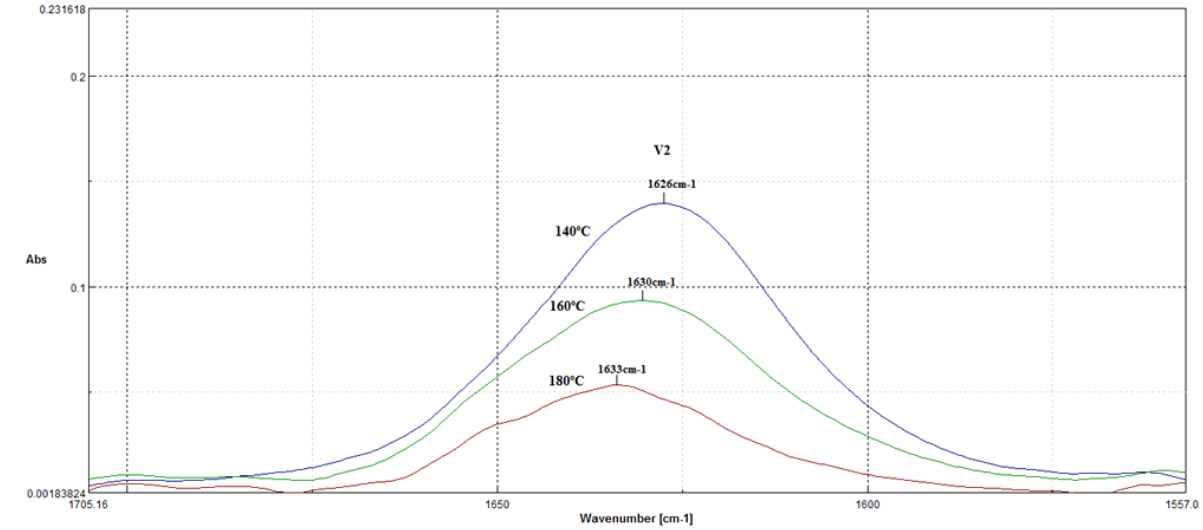

Figure 15b: Spectrograms in the HOH-bending region of Ca-SAz-1 thermal dehydration from 140ºC up to 180ºC. The set of curves shows discrete temperature steps of 20ºC, starting at 140ºC.

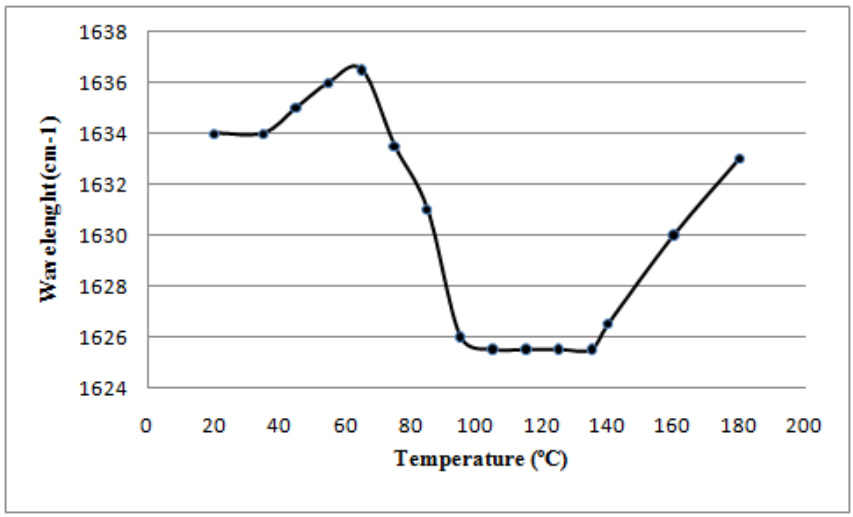

Figure 15c: Curve for Ca-SAz-1 showing the position of the ν_2 mode as a function of the entire temperature range investigated.

In figure 16a-c, spectroscopic results are presented in single figures of Na-SWy-1 temperature-induced dehydration up to 180ºC. An equal division as for Ca-SAz-1, between distinct temperature intervals, does not result in an improved understanding of the process. Relative locations of the ν_2 mode absorption peaks are plotted as a function of the full temperature range in figures 15c and 16c, respectively for Ca-SAz-1 and Na-SWy-1. It was not possible to accurately read out the ν_1 position at all times (e.g., in fig. 14a) as the band gradually gets taken up in the structural OH stretching absorption band. Also, effects of atmospheric water are evident from the crimped shape of the ν_1 peak, in particular during the first temperature steps (e.g., fig. 14a/16a). For these reasons, no detailed information is provided of the OH-stretching region beside the most obvious trends. We explained in section 3.3 that the fundamental vibrations of water molecules are affected by peak shifts and/or band intensity decrease upon dehydration (e.g., Xu et al., 2000). This is clearly supported by the spectral results obtained in this work; at lower water content the absorption characteristics change significantly.

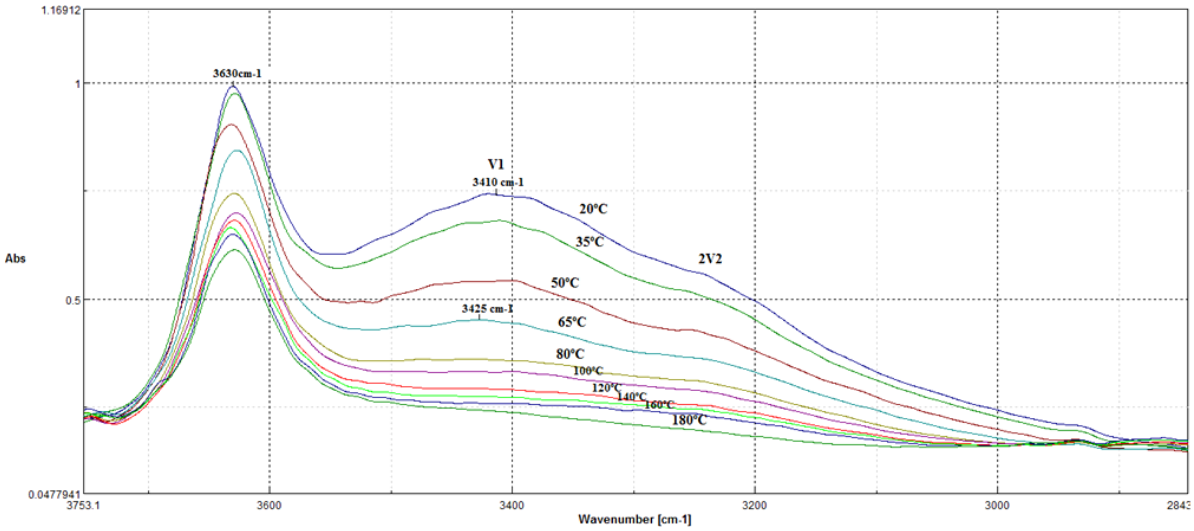

Figure 16a: Spectrograms in the OH-stretching region of Na-SWy-1 thermal dehydration starting at 20ºC to 180ºC. The set of curves shows discrete temperature steps of 15ºC or 20ºC (indicated in the figure). The crimped shape of the 20ºC, 35ºC and 50ºC curves is related to influences of atmospheric water vapor. The bottom curve is taken at 180ºC. The position of the ν_1 peak is approximated for the first curve, and showed for a temperature of 65ºC (ν_1= 3425cm^{-1}), from which it starts to become 'hidden'.

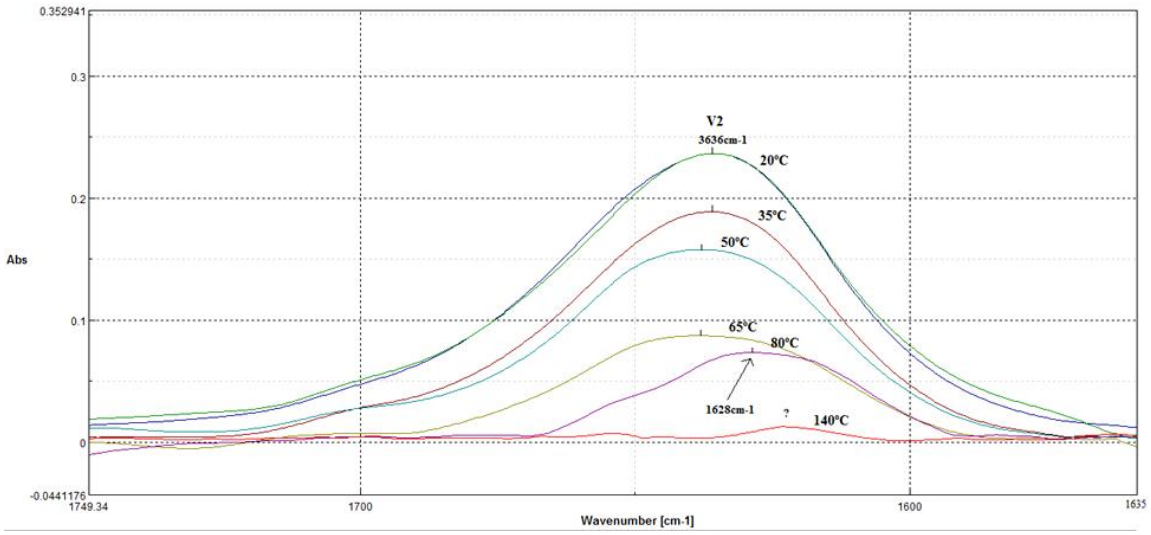

Figure 16b: Spectrograms in the HOH-bending region of Na-SWy-1 thermal dehydration starting at 20ºC to 180ºC. The set of curves shows discrete temperature steps of 15ºC or 20ºC. From 80ºC to 140ºC, the peak position remains identical and beyond 140ºC it remains uncertain whether there is still a peak detectable, or the remaining curvature is due to atmospheric water vapor.

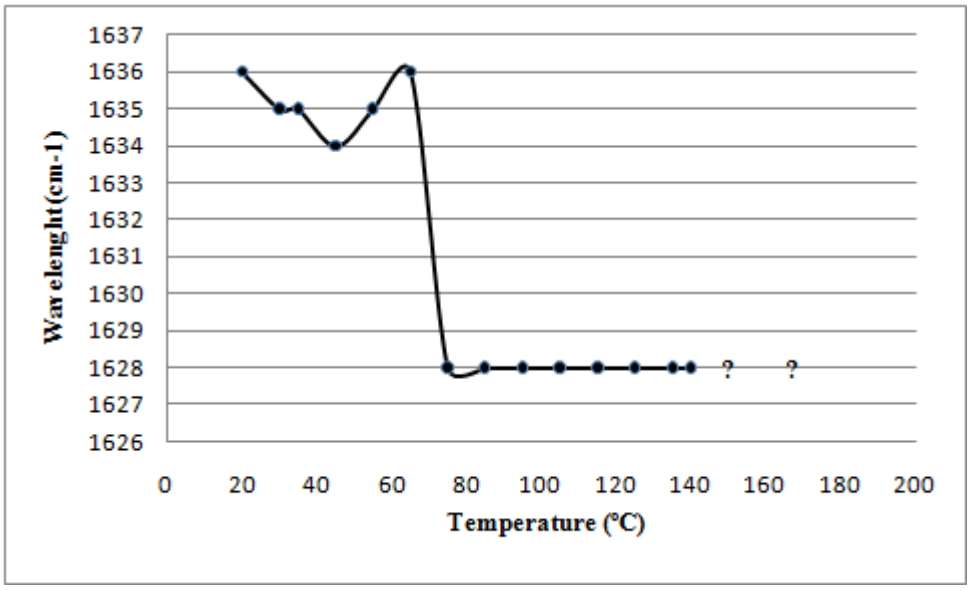

Figure 16c: Curve for Na-SWy-1 showing the position of the ν_2 mode as a function of the entire temperature range investigated. After 140ºC, the remaining ν_2 absorption band is indistinguishable.

The ν_1 position of Ca-SAz-1 shows a successive increase in frequency and decrease of absorption intensity at ongoing dehydration (fig. 14a.). The latter effect seems to be more pronounced during the first temperature steps. At temperatures exceeding ~80ºC, less impact is seen of water-loss until 140ºC is reached. Note that near 100ºC the band cannot be distinguished any longer, but is still 'hidden' underneath the sharp absorption band of structural OH groups at ~3620cm^{-1}. The ν_1 mode occurs as a broad peak, for this reason the structural band is co-affected upon dehydration by intensity reduction. Another absorption

band occurs near 3250cm^{-1}, which corresponds to the bending overtone ($2\nu_2$) of water, its position remains unchanged at higher temperatures. Beyond 140ºC, successive dehydration leads to recurrence of the ν_1 peak at 3533cm^{-1} (fig. 15a.). This gives rise to an apparent position shift of >300cm^{-1} and the remaining water molecules show a distinct OH-absorption that is still noticeable at 180ºC. The position of the ν_2 mode in the initial state is 1634cm^{-1} (fig. 15b), which is different from the value of 1643.5cm^{-1} reported for bulk water (Venyaminov et al., 1997). Dehydrating the structure results at first in a very small frequency increase, followed by a major drop until the mode is located at 1625cm^{-1}. This wavelength is reached at temperatures of ~95ºC and unaffected by ongoing heating to 140ºC (fig. 15c). In comparison, this dehydration-induced peak shift is opposite to the trend seen for the ν_1 position. Around 140ºC, the remaining water molecules still give rise to lower frequency ν_2 absorptions, although ongoing heating leads to a shift back in the opposite direction (fig. 15b). This trend is clearly shown in figure 15c.

The result of Na-SWy-1 (fig. 16a) temperature-induced dehydration shows basically the same opposite trend as was found for Ca-SAz-1. At 20 ºC the ν_1 mode occurs near ~3410cm^{-1}, while upon dehydration the absorption intensity strongly reduces and the peak position shifts to higher frequencies. Those effects are clearly displayed at low temperatures, whereas from 80ºC to 180ºC, the band seems to disappear into the structural peak of 3630cm^{-1}. The ongoing intensity reduction is less pronounced at temperatures higher than ~80ºC. In contrast to Ca-SAz-1 (fig. 15a), it remains rather unclear whether there is still water present at 180ºC. A very weak and broad absorbance region is detectable in figure 16a, but does not allow distinguishing separate bands. The ν_2 position (fig. 16b) displays an equal trend as observed earlier in figure 14b. An initial frequency increase is followed by a major drop, occurring over a relative small temperature step (~15ºC). From this stage, the position remains identical as the background noise increases. At the highest temperature it is therefore hard to conclude whether there is still water present, or if the structure can be regarded as fully dehydrated. No evidence is found for an opposite shift occurring at temperatures higher than 140ºC, which was observed for Ca-SAz-1 in figure 15c.

Both temperature-induced dehydration experiments on Na-SWy-1 and Ca-SAz-1 show that upon the removal of water molecules, the effects of hydrogen bonding are reduced. This is explained by the rising influence of exchangeable cations that give rise to relative strong ion-dipole attractions. At low temperatures (~40ºC), the most obvious absorption intensity reductions occur (fig. 14a/b, 16a/b), but no significant peak shifting is observed yet. This is consistent with the theory of condensed water removal in pore space and of neutral or free

surfaces. These molecules are weakly attracted by double-layer forces, consisting of van der Waals and London dispersion forces. Removal of those molecules results primary in less absorption signal. Slightly higher temperatures (60-70ºC) are needed to start observing a shift to higher OH-stretching and lower HOH-bending frequencies, which takes place over a relative small temperature step. These observations agree with comparable experiments performed by Johnston et al. (1992); Xu et al. (2000) and earlier suggestions of Russell and Farmer (1964). The ratio of water molecules directly associated with the cation hydration sphere increases causing a shift in absorption signal. At this stage, the position of the ν_2 mode is relatively unchanged, while the exact ν_1 position is 'hidden' (e.g., fig. 14a/16a). It appears from our experiments that the ν_2 mode frequency is a better indicator of the dehydration process, for the reasons that its position can be read-off more easily (no influence of the structural OH stretching vibration) and the fact that its peak is less affected by noise from atmospheric water. The characteristic absorption frequency of ν_2 maintains until ~140ºC is reached, from which intensity reduction increases again. Removal of this remaining water should correspond to the last layer present in both clay structures (see section 5.1). In the results, for Ca-SAz-1 an opposite shift (fig. 15b) of the ν_2 mode back to its original position is detected. The according ν_1 mode comes out again in figure 15a, but is not shifted further. Na-SWy-1 shows no clear indication of water present beyond 140ºC (fig. 16b), once the last layer is removed, the absorption signals become almost zero. An explanation for this discrepancy seen between the two smectite specimens is looked for in section 6.1.

5.3 Infrared spectroscopy

Normal stress-induced dehydration (HPIR apparatus)

Infrared spectra of montmorillonites subjected to a uniaxial load were obtained *in-situ* under constant temperature and relative humidity (see table 4). The dehydration process is allowed to equilibrate with in this case external pressure, but at present over longer timescale as one could expect the influence of diffusion involved transport mechanisms. We present here only the spectral results of experiments using the highest load. This is because it was found that the dehydration effects at lower stresses are less pronounced and basically show an equivalent trend as is seen for the figures 17 and 18. The results of dehydration effects in the OH-stretching region, at the maximum achievable value of 41(± 6) MPa, are shown in figures 17 and 18, for Ca-SAz-1 and Na-SWy-1 respectively. Compared to the temperature-induced dehydration experiments (fig. 14, 15 and 16), the existence of a slightly different vapor

pressure at the onset is the explanation for the small difference observed in initial absorption intensity, measured at room conditions.

In figure 17, the spectrogram is presented of Ca-SAz-1 showing the initial ν_1 position, which is similar to the starting position of figure 14a. At the moment the load is applied, peak intensity reduction occurs, which initially is characterized by a relatively fast rate. The second curve (green) is taken after 15min of loading time and it shows clearly intensity reduction, also the absorption band of structural OH seems to be co-affected. The red and light-blue spectrograms are collected after 2 and 8 successive hours resp. These curves show that the intensity reduction rate is decreasing with loading time. After ~8 hours, the signal changes no longer (i.e. the water bands remain at similar absorption intensity). This is confirmed by an additional time-step of 48h., showing an exact duplication of the last plotted spectrogram (after 8h.). As can be inferred from figure 17, the characteristic absorption wavelength of ν_1 is not changed due to the water removal. At the lowest absorption intensity (>8 hours), its position still remains identical to the unloaded state.

Normal stress-induced dehydration in the OH-stretching region of Wyoming montmorillonite at 41(±6) MPa is shown in figure 18. The blue spectrogram represents the initial state (ν_1~3410cm^{-1}), which agrees reasonably well with fig. 16a. The second (green) curve is taken after 15min loading time, where clearly absorption intensity reduction is shown. After ~8hours the signal remains identical which is verified by a measurement after 48h, reporting no further modifications. The ν_1 band position is unaffected by water removal, which is also observed for spectral results of the HOH-bending region, showing a constant band at 1633cm^{-1}. Peak intensity reduction rates are found to be high directly after loading and gradually slowing down at longer timescales, becoming zero after a few hours. We notice that the normal-stress induced dehydration character of both montmorillonites (Na-SWy-1 and Ca-SAz-1) does not show any major alterations.

It has to be taken into account that the precise moment of ‘zero dehydration rate’ is not investigated with great precision. Background noise causes the different signals to approach each other at longer time steps, making it difficult to detect absolute changes in absorption intensity. Duplicate runs of both materials at the same applies normal stress have replicated the proposed time-pressure dehydration relation as described, although the absolute total time step was slightly different from the first set (±1.5 hours). Yet it appears that normal stress induced-dehydration occurs considerably slower compared to what was found earlier for a thermally activated process. While taking place fast (in the order of minutes) at elevated temperatures, under a normal load it requires several hours to start observing significant

changes. Rehydration of both montmorillonites (Na-SWy-1 and Ca-SAz-1) after removal of the load occurred at the same rates as we reported earlier in section 5.2; within several minutes the signals were equivalent as in the initial state

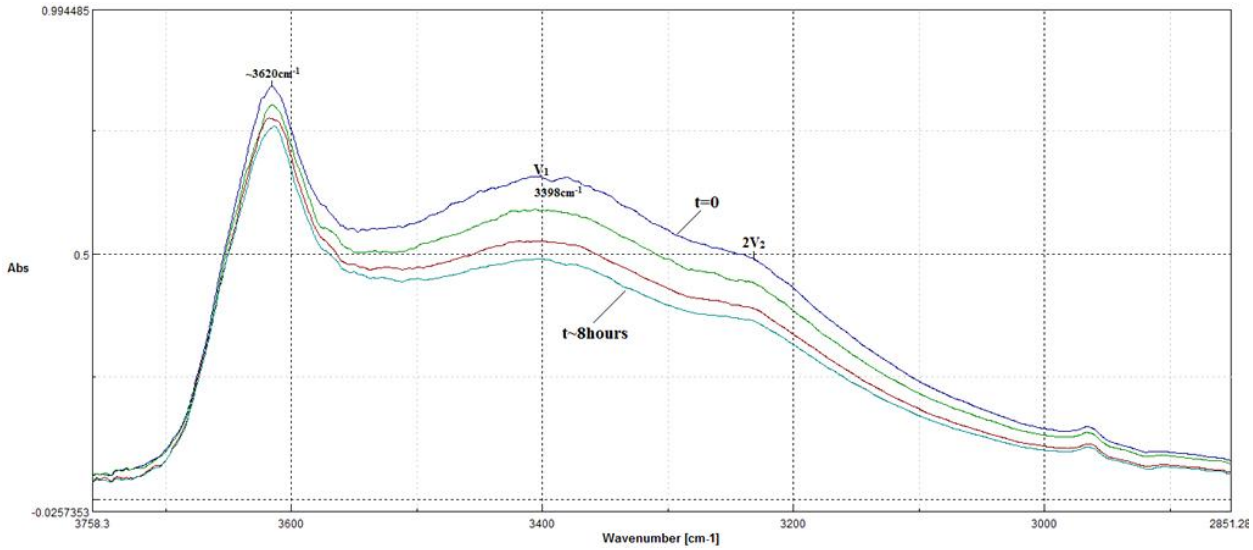

Figure 17: Spectrogram of Ca-SAz-1 normal stress-induced dehydration at 41(± 6) MPa in the OH-stretching region. The top graph corresponds to the initial state where no load is applied yet. Subsequent graphs represent the hydration state at particular time-steps of which the first is taken after 15min, the second at 2h and the third after 8h. More time steps could be showed, but this would lose the overview. After 8h., no further signal change is observed. The crimped shape of the initial state is related to influences of atmospheric water vapor.

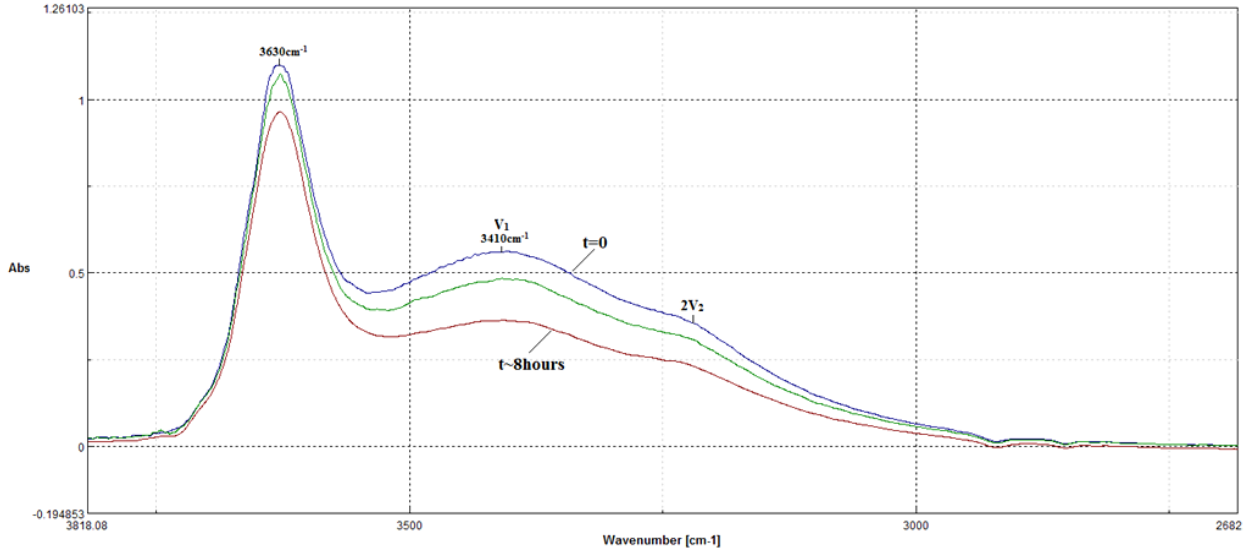

Figure 18: Spectrogram of Na-SWy-1 normal stress-induced dehydration at 41(± 6) MPa in the OH-stretching region. The top graph corresponds to the initial state where no load is applied yet. Subsequent graphs represent the hydration state at particular time-steps of which the first is taken at 15min and the second after ~8h. The last position is observed as the final state where no further signal change occurred.

5.4 Infrared spectroscopy

KBr pellets

Traditional infrared transmission methods such as KBr-pellets are still widely used for mineral identification purposes and the study of structure modifications. On the other hand making use of KBr pellets for studying smectite dehydration is not advantageous as it is widely recognized that the preparation method, which involves grinding and crushing of the samples in a KBr matrix, attracts water vapor. The matrix itself is known to be hygroscopic and it is impossible to distinguish between surface adsorbed water films caused by KBr or the sample of interest. In contrast, because the preparation process to some extent 'forces' water molecules to enter the sample, it is possible to study the ensuing infrared absorption bands as if the system would be 'water saturated' (i.e. experiments conducted at 100% relative humidity). We assume however that the KBr method is better to achieve this, primarily due to grinding and involved grainsize reduction. In other words, the KBr method allows probing water interactions with mineral structures as if the measurement was conducted at high water activity. The experiments performed in this section (see table 4) consist of making mineral fingerprints at room conditions (relative humidity = 40%/temperature=20ºC), nevertheless the according results have to be compared with fingerprint experiments performed at high relative humidity.

In figure 19, the mineral fingerprint in form of the water ν_2 absorption band is shown for a typical KBr experiment, in this case of Wyoming montmorillonite. From this example a clear shoulder at 1627cm^{-1} is detected beside the mean absorption peak at 1638cm^{-1}. We define at this point ν_{2S} that corresponds to the location of the shoulder. The according infrared absorptions from the OH-stretching region do not display a similar distinction and are therefore not included here. In table 5, the rest of the mineral fingerprint results in the HOH-bending region (ν_2 and ν_{2S} band positions) are presented for the following clay minerals: Na-SWy-1, Ca-SAz-1, muscovite, kaolinite and pyrophyllite. Also we measured a sample of pure quartz to verify its hydrophobic nature. From the experiments, it turned out to be that for most samples, an equal distinction could be made in the HOH-bending region between ν_2 and ν_{2S}. In cases where no water bending absorptions had been found, this is indicated with 'x'.

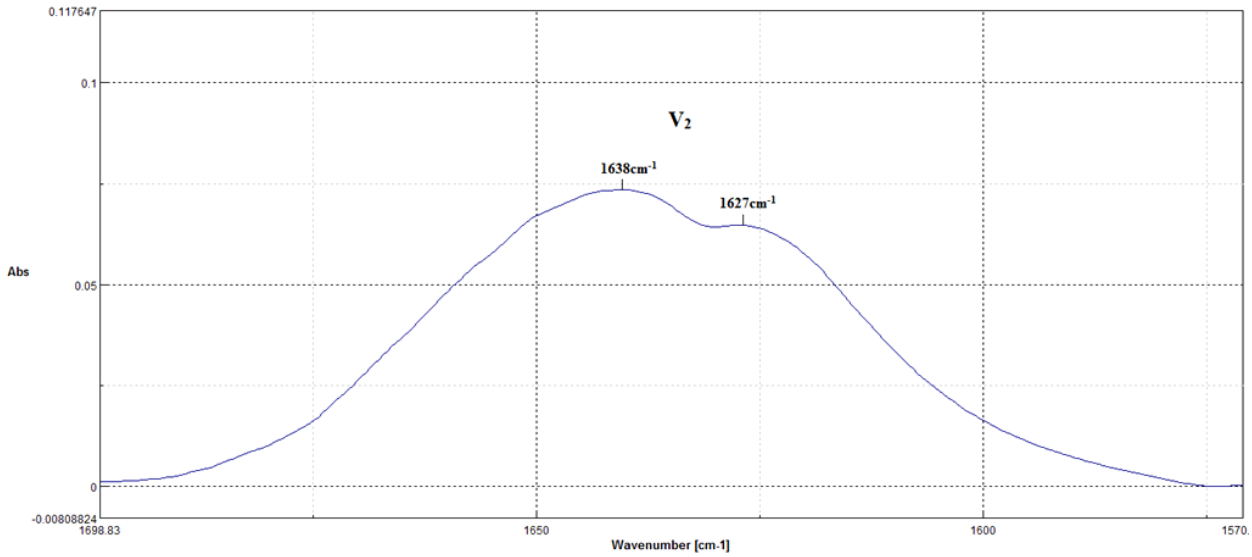

Figure 19: Spectrogram of Na-SWy-1 montmorillonite in the HOH-bending region at room conditions, analyzed with a KBr pellet. The curve displays two types of ν_2 modes, a low and high frequency type.

Clay mineral	ν_2 (cm^{-1})	ν_{2S} (cm^{-1})
Na-SWy-1	1638	1627
Ca-SAz-1	1640	1628
Muscovite	1638	1623
Kaolinite	1638	1626
Pyrophyllite	1636	x
Quartz	x	x

Table 5: Position of water absorption peaks (main peak: ν_2 and shoulder: ν_{2S}) for a number of phyllosilicates in the HOH-bending region

The spectral results of Na-SWy-1 and Ca-SAz-1 demonstrate that a distinction is made between a low and high frequency absorption band in the HOH-bending region. This division was not observed earlier (e.g. fig. 14b & 16b) and it appears that the preparation method influences the infrared absorption character. For Na-SWy-1 and Ca-SAz-1, apparent shoulders are detected on the same position where one would expect the location of water directly attracted to the exchangeable cations (e.g. in fig. 16b). In other words, compared to the temperature-induced dehydration experiments, the locations of the shoulders are in reasonable agreement with the observed peak shifts that start to occur at dehydration temperatures of 60-80º C. We argued that the absorption location of ν_{2S}, to where the shoulders belong to, represent the direct water contribution (to the total water content) of strongly bound water coordinated to exchangeable cations. We also note that the main ν_2

peaks occur at slightly higher frequencies than observed for instance in the figures 14b and 16b, approaching bulk water characteristics.

While recording a background spectrum of pure KBr, the infrared absorptions of water molecules associated with the matrix are selectively removed from the signal. Those molecules are principally attracted to the crystal surface of KBr by means of multilayer adsorption, involving double-layer attractions. We argue that the preparation method involves a mechanism of 'enhanced water layer adsorption' on surfaces of the samples. In other words, all fingerprint measurements should be taken as they were conducted at high relative humidity. This is main reason why the ν_2 band not occurs as a single peak. We demonstrated earlier in section 5.2 that the ν_1 mode shifts to higher frequencies, once remaining water is principally attracted to the exchangeable cation. However probably due to the overlap in the OH-region, caused by contributions of absorptions from structural OH, ν_1 and ν_3 modes, no comparable peak splitting is seen for this region.

The ν_2 band position of muscovite and kaolinite show an equivalent distinction between two types of water molecules occurring in the structure (table 5). Compared to smectites, the according band intensities are less pronounced, which is a direct consequence of the lack of containing interlayer water. Water adsorption happens in both cases solely on external surfaces and in pore space, which means that the total hydratable surface area is less. It appears however that for these clays, despite the absence of swelling properties, the signal still shows different types of bound water molecules. Beside the major peak (ν_2), related to porous and multilayer sorbed water, the shoulders (ν_{2S}) occur at the position where effects of hydrogen bonding are reduced.

6. Discussion

6.1 TGA signal

The peak and shoulder positions of the dehydration reactions, obtained in this study for Na-SWy-1 and Ca-SAz-1 (fig. 9 and 10), are in good agreement with provided data of Guggenheim and Koster van Groos (2001). These authors present an overview of collected TGA data on the source clays of the Clay Mineral Society. Their accumulated analyses are performed with different TG instruments and whether or not the usage of purge. Initial sample weight also varies among the different analyses, but the source clays were not pre-treated prior to testing. TGA curves of two SWy-2 samples (chemically equivalent to SWy-1) display, beside the low and high T peak, a comparable minor peak as seen in my results (fig. 12) near ~100ºC. Also, from >200ºC to the onset of dehydroxylation, the materials lose barely an additional wt%. The provided overview in Guggenheim and Koster van Groos (2001) of SAz-1 dehydration agrees also with our findings (fig. 13), regarding the position of the two major peaks. The shoulder arising ~70ºC is less apparent from their curve, but is still included in the according table (see table 2 in Guggenheim and Koster van Groos, 2001).

We can now evaluate these results to those obtained from other experimental work (e.g., Koster van Groos and Guggenheim, 1984; Guindy et al., 1985; Bish and Duffy, 1990; Schilling, 1990; Zabat and Van Damme, 2000), of which the results are summarized in table 3. A direct comparison however can be difficult as in most cases, all samples had been pre-treated prior to heating (e.g. by ion-exchange procedures). Nonetheless, the observation of two major dehydration peak temperatures below 200°C is common in TGA plots of Na and Ca-montmorillonites. The highest temperature peak is generally significantly smaller than the lower temperature one and both peaks for Ca-montmorillonites occur at slightly higher temperatures than for Na-montmorillonites (Guindy et al., 1985; Zabat and Van Damme, 2000; Guggenheim and Koster van Groos, 2001). This is in agreement with the present results and the implication that the hydration energy of calcium is larger than for sodium. The additional shoulders found in this work suggest that besides the nature of the interlayer cation, the structural type of montmorillonite is important for other sorption sites.

The presence of such shoulders has also been reported in the literature (e.g., Guindy et al., 1985; Koster van Groos and Guggenheim, 1984). A discrepancy is found to exist between two main groups, relating the position of shoulders to the temperature of the second dehydration event near ~140°C. Some studies report on an additional shoulder following this

peak, whilst others only support the existence of shoulders prior to this peak. In Koster van Groos and Guggenheim (1984), the effect of the external hydrostatic pressure on the dehydration reactions of Na-SWy-1 was investigated using DTG analyses. Their experiments performed at 1bar indicate the presence of a shoulder at 200°C after the main peak at 140°C (see also van Olphen and Fripiat, 1979). Other studies only report the presence of shoulders prior to this temperature (Zabat and Van Damme, 2000) or no shoulders at all (Bish and Duffy, 1990; Schilling, 1990). To a large extent, these discrepancies can be directly related to factors that are a function of the preparation method or controls on the analysis (e.g. the usage of different heating rates). Experiments performed at high heating rates, when samples are heated rapidly and so not allowed to 'equilibrate' with each new state, yield different peak temperature data. For instance, the reason why Zabat and van Damme (2000) only report a single peak for Na-montmorillonite could be due to the fact that they used relatively fast heating rates (10gr/min). In this study, it was found that for Na-SWy-1, the high temperature peak corresponds to very little extra weight-loss (<1wt %), and is therefore easy to remain 'hidden' under the bulk signal or noise.

The high temperature shoulders, as reported in Guindy et al. (1985) and Koster van Groos and Guggenheim, (1984/1986), are found on homo-ionic source clays and/or unknown sample material regarding its structure. At this stage, we cannot think of a possible explanation related to this occurrence. Again, the TGA results of Guggenheim and Koster van Groos (2001) are best compared with the present findings, with respect to similar material type and experimental conditions.

As pointed out in section 5.1, the low temperature (~40ºC) peak in typical TGA curves is related to removal of free water occurring in multilayers and in pore space; the high temperature (~140ºC) peak is associated with dehydration of the cation hydration sphere. To describe the dehydration process in more detail, we have to take into account the initial hydration states of Arizona and Wyoming montmorillonite in our experiments. With respect to the local environment, at 20ºC and atmospheric pressure, the hydration state of smectite is solely a function of vapor pressure. According to the phase-diagrams of Bird (1984), at the average 40% relative humidity in the laboratory, the initial hydration states of Ca-SAz-1 and Na-SWy-1 correspond to a 2 and 1-layer state respectively. Although the standards of Bird (1984) were made for homo-ionic source clays (in comparison to non pre-treated samples in this work), we assume that the diagram still holds. This is because as for both montmorillonites, 40% is not in the vicinity of hydration state boundaries. Moreover, the predictions are in agreement with comparable phase diagrams of Sato (1992). Because of the

strong poly-ionic nature of the exchangeable cations in K-10 montmorillonite, and the unspecified additional information concerning its structure, it was chosen not to analyze its signal (fig. 11) in more detail. We explained that in this case, the absence of a second high temperature peak is the direct effect of this poly-ionic nature. The mixture of exchangeable cations is coupled to each cation having its own energy barrier to overcome upon releasing hydrated water, resulting in a scattered signal.

Starting with Na-SWy-1 (fig. 9 and 12), the peak arising at 130-139ºC represents not only dehydration of the last remaining water layer present, but also of the hydration sphere occurring on the external surfaces. For this particular case, there is no significant contribution of the 2-layer state. It was pointed in section 3.2 that mixed hydration states occur, even at low water contents (e.g., da Silva et al., 2003). On this scale, the role of a possible 2-layer state appears to be negligible nonetheless. It is possible that the irregular decline between 60 and 80°C in figure 12 represents remnants of the two-layer state. The sharp peak at ~100ºC in figure 12 is not explained yet in terms of sorption sites. Its shape indicates that a specific group is suddenly affected by the temperature, although the according weight-loss step is very small (≤1%). Wyoming montmorillonite contains tetrahedral substitutions and therefore has charge localization on the internal and external surfaces. Water molecules can form hydrogen bonds with these tetrahedral sites, in the sorption site model of figure 6 this is indicated by ´internal/external surface site'. It is proposed here that the ~100ºC peak represents water-loss associated with this site. The sorption strength appears to be lower than for the cation hydration sphere, but higher than the attraction arising through double-layer forces and capillary condensation, which agrees with the adsorption theory of Prost et al. (1998). From this interpretation it follows that the amount of H_2O involved is very little, most likely 'wetting' the surface as a monolayer of water molecules. Once the cation hydration sphere starts to become dehydrated at 130-139ºC, it remains unclear from figure 9 whether the reaction is completed at the onset of dehydroxylation. It seems that in this interval the material continues losing some weight, which might represent the last one or two molecules associated with the cations.

Ca-SAz-1 montmorillonite has a two-layer hydration state at the start of the analyses. The dehydration curves (fig. 10 and 13) display a similar distinction as was seen for Na-SWy 1, between a low- and high temperature peak, related to weakly and strongly cation bonded water molecules. An apparent shoulder arises at 70ºC (fig. 13) and it is suggested here that its appearance is related to expulsion of the second-layer. This is because we argued in section 3 that this layer is weakly attracted to the exchangeable cation, and requires less energy upon

removal. This interpretation is in qualitative agreement with the conclusions of Bray et al. (1998) and Ferrage et al. (2007), although the latter study indicates slightly lower temperatures for the transition to a one-layer state. The last peak at 138-140ºC is also here associated with removal of the remaining layer, belonging to the cation hydration sphere (thus located in the interlayer and on the external surface). The structure of Arizona montmorillonite is characterized by octahedral site substitutions only, letting its sorption properties for a large part to rely on the attraction of exchangeable cations. The rest of the surface is considered rather hydrophobic, which is in accord with the TGA signal, i.e. no additional peaks have been observed. As was concluded for Wyoming montmorillonite, it remains uncertain if the final dehydration reaction is completed before the onset of dehydroxylation (fig 10).

From the TGA results on natural montmorillonites (fig. 12 and 13), it appears that both main peaks (at ~40ºC and 140ºC) correspond to more weight-loss in the case of Ca-SAz-1. This observation is in agreement with Bird (1984) and Bishop (1994). However on the basis of the CEC difference solely between both samples, one would expect an opposite trend. It was argued in section 2.3 that the tendency of smectite clays to swell is primary a function of the interlayer charge. 2:1 structured phyllosilicates have not been observed to swell if their charge is above -0.9e, and decreased swelling is generally observed with high charge. Few authors have put forward the opposite relationship (e.g., Laird, 1999). In this study, the influence of layer charge on the hydration of Mg-saturated smectites was investigated where it was experimentally shown that the water retained by clays increased with amount of layer charge. The increase in water content was however attributed to increase along the external surface solely. Chiou and Rutherford (1997) observed higher H_2O contents for SAz-1 than for SWy-1 over the full range of vapor pressure, which in agreement with the results presented in section 5.1.

The suggestion that charge location can be equally important in controlling the hydration properties of smectites is put forward by experiments of Sato (1992), who showed that basal spacings are larger when the charge is located in octahedral sheets. The results of the present experiments in section 5.1 are in agreement with this interpretation, Arizona montmorillonite contains more interlayer water than Wyoming montmorillonite. When the charge derives from the tetrahedral sheet (as in Na-SWy-1), limited expansion is possible due to a stronger attraction force between the clay platelets. Note however that for direct comparisons to explore the role of layer charge among different TGA studies, to exclude the

effects of cation type and charge location, it is critical to ensure that the clay specimens are identical.

6.2 Temperature-induced dehydration

Upon dehydration of both investigated natural montmorillonites (fig. 14a, 14b and 16a, 16b) the position of the HOH bending (ν_2) vibration shifts to a lower frequency. The OH stretching modes (ν_1 & ν_3) show an opposite shift and shift to higher frequencies. This trend is explained in sections 2.3 and 5.2 as a result of reduced effects of hydrogen bonding when the infrared absorption signal represents an increasing contribution of water molecules that are directly associated with the cation hydration sphere. These observations are in qualitative agreement with the conclusions of Russell and Farmer (1964). More specifically, in the FTIR dehydration experiments of Johnston et al., (1992), it was shown that the ν_2 position of homo-ionic Na^+/Cu^{2+} and K^+ exchanged SAz-1 remains identical for an hydration state over 8-10 water molecules per metal cation. Below this 'threshold', the absorption peak starts to shift to e.g. 1629cm^{-1}, for Na^+-SAz-1, when only 1 or 2 water molecules per cation are left over. This trend is of a similar type as seen in our results (fig. 15c and 16c).

Comparable experiments as Johnston et al. (1992) were performed by Xu et al. (2000) who probed the infrared spectra as a result of dehydration for two cation-exchanged (Na^+-SWy-1 and Ca^{2+}-SAz-1) source clays. Since the sample materials used in this study are comparable to our samples, it is possible to make a more thorough comparison. For Wyoming montmorillonite, the spectral results of Xu et al. (2000) show that for going from high water content (>20$H_2$0/cation) to ~8H_2O/cation, there is an initial small frequency increase of ν_2. This is followed directly by a major drop to 1625cm^{-1} at nearly dehydrated conditions. Arizona montmorillonite displays a related trend, although here the frequency drop begins already at 15H_2O/cation and no measurements were included for hydration states lower than ~12H_2O/cation, of where the corresponding absorption position equals 1628cm^{-1}. The according ν_1 trend for Wyoming and Arizona montmorillonite starts to be affected at similar hydration states as is seen for ν_2, i.e. for shifting from initial positions of 3420 to 3430cm^{-1} at 3-4H_2O/cation and 3420 to 3455cm^{-1} at ~12H_2O/cation, for Na-SWy-1 and Ca-SAz-1 resp. The spectral results of Ca^{2+}- exchanged Arizona montmorillonite deviate from the rest of the data set in Xu et al. (2000), as the signal gives the impression to be comprised of cation hydration water already at 12H_2O/cation. In that study, no explanation is provided for this apparent discrepancy.

The spectral results of Na^+- exchanged Wyoming montmorillonite in Xu et al. (2000) show that the water band frequencies commence to shift at hydration states of 7-8H_2O/cation, corresponding typically to a two-layer hydration state (Bird et al., 1984). At the point where the one-layer layer state would have been reached (3-4H_2O/cation), the according ν_2 position (~1628cm^{-1}) agrees reasonably well with our equivalent result of at least 70ºC thermal dehydration (fig. 16c). Because in the one-layer state the majority of the water molecules are coordinated to the exchangeable cations, this correlation provides evidence that water belonging to the direct cation hydration sphere is left-over already at this temperature. This remaining water is expelled near 140ºC, which was suggested earlier in section 5.2. In between 70ºC and 140ºC, it was showed that the ongoing absorption intensity decline is less pronounced (fig. 14a/16a), suggesting that little dehydration takes place during that stage. Note that in the present study initial ν_1 positions for both clay samples are slightly offset (fig 14a/16a), compared to the study of Xu et al. (2000). This could be explained by the usage of non pre-treated specimens in this work, without chemical treatment prior to testing. Note also that it is hard to exactly determine the location of the absorption peaks in figure 14a and 16a due to resolution loss from atmospheric water.

In both studies of Johnston et al. (1992) and Xu et al. (2000), the hydration state is controlled using water-vapor sorption isotherms coupled to a microbalance. This set-up allows gravimetric and IR-spectroscopy data to be collected simultaneously and therefore to predict the hydration state of the exchangeable cations. However it is noted here that this value (e.g. 10 H_2O/cation) is misleading. It was argued earlier that a significant contribution of the total water content in the interlayer region is coordinated outside the direct cation hydration sphere (e.g., Bray et al. 1998; Tenório et al., 2008). On external surfaces the same distinction between two types of water molecules applied, although here is referred usually to the formation of multilayers on neutral surfaces, for water that is coordinated outside the cation hydration sphere. This type of adsorption is more enhanced at high water activity, but was also shown to be present in the one-layer state (Tambach et al., 2006). As a result, the hydration state number presented by Johnston et al. (1992) and Xu et al. (2000), represents the total amount of water molecules that will on average be ‘associated’ with a single exchangeable cation. Considering the fact that all molecules are not adsorbed in equal fashion, as the direct cation hydration sphere is fairly small, those hydration numbers are more exact when the infrared frequency shifts start to be observed. This is because only then it can basically be said that the signal is comprised mainly of cation hydration water.

It was shown in the present temperature-induced dehydration experiments (e.g., fig. 14b) that for both samples at low temperatures (~40ºC), solely absorption intensity reduction occurs for both ν_1 and ν_2, which is explained by the removal of water located in pore space and along free surfaces. At higher temperatures (70ºC) peak shifting starts to take place (e.g., fig. 14b), indicating that the ratio of H_2O associated with the cation hydration sphere increases. In particular the ν_2 mode maintains a characteristic frequency, until the remaining water molecules start to be removed at ~140ºC. Taking into account the assumed hydration states at the start (i.e. 2-layer and 1-layer for Ca-SAz-1 and Na-SWy-1 resp.), dehydration of Na-SWy-1 to ~140ºC is consistent with removal of the last water layer.

Removal of the second layer hydrate in Ca-montmorillonites was suggested to occur at fairly low temperatures <50ºC (Ferrage et al., 2007). For this reason, dehydration of the second-layer state in Ca-SAz-1 used in the present work is assumed to take place slightly after or simultaneous when water molecules are being removed from multilayers on external surfaces. This would be in agreement with the theory that the second-layer might be relatively loosely bound in the interlayer (Bray et al. 1998), compared to the final layer which is dehydrated near ~140ºC. It was shown that after reaching 140ºC, the absorption intensity of ν_2 clearly reduces, although the remaining band position shifts back to higher frequencies (fig. 15b). This occurs while the corresponding ν_1 position remains equal (fig. 15a). Up to now, no apparent reason could be found for this remark. It could indicate that the effects of hydrogen bonding are increasing again, after only one or two molecules per cation are still remaining. In comparison to Na-SWy-1, Ca-SAz-1 shows clear evidence that still a few water molecules are present at 180ºC (fig. 15a/b). This effect is attributed to the stronger hydration energy of calcium ions. A similar effect is expected for the temperature at which the final water layers are expelled, if an accurate analysis would be made of the 125-145ºC dehydration regions. This effect is not apparent from the present temperature-induced dehydration experiments.

6.3 Integrating the TGA and FTIR spectroscopy results

Both macroscopic experimental techniques can be combined to provide additional details on the dehydration character of the studied montmorillonites. The inferred dehydration temperatures of ~40ºC (see sections 5.2 and 6.2) from IR spectroscopy, associated with the removal of free water or water derived from capillary condensation, are consistent with the temperature range of the first peaks as observed in the TGA plots of figure 9, 10 and 11. In the curves of figure 9 and 10 the low temperature peak, arising at ~40 and ~50ºC for

Wyoming and Arizona montmorillonite resp., agrees with the inferred IR spectroscopy trends (i.e. no peak shifting of ν_1 and ν_2) from section 5.2. Absorption intensity reduction occurs during this low temperature interval, removing water molecules located on neutral surfaces. In terms of temperature steps, on which the IR measurements were taken (e.g., 15ºC in fig. 14a), the accuracy does not allow distinguishing the slightly higher peak dehydration temperatures of Ca-SAz-1 compared to Na-SWy-1, as was seen in figure 12 and 13.

Dehydration of Wyoming montmorillonite displays a characteristic peak at ~100ºC (see fig. 9 and 12), which was proposed to follow from the removal of H_2O molecules sorbed around tetrahedral substituted surface sites. No equivalent peak is detected for Arizona montmorillonite in figure 10 and 13, which is the result of its rather hydrophobic surface. In the present spectroscopic results of figures 14-16, no evidence is found for a related trend, which is in agreement with the conclusions of Xu et al. (2000). One of the reasons why this type of sorbed water does not show a clear signal could be that it involves only a very small quantity of molecules. The TGA curve (red line in figure 12) indicates that the according amount of water liberated is very little (<1wt %). The sorption mechanism of these surface sites consist of attractions through hydrogen bonds with ions of substituted tetrahedra. The removal of those sorbed water molecules thus reduces the total amount of hydrogen bonding in the signal. The associated infrared spectra of Na-SWy-1 and Ca-SAz-1 (fig. 14-16) show that the position and intensity of water absorption bands, between 90ºC and 140ºC, are relatively unaffected. Absorption intensity reduction occurs mainly over this interval, but no clear effect is seen of dehydration from the hydrogen bonded surface sorption sites (see fig. 6). Hence, it is concluded only from TGA that the peak seen at 100ºC in figure 12 follows from dehydration of the crystal surface (molecules that H-bonded to the surface).

Spectroscopic evidence for dehydration of the second-layer state is not explicitly shown. The major difficulty arising here is the physical distinction between the second and third (or final) layer. The hydration state (in terms of number H_2O molecules/cation) from which interlayer water is only associated with the hydration sphere of the exchangeable cation, is poorly defined. This is because for example in the two-layer state, only a certain amount of molecules is associated with the direct cation hydration sphere. The rest of the adsorbed water molecules are located outside this sphere, either forming H-bonds with the surface or moving more freely in the interlayer region. The latter type of water molecules are equivalent to ‘outside cation hydration water’ in figure 6. Dehydration of Arizona montmorillonite shows a clear shoulder near ~70ºC in figure 13, which was proposed to be attributed to expulsion of this second layer. It appears that this temperature corresponds well

with the onset of in particular the ν_2 shift to lower frequencies (see fig. 15c), suggesting that beyond this hydration state, the remaining molecules are orientated primary to the cation hydration sphere. This implies directly that water molecules of the second layer state are rather weakly adsorbed in the interlayer region, which is in agreement with the conclusions of Bray et al. (1998). The TGA plot of figure 13 shows that the corresponding sorption strength is a little higher than water sorbed exclusively as a result of double-layer forces on the external surface. The present spectroscopic results suggest that on the basis of infrared spectroscopy solely, no distinction can be made between different hydration states in terms of a specific number of water-layers. Hence, it is not possible to differentiate between three or two-layer hydrates. The one-layer state can be determined by IR spectroscopy only because the associated water content is comprised mainly of cation attracted water molecules.

Removal of the last layer in the interlayer region, and of the hydration sphere of exchangeable cations on external surfaces, occurs at slightly higher temperatures for the calcium dominated structure than for sodium (see fig. 12 and 13). This effect is not seen in the infrared spectra of figures 14-16, probably due to the relatively large steps of the chosen temperature intervals. After removal of the cation hydration water, from the TGA curves (fig. 9 and 10) it was suggested that the reaction probably did not finish before the onset of dehydroxylation. This theory is in agreement with the spectroscopic data taken at temperatures higher than 140ºC (fig. 15a/15b). In particular for Arizona montmorillonite, as the ν_1 peak indicates (fig. 15a), there is definite evidence that some water molecules are still in the structure at the highest temperature. Whether Wyoming montmorillonite still contains H_2O at 180ºC is questionable. Spectroscopy puts forward that the material is close to dehydrated (fig. 16b) and TGA indicates that the sample loses less than 1 wt% going from 175ºC to the onset of dehydroxylation (fig. 10). Therefore it seems to be a very small contribution.

6.4 Normal stress-induced dehydration

In the normal stress-induced dehydration experiments on Na-SWy-1 and Ca-SAz-1, dehydration is expected from a ‘squeezing’ effect. The stress is transmitted through the clay platelets, in that way breaking bonds between water molecules and sorption sites. If we compare the corresponding spectral results of figure 17 and 18 with the observations made in section 5.2 on temperature-induced dehydration, at present both montmorillonites have not shown evidence yet of ν_1 and ν_2 peak shifting. It was demonstrated in figures 14 and 16 that

initially absorption intensity reduction occurs, analogous to low temperature dehydration of ~40ºC. Subsequently the location of the ν_1 peak starts to shift, although this exact point is weakly defined in figure 14a and 16a, while atmospheric water influences the resolution of the signal. This interpretation shows from analogy that the normal stress-induced effect in figures 17 and 18 is consistent with water removal from the pore space and from free surfaces. These molecules are attracted through capillary condensation and multilayer adsorption, which can be more easily squeezed out by imposed stress.

The observed difference between reaction rates caused by temperature and normal stress effects, in the figures 14-16 and 17-18 respectively, are attributed to consequences of a diffusion involved transport mechanism in the latter case. For both dehydration methods, after the water adsorbed in multilayers on external surfaces has been partially removed, the dehydration rate ceases as it requires more work to remove molecules located on stronger sorption sites. The rate would increase if the imposed relative humidity gradient between clay film and atmosphere is higher, creating a higher chemical potential gradient. This however introduces a coupled effect as allowing a local change in relative humidity causes the structure of the clay already to shrink. The change in vapor pressure is able to dehydrate the structure by itself. Effects which are solely induced by external pressure cannot be easily separated from changes in environment. A systematic description of smectite dehydration can therefore only be made if just one hydration state parameter is varied per analysis. For this reason, it is argued here that a comprehensive view of (normal stress-induced) smectite dehydration requires the availability of constant vapor pressure.

From the spectral results of figure 17 and 18, it appears that only free water is affected by the imposed stress. In section 3 it was mentioned that the larger part of this water is located outside the interlayer region, but can also occur in the interlayers (e.g., Tambach et al., 2006). The fact that no peak shifting is observed implies that the (interlayer/exchangeable) cation hydration sphere remains intact. The absorption ‘fingerprint’ of both Na-SWy-1 and Ca-SAz-1 after 48hours is still dominated by water located outside the cation hydration sphere. Whether other water molecules (e.g. outer cation hydration water in fig. 6) in the interlayer region start to become expelled or not, cannot be solely stated using these results. Dehydration of Wyoming montmorillonite at approximately 41MPa normal stress has probably not resulted in expulsion of interlayer water. This is because the larger part of the initial water content is assumed to occur in the one-layer state.

It was argued that the second-layer may be relatively loosely bound to other water molecules and is affected already <50ºC (Bray et al., 1998). In Bray et al. (1998), the

structural type of montmorillonite is not defined, this allows no direct comparison to be made. A scenario for dehydration of the two-layer state would be possible only for Arizona montmorillonite, as it has two water layers at the start. It follows from the present work (fig. 16 and 17) that the normal stress effect is analogous to low temperature dehydration of ~40ºC. This implies that no effects from dehydrating the second layer should be observed yet. It is noted though that the exact temperature of expulsion from the second layer is uncertain. In the present temperature-induced FTIR-spectroscopy experiments, the precise time-temperature relation has not been investigated with great accuracy. If the proposed temperatures (60-70ºC) of onset in peak shifting represent an upper bound, as a result of transport delayed effects, then the second-layer might start to become expelled at slightly lower temperatures. However still, if the normal stress-induced effect represents removal of the second-layer state, then you would expect to see peak shifting in figure 16 and 17, where evidence for is lacking. In other words, despite the fact that the second layer may be bound relatively loosely, for instance because some of the molecules are adsorbed not directly to the interlayer cations, the present experiments have not found direct evidence for interlayer water expulsion of Arizona montmorillonite at 41(±6) MPa. In any case, the (interlayer) cation hydration sphere (≈first-layer state) remained unaffected by the stress of both samples.

Whilst the normal stress is estimated at 41(± 6) MPA, the effective normal stress on the clay film could be lower. Both clay samples have initial hydration states distant from saturated condition (100% relative humidity). The pore space is therefore considered to be partially filled with capillary condensed water. The external surface, directly adjacent to the platelets, is covered with multilayers of which was proposed that the normal stress removes part of this cover. Those molecules are squeezed out of the structure and it is not impossible that the fluid pressure in the pores temporarily rises, thereby lowering the effective normal stress. This theory can be extended to explain as well the reason why dehydration ceases after a number of hours. Because multilayers are effectively removed from the clay surface, the transient pore-fluid pressure increases. When the molecules are diffusing to the outer side of the clay film, they are not easily released into the atmosphere since the vapor pressure gradient is low. This implies that at the edge of the film, an increased H_2O concentration could develop in the pores. The result of such happening is further enhanced on the longer timescale, when more water is diffused to the film edge. A scenario as described here would promote the development of high pore fluid pressure with ongoing dehydration, gradually lowering the effective stress exerted by the spring. This hypothesis provides an alternative explanation why the dehydration reaction stops after several hours.

At the moment, we have no particular evidence that this lowering of effective stress could be occurring. Considering the unconsolidated nature of the clay powder at initial state, without external pressure, the porosity is assumed to be higher than sheared clay. The load reduces the porosity, while it squeezes surface adsorbed water films into the pores that diffuse out of the structure. This collaboration of processes may lead to local increases of fluid pressure and subsequent lowering of effective stress. Such a relation has to be considered systematically in the future, by measuring constrains on porosity and local changes in water concentrations, for different parts in the clay film. This raises new challenges as the clay film thickness is not constant over the entire surface. It also needs information on the molar absorptivity of water, which is shown to be a strong function of the hydration state (Xu et al., 2000). Despite the fact that locally the effective stress may have been lower, it does not seem that the spectral results would be altered to a large extent. This is because the experiments were conducted at under-saturated conditions, where still a considerable volume of pore space is assumed to be empty. Porosity measurements before and after the experiment (and during) could provide a more quantitative approach.

It was inferred experimentally that the third-layer state of montmorillonites is easily lost upon dehydration at elevated temperatures of ≤60ºC (Bray et al. 1998). This is in agreement with experimental evidence of Fitts and Brown (1999), who showed indirectly that smectites can partially dehydrate to two-layer states at effective normal stresses ~1.5MPa. From the IR-spectroscopy studies of Johnston et al. (1992) and Xu et al. (2000), it appears that the spectral properties of water molecules in smectites are not typically modified beyond a two-layer state. For this reason, the normal stress-induced dehydration of material having three water layers at the onset will primarily result in absorption intensity reduction. The difference in thermodynamic state of water belonging to the three- or two-layer state is poorly defined. It is argued therefore here that the present method is not particularly useful to demonstrate interlayer water removal belonging to the third-layer state.

From the literature review in section 3.6, it was mentioned that several thermodynamic calculations indicate expulsion of the second-layer state (at room temperature and 40% RH) occurring at slightly higher normal stresses. The second water layer needs conditions in the order of 38-60 MPa differential stress to dehydrate (Bird, 1984; Colten-Bradley, 1987). Other estimations go up to as high as 100MPa for Na^+-smectite (Colten-Bradley, 1987), depending strongly on constrains regarding the interlayer water density, which is known only very limited. To compare with, simulation models indicate that Na^+-SAz-1 and K^+-SAz-1 require normal stresses between 187-487MPa and 10-375MPa resp., to go from a two-layer to a one-

layer state (Tambach, 2005). These values depend on the ambient relative humidity and given here are lower and upper bounds, corresponding to 8.9 and 67% RH respectively. The results overview as shown here and in section 3.6 denotes the existence of large variations among the predictions. This can have a more structural (e.g. different crystal structure) or lack of thermodynamic data origin.

By comparison, in the present work it is inferred from figure 17 and 18 that both cation hydration spheres remain intact at ~41MPa normal stress. In other words, dehydration of the one-layer state has certainly not occurred in both smectite specimens. At the present, the time dependency of the dehydration reactions has been studied on a long timescale (48h) and showed no variations compared to the signal at ~8h. The maximum attained normal stress (41MPa) approaches some of the values as found in section 3.6. For instance, the estimations of Bird (1984) are only a few units away from this value. In general, the predictions of Tambach (2005) are fairly high but do show the effects of ambient relative humidity. When the water vapor concentration in the atmosphere is low, the water molecules will diffuse into the gas phase more easily. This has dramatic effects on the required differential pressures. Due to limitations regarding the size of the spring, it was not possible to conduct loading experiment under higher normal stresses. This could be improved in the future to allow measuring up to 90MPa. Going from a one-layer state to dehydrated conditions needs at least 38-142MPa for Na^{+}-SWy-1 and 363MPa for Ca^{2+}-SAz-1 (Bird, 1984). The wide differential pressure ranges here shown for Wyoming montmorillonite is caused by an overlap of stability fields. According to these calculations, in the present experiments the dehydration of Na SWy-1 should already have been started, which is clearly not supported by the present result (fig. 18).

The results of this work are best compared with predictions on smectites having identical crystal structures, for instance as used in Bird (1984). It remains a challenge to accurately assess other findings (e.g., Colten-Bradley, 1987; Tambach, 2005). The present results could be used in future calculations and modeling work as an evaluation on differential stress-induced dehydration of these source clays. As pointed out in this section, if it is achievable to measure the dehydration effect at normal stresses up to ~100MPa, then presumably the structures would start to expel water molecules belonging to the direct cation hydration sphere. Theoretically these stresses have suggested to be in the order of a few hundred MPa (e.g., Colten-Bradley, 1987). Experimental verification is compulsory in order to confirm these calculations. The present dehydration effect for both clays (at 41MPa normal stress) shows no particular evidence of dehydration resulting from the cation hydration

sphere, hence part of the interlayer region. The shown effect is the result of water removal on multilayers, which is weakly adsorbed or capillary condensed in the pores of the structure. At this stage, we do not exclude that part of the interlayer water might have been dehydrated, particularly for Ca-SAz-1 as it starts with a two-layer state. This is because part of the interlayer water in the second-layer occurs outside the direct cation hydration sphere (see fig. 6). This water is more weakly attracted and cannot be easily distinguished from water occurring in multilayers on external surfaces.

6.5 Adsorbed water films on clays: KBr pellets

It was shown in table 5 that the ν_2 band positions of muscovite and kaolinite show a comparable distinction as seen in smectites, between two types of water molecules. This is direct evidence that the swelling properties of smectite clays do not affect the infrared water absorptions in a fundamentally different way as to other non-swelling clay minerals. Both swelling and non-swelling clays can contain exchangeable cations, while only the first group has a portion of the total water content incorporated in the interlayer region. This water is to a certain extent directly attracted to the interlayer cation, of which the according ν_2 band is located at relative low frequencies. It is thus showed here that the properties of both ions are not distinct, with respect to the associated hydrogen bond energy. For this reason, we put forward that water molecules around interlayer cations are quite similar from those coordinated to exchangeable cations. The crystal structures of the investigated minerals from table 5 are now discussed separately in the following in more detail.

Muscovite contains solid substitutions in the tetrahedral sheet, but as the charge deficiency is too high ($\geq$-1.0*e*), the interlayer hydration force is not strong enough to overcome the electrostatic attraction between the ions and clay platelets. Consequently, muscovite has no swelling properties attributable to water adsorption in the interlayer region. It appears from table 5 that the structure is still able to adsorb water on external surfaces. This water is physically distinct compared to water derived from capillary condensation and is evidently affected by the exchangeable cations, forming a hydration sphere.

The mineral kaolinite is considered as having a rather ‘perfect’ 1:1 crystal structure. Some discussion exists however on whether its low CEC nature is explained by the occurrence of isomorphic substitution and/or the ability to protonatize exposed hydroxyl groups (e.g., Zhou and Gunter 1992; Ma and Eggleton, 1999). According to the present spectroscopic results, at least a fraction of the total water content is associated with the

hydration sphere of ions. If the crystal structure would have been 'perfect', no low frequency shoulder (ν_{2S}) could be identified. As was found for muscovite, also in this case there is clear evidence for the existence of water molecules associated with the cation hydration sphere on the external surface of the crystallite.

Pyrophyllite has a perfect 2:1 crystal structure with no solid substitutions. This is confirmed by its infrared signal displaying only a single peak at 1636cm^{-1}, representing condensed and multilayer sorbed water. It appears that to some extent, the exposed cleavage planes and neutral surfaces are able to attract water molecules. This is mainly the result of van der Waals forces. Exposed crystal edges can lead to some hydrophilic character, even though the cleavage plane is hydrophobic. It is noted however that the intensity of the 1636cm^{-1} peak is rather low. No ν_{2S} shoulder could be detected in this case, indicating the lack of a cation hydration sphere.

The crystal structure of quartz is not charged and therefore has no lubricating effects. The lack of spectroscopic signal is in correspondence with this view. No indication is found for water in any form, whether it would result from adsorption on KBr surfaces, or on quartz itself. It appears that the surface of quartz is highly hydrophobic and shows no sign of water attraction. This conclusion is consistent with the assumption made earlier: by taking a blank spectrum prior to each measurement, the infrared absorptions of water molecules associated with the KBr matrix are selectively removed.

6.6 Weakening mechanism of clay minerals

Fault gouge containing considerable quantities of clay phases has long been pursued as a potential source of fault weakness, due to the exceptionally low strength of these phases under particular conditions (e.g., Saffer et al., 2001). Morrow et al. (2000) showed that the frictional resistance of 'dry' phyllosilicates (heated to 180ºC), for different structural groups, can be directly related to their interlayer bond strength (see also table 2 and section 2.7). Above a certain strength threshold, the dry coefficient of friction approaches Byerlee's law ($\mu \approx 0.8$), from which it is well-known that strain is accommodated through typical brittle processes (e.g., Paterson, 1978). An exception to this relation is montmorillonite, which on basis of its interlayer bond type would expected to have a lower friction coefficient than the value of ~0.8, as determined experimentally (e.g., Moore and Lockner, 2007). Below the strength threshold, a correlation was found between μ (dry) and interlayer bond strength (table 2), suggesting that shearing occurs by cleaving through the d_{001} plane (e.g., Moore and Lockner,

2007). Moore and Lockner (2004a) argued that this mechanism is favored above shearing along grain surfaces.

To recap from sections 2.5-2.8, the frictional strength of 'dry' (heated to 125ºC) montmorillonite was found to be rather high at 100MPa effective normal stress ($\mu \approx 0.7$-0.8) (e.g., Moore and Lockner, 2007). With the introduction of water this value is reduced significantly to $\mu \approx 0.2$ at saturated conditions (e.g., Morrow et al., 2000; Ikari et al., 2009), hence if the development of excessive pore-fluid pressure is considered to be negligible. However friction measurements of pyrophyllite, which is crystallographic similar to montmorillonite but then without an interlayer charge, at comparable conditions (wet) showed that its strength is only a fraction higher with $\mu \approx 0.28$ (table 2). The discovery of this similarity led Moore and Lockner (2004a) to propose that the mechanical properties of montmorillonite at water-saturation are actually analogous to what is expected on the basis of its crystal structure solely. This is because due to its hydrophobic nature, the strength of pyrophyllite is not expected to be influenced by addition of water. In other words, the swelling properties of montmorillonite could be inappropriate for controls on its frictional strength. In experiments, this would be only 'true' if careful handling is employed concerning the generation of excess pore pressures (e.g. by conduction friction experiments at water saturation). A limitation to this strength hypothesis of Moore and Lockner (2004a) is that it is based on montmorillonite with octahedral substitutions only. In reality, the mineral might have a charge deficiency distributed over both sheets. This is strongly depending on the type of montmorillonite. The association would be different if a more complete range of structural types is considered. Ion substitutions in the tetrahedral sheet are in close vicinity of water molecules located on the surface, allowing the creation of strong hydrogen bonds with the interlayer/external surface (see fig. 6). For talc (having a perfect tri-octahedral crystal structure), it was made clear by Morrow et al. (2000) that the difference between wet and dry friction is very small (table 2), which is in agreement with the hypothesis of Moore and Lockner (2004a.).

It has been argued that the high strength of thoroughly dried montmorillonite is remarkable (Moore and Lockner, 2007). On the basis of predictions concerning its interlayer bond separation energy, one would expect a lower coefficient of friction than the experimentally observed value of ~0.7-0.8 when dried sufficiently (Moore and Lockner, 2007). An important observation is that montmorillonite does show unusual weakening behavior, although it seems that this fact is primary caused by its high 'real dry' strength. We also denoted that the strength of wet pyrophyllite is very close to water-saturated

montmorillonite (0.28 vs. ~0.2 for μ resp.), letting Moore and Lockner (2004a) to propose that the weakening effect is irrelevant to the fact that montmorillonite has interlayer water. In order to improve the current understanding of this correlation, there is need for knowledge of pyrophyllite dry strength. We can expect this strength reduction, going from dry to wet pyrophyllite, to be negligible as found for talc (Morrow et al., 2000), because the structure is not charged. If this is experimentally validated, then it should be the high friction coefficient of 'real dry' montmorillonite that requires explanation, in terms of absolute strength reduction. To compare with, minerals from the serpentine group (e.g. chrysotile) also display great weakening upon water saturation (see table 2), and neither contain interlayer water. The serpentine minerals have tri-octahedral 1:1 crystal structures and show a similar strength reduction trend upon the introduction of water as di-octahedral kaolinite (Moore and Lockner, 2004a).

Whereas a weakening trend, upon the introduction of water in typical friction experiments on clay minerals is evident, the mechanism by which this effect occurs is not. Our present discussion starts with the smectite clay group while since its discovery as a potential source of fault weakness (e.g., Wang et al., 1980), a number of water-assisted weakening mechanisms have been proposed (e.g., Moore and Lockner, 2004a). Most of these hypotheses address its low strength, measured under 'room-dry' or wet conditions, to the stress-induced effect of interlayer water expulsion (e.g., Fitts and Brown, 1999), which reduces friction by increasing the pore-fluid pressure (defined here as the water-assisted *indirect* weakening mechanism). Although this mechanism might explain part of the published strength data, for instance of the friction experiments performed at partially saturated condition (hence, equivalent to conditions of room temperature), it was also explained that montmorillonite weakens in the case of fluid saturation (Moore and Lockner, 2007), thus when the pore-fluid pressure increase is limited. This suggests that there exists more than one particular weakening mechanism for smectites.

Another smectite weakening hypothesis mentioning specifically the role of interlayer water was proposed by Bird (1984). In this theory, the interlayer water supports the normal stress on its own and allows slip to occur at low effective normal stress. Because the friction experiments of Bird (1984) were performed under conditions that did not allow changes in the hydration state, the effect of water expulsion (and so the *indirect* weakening mechanism) could be excluded. Currently, there is however insufficient evidence that this is occurring on the microscale. Bird (1984) did not consider the shear through surface adsorbed water films,

which have shown to exist also on the external surfaces of smectites (e.g., Ormerod and Newman, 1983; Güven, 1992).

Since the identification of non-swelling clay minerals as weak phases when sheared under wet conditions (Morrow et al., 2000), there was a need for a new type of weakening mechanism to explain the fact that beside smectite, the strength of other (non-swelling) clay minerals can also be affected by the introduction of water. Moore and Lockner (2004a) explained their observed water-assisted weakening trend, and the results obtained by Morrow et al. (2000), for a range of phyllosilicates (micas and clay minerals) as a result of shear through surface adsorbed water films. The lubricating effect of the externally adsorbed water films was proposed to lower the friction coefficient, depending on the bond strength (or hydration energy) between the water molecules and the surface sorption sites (Moore and Lockner, 2004a). In section 3 it was explained that for swelling and non-swelling clay minerals, there exist two of these sorption possibilities: water molecules can be either adsorbed to the exchangeable cation or directly to the surface through hydrogen bonding with the surface (see also figure 6).

The FTIR spectral results (using the KBr method) obtained in this study support the hypothesis of Moore and Lockner (2004a). In the present work we verified the existence of a particular type of surface adsorbed water molecules on clay structures that contain no interlayer water. Those water molecules are coordinated around and attracted by exchangeable cations. It turns out that their properties are quite similar to that of interlayer water adsorbed directly to the interlayer cation (see table 4). The presence of these water films can reduce the frictional resistance and thus give rise to the weakening effect as was observed by Morrow et al. (2000) and Moore and Lockner (2004a). This mechanism is defined here as the *direct* water-assisted weakening mechanism. The present findings thus provide more evidence for the fact that the swelling properties of smectites *can* be irrelevant regarding its weakening effect, as was concluded by Moore and Lockner (2004a). This is because smectite is also able to adsorb water films on external surfaces (e.g., Ormerod and Newman, 1983). We emphasize though that it is *only* irrelevant when the other water-assisted weakening mechanism (*indirect*) for smectites is considered to be negligible. In other words, under lab experiments when effects of local pore-fluid pressure changes are considered to be negligible (e.g. by usage of water-saturation in typical friction experiments). In natural fault zones the chance of interlayer water expulsion and so local increases in pore-fluid pressure, as a result of elevated temperature and/or differential stress, should always be taken into account.

In the present work, we also showed in section 5.3 that for normal (or differential) stresses up to 41(± 6) MPa and initial hydration states belonging to the two- or one-layer state, no significant effect of interlayer water expulsion can be expected. In the future, the stress threshold for interlayer water expulsion needs to be constrained for a systematic range of parameters (e.g. different types of smectites and range of initial hydration states). Only if such stress data is identified, then more detail can be provided for the contribution to the total weakening effect of the interlayer water expulsion (and so local high pore-pressure) weakening mechanism. For a more complete description, relevant for existent geological situations, such calibration has to be extended afterwards to account for the combined dehydration effect of elevated temperature and different pressure conditions.

6.7 Influence of effective normal stress on friction experiments of clay minerals

In order to make consistent frictional strength comparisons in the sections 2.5-2.8, the mechanical properties of several clay minerals (under wet/dry conditions) were discussed measured at constant effective normal stress of 100MPa. In the following, the dependency of these results on effective normal stress is investigated. We start with smectite and then go on to extend the inferred hypothesis to other non-swelling clay minerals.

In the review of Moore and Lockner (2007), an apparent difference on effective normal stress dependency was noticed among collected data sets on the frictional strength of montmorillonite. The data that correspond to experimental conditions performed under water-saturated conditions (equilibrated pore-fluid pressures) show that μ increases with increasing normal effective stress. For example, Morrow et al. (1992) found an increase of 0.12 for μ measured at 100 to 300MPa σ_n^e. This is in contrast to what is found typically for friction experiments performed under partially saturated conditions (e.g. experiments under room-dry conditions with under-saturated pores). For example, data from Saffer et al. (2001) show a decrease of 0.16 for μ measured at 5 to 50MPa σ_n^e. In particular the possible drop in μ at higher effective normal stress is confirmed by several other studies (e.g., Bird, 1984; Saffer and Marone, 2003; Ikari et al., 2007).

One reason for the negative μ - σ_n^e slope is due to the *indirect* water-assisted weakening mechanism as a result of higher effective normal stress, which could squeeze out some of the interlayer water. It was argued in section 2.8 and from Wang et al. (1980) that usage of partially saturated conditions in friction experiments on smectites can be problematic due to possibly undetected high pore-fluid pressures. This would lead to inferred friction

coefficients that are taken too low. The effect of higher effective normal stress on the friction coefficient is however fully consistent with the *direct* water-assisted weakening mechanism and the reduction in friction hypothesis of Moore and Lockner (2004a), as a result of shear along surface adsorbed water films. At higher σ_n^e some interlayer water expulsion threshold can be reached which promotes lubrication of the external surfaces, and therefore the reduction in shear strength. In other words, due to the imposed stress condition water is squeezed out of the interlayer region and these molecules can contribute to the water content along the surface of the grains. This mechanism explains why smectite weakens furthermore upon increasing the effective normal stress in friction experiments using partially saturated clay gouge.

A positive μ - σ_n^e slope is achieved in friction experiments on montmorillonite using water-saturated conditions (e.g., Moore and Lockner, 2007). Yet again this trend is fully consistent with the reduction in friction hypothesis due to shear along surface adsorbed water films of Moore and Lockner (2004a). In this case the *indirect* water-assisted weakening mechanism can be ignored. The influence of higher effective normal stresses on the remaining *direct* weakening mechanism, the lubrication effect along the surface of the grains, is now easily explained. In saturated clay gouge composed of montmorillonite all the grains surfaces are assumed to be wetted with water molecules. A higher value of σ_n^e will reduce this lubricating ability, driving off the water films, and in consequence raising the frictional strength of the gouge. It is thus concluded that the hypothesis of Moore and Lockner (2004a) explains both types of observed relations of the friction coefficient to the effective normal stress for smectites.

If the hypothesis of Moore and Lockner (2004a) is also valid for other clay minerals, then there should exist no (or negligible) dependency of frictional strength on effective normal stress, for clay gouge composed of hydrophobic clay minerals. This supposition was experimentally confirmed by triaxial friction experiments on water-saturated talc gouge at room temperature by Moore and Lockner (2008). The non-swelling clay structure of talc does not contain any solid substitutions and therefore its surface is hydrophobic. In the according results it was shown that for going from 100 to 300MPa σ_n^e, the coefficient of friction increased only slightly with 0.03.

On the other hand, an apparent positive effective normal stress dependency has been observed, for other water-saturated room temperature friction experiments, on different hydrophilic clay minerals beside smectites. For example, Moore et al. (2004) showed that for chrysotile μ increases respectively from 0.15 to 0.32, when going from 40 to 300MPa normal

effective stress. Also for muscovite such positive correlation is inferred for a compilation of data from different friction experiment (see fig. 8 in Moore and Lockner, 2008). The stress drives off externally adsorbed surface water films and thus increases the shear strength.

6.8 Proposed fault weakening model

From sections 2.5-2.8 and in section 6.6, we showed that different phyllosilicate groups weaken to various extents, when sheared under 'real dry' or wet conditions (Moore and Lockner, 2004a). This was explained by the fact that shear becomes localized along surface adsorbed water films, which interact in different ways with each mineral surface (the *direct* water-assisted weakening mechanism). Smectites provide no exception to this hypothesis as it contains significant amounts of surface adsorbed water molecules, on top of its interlayer water (e.g., Ormerod and Newman, 1983; Prost et al., 1998; Knudsen et al., 2003). Smectites however do have an additional waster-assisted weakening mechanism (*indirect*), which is caused by local elevated pore-fluid pressures, due to interlayer water expulsion. The externally adsorbed water molecules occur in different states, from multilayer to exchangeable cation adsorbed water (see also fig. 6). We showed in section 5.4 that the molecular properties of the latter (relative strong) adsorbed films are not different from water molecules coordinated to interlayer cations in smectites. With this analogy, we support the presence of strongly adsorbed surface water films on other non-swelling clay minerals beside smectites, and that the removal of such films at high differential stress can explain the proportionality of friction to effective normal stress at room temperature under water saturated conditions (e.g., Moore and Lockner, 2007; Moore et al., 2004). The mutual effects of clay gouge fabric, water content and mineral composition, on the frictional strength of shallow crustal faults can now be integrated to provide a framework that evaluates the possibilities of fault zone weakening in the upper crust.

Fault weakness of many crustal faults is controlled by a number of dynamic and static weakening mechanisms. In the present fault weakening model, the focus is laid on the weakening effect of fault gouge containing clay minerals, and in particular smectite, of which both have shown to act under specific conditions as weak phases. The groundwork of the model was laid by a study of Collettoni et al. (2009a), who addressed specifically the role of fault zone fabric in controlling the frictional strength of a natural fault zone containing clay minerals. From section 2.6 it was argued that the alignment of clay minerals into preferred lattice orientations is commonly observed during friction experiments (e.g., Saffer et al.,

2001). The work of Collettini et al. (2009a) showed that the frictional strength of intact fault rocks (with pronounced foliation) sheared in *in-situ* geometry is clearly lower compared to their powder equivalents. In here, the total clay content of the specific fault rock was estimated to lie between 20 and 30%, including 14 to 19% of smectites and 6 to 15% of talc, with the rest of the composition made up of calcite and amphibole (tremolite). The micro-structures of the sheared samples of Collettini et al. (2009a) reveal an apparent distinction between intact fault rocks versus powder equivalent. The analyses on intact fault rocks showed that frictional sliding occurs along very fine-grained talc and smectite foliations, which form due to translation and rotations of the phyllosilicates, an interconnected network of slipping planes. This is in contrast to what is observed for the powered rocks that show typical cataclastic micro-structural features like R1, Y and B shear bands. Although most frictional experiments of Collettini et al. (2009a) were conducted at room conditions, the tests performed at water-saturation indicated further weakening of both the intact fault rock and the powder equivalent, compared to the room-dry experiments (see also fig. 2b in Collettini et al., 2009a). However the smectite minerals sheared at room conditions still had initial conditions corresponding to one or two water layers in the interlayers, and an equivalent of surface adsorbed water films, depending on specific crystallographic controls and relative humidity. In other words, most of the foliated surfaces in the intact fault rocks were assumed to be lubricated during the experiments performed at room conditions.

The conclusions of Collettini et al. (2009a), who describe fault weakening as a result of growth of an interconnected anastomosing network of phyllosilicate phases, from which frictional sliding occurs, is fully consistent with the weakening hypothesis of Moore and Lockner (2004a). Our current work supports this model and provides additional evidence for the presence of strongly surface adsorbed water films on non-swelling clay minerals. Because these films have the physical properties equivalent to the last remaining water layer in the interlayer region of smectites, which is strongly adsorbed (i.e. generally need temperatures higher than 140ºC or a few hundred MPa differential stress upon removal), it is assumed here that they can persevere hydrating the phyllosilicate foliation up to significant depths (5-8km). For instance, the films are believed to withstand effective normal stresses up to 800MPa (Renard and Ortoleva, 1997). Yet it is hard to constrain this depth accurately due to the combined dehydration effect of elevated temperature and stress (hydrostatic versus differential), of which experimental evidence is still lacking.

Despite the fact that clay fabric plays an important role in explaining some weak faults, we argue that the presence of weak phyllosilicate phases in fault gouge, which are

capable of adsorbing surface water films (e.g. smectite, muscovite, chrysotile, kaolinite, lizardite, chlorite, illite) is the most important element of the weakening model (the *direct* water-assisted weakening mechanism). Alternatively, if phases such as talc are sufficiently present, both the *direct* and *indirect* water-assisted weakening mechanisms become less important. This is because talc has shown to be consistently weak (μ~0.2) over a range of conditions (Moore and Lockner, 2008; Collettini et al., 2009b). The structure specific *indirect* water-assisted weakening mechanism of smectites (interlayer water expulsion and pore-fluid pressure increase) can play an important role as well in controlling fault weakness. This impact depends on the overall permeability of the fault gouge, which is a dynamic feature (depending on the amount of shear) and a function of gouge mineralogy (Ikari et al., 2009). In friction experiments on smectites the influence of this particular mechanism can be minimized by using water-saturated conditions. In natural smectite-bearing fault zones, the phyllosilicate-rich networks can be easily reactivated by the two *direct* and *indirect* water-assisted weakening mechanisms, and by doing so contributing to significant fault weakening at shallow depths.

6.9 Application to natural fault zones

The relevance of the present upper crustal weakening model, with two different water-assisted weakening mechanisms (*direct* and *indirect*), for fault gouge containing clay minerals is now evaluated for specific case-studies.

In Numelin et al. (2007), the frictional properties of a natural low-angle normal fault, in Panamint Valley, California, were determined at room temperature to investigate the influence of clay minerals on fault weakness. The clay mineral content of the particular fault zone appeared to be strongly heterogenic, with smectite making up 10 wt% to 40 wt% of the total clay content, which ranged from 15 wt% to 62 wt% of the total rock composition Two important conclusions were made in the study of Numelin et al. (2007) that support the present weakening model. The first conclusion is based on the observation that friction decreased with increasing total clay content, rather than with swelling clay content. This is consistent with the fact that the additional *indirect* weakening mechanism of smectite clays can be irrelevant for the total weakening effect of smectite-bearing fault gouge. Because the experiments were conducted at room temperature, all hydrophilic phyllosilicates (incl. smectite) contained surface adsorbed water films, which acted as gliding surfaces. Hence, the observed weakening effect of Numelin et al. (2007) is thus probably the result of the *direct*

water-assisted weakening mechanism only. The second conclusion that was made supports the positive inferred correlation in section 6.8 between clay content, fabric intensity and low friction. The authors proposed a weakening model that is based upon the development of foliations, which act as gliding surfaces, and the presence of sufficient (>50 wt%) weak phyllosilicate phases. This model description is consistent with our present view of weak faults as explained in section 6.8.

Similar studies as Numelin et al. (2007) report on the specific influence of clay minerals in controlling fault weakness. For example, Jefferies et al. (2006) explained the long-term weakening of the Median Tectonic Line (MTL) in Japan as a consequence of the development of phyllosilicate-rich fault rocks that are able to form an interconnected thin layer of weak material, which extends on the (tens of) kilometer scale. The existence of surface adsorbed water films on the corresponding clay minerals will contribute to this weakening process. In Solum and van der Pluijm (2009), the influence of clay mineral composition and fabric was investigated to determine fault behavior of the Carboneras fault, Spain. This particular fault zone contains no smectite but illite, muscovite and chlorite. Still it was concluded by Solum and van der Pluijm (2009), who quantified the clay fabric, that the fault is weak due to the presence of these clay phases that rotate into networks of connected minerals. The presence of strongly surface adsorbed water films, which was in the present work found to exist on muscovite, will contribute to this weakening effect.

7. Conclusions

In the present work we study the influence of water in controlling the frictional strength of fault gouge containing clay minerals. In particular, the weakening effect of swelling smectite clays (containing interlayer water) is investigated. To challenge this, we use comprehensive literature reviews and report on new qualitative laboratory data using TGA and FTIR-spectroscopy of the *in-situ* temperature- (20-180ºC) and normal stress-induced (to 41 ±6 MPa) dehydration character of two well-known montmorillonite source clays (Ca-SAz-1 and Na-SWy-1). We also investigate the interaction of water molecules with the mineral surface for a number of non-swelling clay minerals. From the (experimental) results we conclude the following:

1. The temperature-induced dehydration signal of Na-SWy-1, Ca-SAz-1 and K-10 montmorillonite, using TGA and FTIR spectroscopy, has led to an improved and thorough understanding of the dehydration process occurring at the macro- and microscale. The hydration properties, as a result of differences in interlayer cation (Ca^{2+} vs. Na^{+}), initial hydration state (two-layer vs. one-layer) and charge location (octahedral substitutions only vs. substitutions in both sheets) are clearly displayed in sections 5.1-5.3, for Ca-SAz-1 and Na-SWy-1 respectively.

2. The application of confining pressure alone tends to increase the stability of hydration water, resulting in no interlayer water expulsion. In this work, it was shown from normal stress-induced dehydration experiments at room temperature of Na-SWy-1 and Ca-SAz-1 up to 41MPa, that application of an equivalent differential stress results in no obvious interlayer water expulsion. The shown dehydration effect corresponds to removal of water molecules that are weakly bounded to the mineral external surface, attracted through double –layer forces and capillary condensation. It was shown that the cation hydration sphere remains intact for both montmorillonite.

Thermodynamic predictions from the literature of differential stress-induced interlayer water expulsion at room temperature are very scarce, but suggest that the last layer is very difficult to remove, requiring several hundred MPa differential stress. The second water layer needs conditions in the order of 38-60 MPa differential stress to dehydrate and the third layer is easily lost requiring only a few MPa. Although according to the calculations, Ca-Saz-1

would already have started to dehydrate, our spectral results found no evidence for this occurrence. It is emphasized here that the thermodynamic predictions are not accurate, both due to differences in type of smectite structure and missing information relating to specific thermodynamic properties, such as interlayer water density. In the future, the differential stress threshold for interlayer water expulsion needs to be constrained for a more systematic range of parameters (e.g. for different types of smectite structures and range of initial hydration states), and also the combined temperature-differential stress dehydration effect, relevant for subsurface conditions, on the stability of interlayer water needs to be assessed.

3. The usage of *in-situ* XRD studies at elevated differential stress has not been considered as a potential technique for specifying the differential stress ranges under which hydrates are stable. It is argued here that this technique would resolve the problems occurring with infrared spectroscopy as it probes the micro-structure (d_{001} spacing) and provides direct insight on the hydration state. No contributions to the total water content of the mineral surface can be visualized. In this way, it would be possible to constrain accurately the differential stresses needed to expel the specific water-layer of interest.

4. The minerals muscovite and kaolinite contain, beside multilayer adsorbed H_2O molecules, surface adsorbed water films which are attracted directly to the exchangeable cation. It is shown here that the properties of these surface adsorbed water molecules are similar to water molecules directly attracted to interlayer cations. To compare with, pyrophyllite and quartz do not show these characteristic absorptions due to their relative perfect (hydrophobic) crystal structures. Hence, we support the existence of distinct externally surface adsorbed water molecules on non-swelling clay minerals, which require more work to dehydrate than capillary condensed water at elevated pressure and temperature.

5. Friction experiments on clay minerals and micas show that for different crystallographic groups, the effect of adding water leads to weakening of the material. This relation had been inferred earlier for smectites solely and led to some confusion concerning the role of interlayer water in controlling the weakening mechanism. Most friction studies on montmorillonites assign the low inferred coefficient of friction ($\mu \sim 0.2$) to the fact that it can expel its interlayer water and therefore increase locally the pore-fluid pressure (defined as the *indirect* water-assisted weakening mechanism). In our work, we provide additional evidence for the weakening hypothesis of Moore and Lockner (2004a): clay gouge (smectite-bearing or

without smectite) can be weak due to facilitated shear on water layers that are adsorbed on aligned play surfaces (defined as the *direct* water-assisted weakening mechanism). This type of water film occurs also on smectites and can explain fully the observed low frictional strength (at any hydration state other than fully dehydrated), if influence from the *indirect* water-assisted weakening is considered to be negligible.

6. Application of the *direct* water-assisted weakening mechanism for smectite explains fully the experimentally observed twofold dependency of frictional strength on effective normal stress. While a negative correlation (μ drops with increasing σ_n^e) is found for experiments conducted under partially saturated conditions, a positive correlation (μ increases with increasing σ_n^e) is found for experiments performed under water-saturated conditions. This twofold dependency is explained using the weakening hypothesis of Moore and Lockner (2004a). In case of water saturation, effective normal stress drives water off, thinning out the films, and so increasing the shear strength. If smectite is only partially saturated, then increasing the effective normal stress results in two coupled effects that tend to lower the frictional strength. The first develops through increased surface wetting (*direct* water-assisted weakening mechanism) and the second as a result of potential increase in pore fluid pressure (*indirect* water-assisted weakening mechanism). We emphasize that to obtain reliable friction data of smectites, it is compulsory to use water-saturated or thoroughly dried conditions. This will prohibit the influence of possibly high undetected pore-fluid pressures.

7. Thoroughly dried (T>140ºC) montmorillonite is strong with friction values approaching Byerlee's law. The material weakens if water is present due to a *direct* and *indirect* weakening mechanism. In the present work, we looked in particular for the stability range of differential stress associated with the *indirect* mechanism, to study which stress condition is needed to squeeze out interlayer water. It was concluded that for both investigated montmorillonites at 41 MPa differential stress, no evidence is found of interlayer water expulsion.

8. Fault weakness of many crustal faults is controlled by a number of dynamic and static weakening mechanisms. In the present fault weakening model, the existence of some weak faults is explained due to 1. the presence of weak (hydrophilic) phyllosilicate phases and 2. growth of an interconnected anastomosing network of these phases. This model description is consistent with a weakening mechanism based on facilitated shear through surface adsorbed

water films, plus the addition of clay fabric as second important element. The present work supports this model, based on the work of Collettini et al. (2009a), through providing additional evidence for the presence of strongly surface adsorbed water films on non-swelling phyllosilicates (muscovite and kaolinite). In natural smectite-bearing fault zones, the phyllosilicate-rich networks can be easily reactivated by the two *direct* and *indirect* water-assisted weakening mechanisms, and by doing so contributing to significant fault weakening at shallow depths.

Acknowledgements

I would like to thank my main supervisor, prof. Chris Spiers for letting me carrying out this project. His constructive and inspiring view on the problem statement and the approach in this work is unique. Also I thank Tim Tambach (TNO) for some interesting discussions. I also would like to thank the rest of the HPT group for their support, especially Peter van Krieken and Gert Kastelijn for their technical assistance.

References

Anderson, R.L., Ratcliffe, I., Greenwell, H.C., Williams, P.A., Cliffe, S., Coveney, P.V. (2010), Clay swelling – A challenge in the oilfield, *Earth-Science Reviews (98),* 201-216

Bailey, S.W. (1980), Summary of recommendations of AIPEA nomenclature committee on clay minerals, *Am. Mineral*., vol. 65, pp 1-7

Biot, M.A. (1956), Theory of deformation of a porous viscoelastic anisotropic solid, *Journal of Applied Physics 27 (5),* 459-467

Bird, P. (1984), Hydration-phase diagrams and friction of montmorillonite under laboratory and geologic conditions, with implications for shale compaction, slope stability, and strength of fault gouge, *Tectonophysics, 107*, 235– 260

Bish, D.L., Duffy, C.J. (1990) Thermometric analysis of minerals. *In Stuchi, J.W., Bish, D.L., Mumpton, F.A., Eds., Thermal analysis in clay science, p. 96-157.* Clay Minerals Society Workshop lectures, Boulder, Colorado.

Bishop, J.L., Pieters, C.M., Edwards, J.Q. (1994), Infrared spectroscopy analyses on the nature of water in montmorillonite, *Clays and Clay Minerals, 42, no. 6*, 702-716

Bleam, W.F. (1990), The nature of cation-substitution sites in phyllosilicates, *Clays Clay Miner., 38*, 527– 536

Bray, H., Redfern, S.A.T., Clark, S.M. (1998), The kinetics of dehydration in Ca-montmorillonite: an *in situ* X-ray diffraction study, *mineralogical magazine, vol. 62(5),* 647-656

Brindley, G.W., Brown, G. (1983), Crystal Structures of Clay Minerals and their X-ray Identification, Mineralogical Society Monograph No.5, pp. viii + 496pp.

Byerlee, J.D. (1978), Friction of rocks, *Pure Appl. Geophys., 116*, 615–626.

Cebula, D.J., Middleton, S., Ottewill, R.H., White, J.W., Thomas, R.K. (1979), Neutron diffraction from clay-water systems, *Clays and Clay Minerals, 27*, 39-52

Chang, F.R.C., Skipper,N.T., Sposito,G. (1995), Computer simulation of interlayer molecular structure in sodium montmorillonite hydrates, *Langmuir 11, Issue 7*, Pages 2734-2741

Collettini, C., Niemeijer, A., Viti, C., Marone, C. (2009a), Fault zone fabric and fault weakness, *Nature, vol. 462*, 907-911

Collettini, C., Viti, C., Smith, S.A.F., Holdsworth, R.E. (2009b), Development of interconnected talc networks and weakening of continental, *Geology, 37*, 567-570

Colten-Bradley, V.A. (1987), Role of pressure in smectite dehydration — Effects on geopressure and smectite-to-illite transformation, *AAPG Bull., 71*, 1414– 1427

da Silva, G.J., Fossum, J.O., DiMasi, E., Måløy, K.J. (2003), Hydration transitions in a nanolayered synthetic silicate: A synchrotron x-ray scattering study, *Physical review B 67*; doi:10.1103/PhysRevB.67.094114

da Silva, G.J., Fossum, J.O., DiMasi, E., Måløy, K.J., Lutnæs, S.B. (2002), Synchrotron x-ray scattering studies of water intercalation in a layered synthetic silicate, *Physical Review E 66*, 01130

de Pablo, L., Chávez, M.L., Sum, A.K., de Pablo, J.J. (2004), Monte Carlo molecular simulation of the hydration of Na–montmorillonite at reservoir conditions, *J. Chem. Phys. 120, 939*; doi:10.1063/1.1631440

Eisenberg, D., and W. Kauzmann. 1969. The Structure and Properties of Water. New York: Oxford University Press, 296 pp.

Farmer, V.C. (1978), Water on particle surfaces, *Chemistry of Soil Constituents,* D.J. Greenland and M.H.B. Hayes, eds., Wiley, New York, 405-448

Ferrage, E., Kirk, A.C., Cressey, G., Cuadros, J. (2007a), Dehydration of Ca montmorillonite at the crystal scale. Part I: Structure evolution**,** *American Mineralogist, Vol. 92,* pages 994-1006

Ferrage, E., Kirk, A.C., Cressey, G., Cuadros, J. (2007b), Dehydration of Ca montmorillonite at the crystal scale. Part 2. Mechanism and kinetics**,** *American Mineralogist, Vol. 92,* pages 1007-1017

Ferrage, E., Lanson, B., Sakharov, B.A., Drits, V.A. (2005), Investigation of smectite hydration properties by modeling of X-ray diffraction profiles. Part 1. Montmorillonite hydration properties, *American Mineralogist, 90*,1358-1374

Fitts, T.G., Brown, K.M. (1999), Stress-induced smectite dehydration: ramifications for patterns of freshening and fluid expulsion in the N. Barbaros accretionary wedge, *Earth and Planetary Science Letters, 172,* 179 -197 *Geochimica et Cosmochimica Acta, 60*, 4059-4074

Giese, R.F., (1975), The effect of F/OH substitution on some layer silicate minerals, *Z. Kristallogr., 141*, 138–144

Giese, R.F., (1978), The electrostatic interlayer forces of layer structure minerals, *Clays Clay Miner., 26*, 51– 57

Grim, R.E. (1968), Clay Mineralogy, 596 pp., McGraw-Hill, NewYork,

Guggenheim, S., Koster van Groos, A.F. (2001), Baseline studies of the clay minerals society source clays: thermal analysis, *Clays and Clay Minerals, 49, no. 5*, 433-443

Guindy, N.M., El-Akkad, T.M., Flex, N.S., El-Massry, S.R., Nashed, S. (1985), Thermal dehydration of mono- and di-valent montmorillonite cationic derivates. *Thermochimica Acta, 88*, 369-378

Güven, N. (1992), Molecular aspects of clay/water interactions, in Clay-Water Interface and its Rheological Implications, edited by N. Güven and R. M. Pollastro, *Clay Min. Soc. Workshop Lect., 4*, 1– 79

Harward, M.E., Brindley, G.W. (1965), Swelling properties of synthetic smectites in relation to lattice substitutions, *Clays and Clay Minerals, 13*, 209-222

Hawkins, R.K., Egelstaff, P.A. (1980), Interfacial water structure in montmorillonite from neutron diffraction experiments, *Clays and Clay Minerals 28 (1)*, 19-28

Hendricks, S.B., Nelson, R.A., Alexander, L.T. (1940), Hydration mechanism of the clay mineral montmorillonite saturated with various cations. *Journal of American Chemical Society, 62*, 1457-1464

Huang, W.L., Bassett, W.A., Wu, T.C. (1994), Dehydration and hydration of montmorillonite at elevated temperatures and pressures monitored using synchrotron radiation, *American Mineralogist, Vol. 79*, 683-691

Ikari, M,J., Saffer, D.M., Marone, C. (2009), Frictional and hydrologic properties of clay-rich fault gouge, *J. Geophys. Res., 114*, B05409, doi: 10.1029/2008JB006089

Ikari, M.J., Saffer, D.M, Marone, C. (2007), Effect of hydration state on the frictional properties of montmorillonite-based fault gouge, *J. Geophys. Res., 112*, B06423, doi:10.1029/2006JB004748

Ikari, M.J., Saffer, M.S., Marone, C. (2009), Frictional and hydrologic properties of clay-rich fault gouge, *J. Geophys. Res., 114*, B05409, doi:10.1029/2008JB006089

Israelachvili, J. N., McGuiggan, P.M., Homola A.M. (1988), Dynamic properties of molecularly thin liquid films, *Science, 240*, 189– 191

Jefferies, S.P., Holdsworth, R.E., Wibberley, C.A.J., Shimamoto, T., Spiers C.J., Niemeijer, A.R., Lloyd, G.E. (2006), The nature and importance of phyllonite development in crustal-scale fault cores: an example from the Median Tectonic Line, Japan, *Journal of Structural Geology 28*, 220–235

Johnston, C.T., Sposito, G., Erickson, C. (1992), Vibrational probe studies of water interactions with montmorillonite, *Clays and Clay Minerals, 40*, 722-730

Kim, Y., Kirkpatrick, R.J, Cygan, R.T. (1996), Cs-133 NMR study of cesium of the surfaces of kaolinite and illite,

Knudsen, K.D., Fossum, J.O., Helgesen G., Bergaplass, V. (2003), Pore characteristics and water absorption in a synthetic smectite clay**,** *J. Appl. Cryst. 36*, 587-591

Koster van Groos, A.F., Guggenheim, S. (1984), The effect of pressure on the dehydration reaction of interlayer water in Na-montmorillonite (SWy-I), *American Mineralogist, 69*, 872-879

Kramer, L. (2006), Solubility and dissolution rate of CO2 in water and saline solutions: A high pressure FTIR study, Msc Thesis, Utrecht University, 57pp

Laird, D.A. (1999), Layer charge influences on the hydration of expandable 2:1 phyllosilicates, *Clays and Clay Minerals, Vol. 47, No. 5*, 630-636

Lehner, F.K., Pilaar, W.F., (1997), The emplacement of clay smears in synsedimentary normal faults: Inferences from field observations near Frechen, Germany. In: Møller-Pedersen, P., Koestler, A.G. (Eds.), Hydrocarbon seals: Importance for exploration and production. *Elsevier*, Singapore, p.39

Liechtt, R., Zoback, M.D. (1979), Preliminary analysis of clay gouge from a well in the San Andreas fault zone in central California. Proc. Conf. VIII. Analysis of Actual Fault Zones in Bedrock. *U.S. Geol. Surv.* Menlo Park, Calif., pp. 2688275

Ma, C., Eggleton, R.A. (1999), Cation exchange capacity of Kaolinite, *Clays and Clay Minerals, 47*, 174-180

Madejova, J. (2003), FTIR techniques in clay mineral studies, *Vibrational Spectroscopy 31*, 1–10

Meunier, A. (2005), Clays, 472 pp., Springer, Berlin

Mooney, R.W., Keenan, A.G., Wood, L.A. (1952), Adsorption of water vapor by montmorillonite. II. Effect of exchangeable ions and lattice swelling as measured by X-ray diffraction**,** *Journal of the American Chemical Society* 74 (6), pp. 1371-1374

Moore, D.E., Lockner, D.A. (2004a), Crystallographic controls on the frictional behavior of dry and water-saturated sheet structure minerals, *J. Geophys. Res., 112*, B03401, doi: 10.1029/2003JB002582

Moore, D.E., Lockner, D.A. (2004b), The Coefficient of Friction of Chrysotile Gouge at Seismogenic Depths, *International Geology Review, Vol. 46*, 385-398

Moore, D.E., Lockner, D.A. (2007), Friction of the smectite clay montmorillonite: a review and interpretation of data. In: Dixon, T.H., Moore, J.C. (Eds.), *The Seismogenic Zone of Subduction Thrust Faults*. MARGINS Theoretical and Experimental Earth Science Ser., vol. 2, pp. 317–345

Moore, D.E., Lockner, D.A. (2008), Talc friction in the temperature range (25º - 400ºC): Relevance for Fault-Zone Weakening, *Tectonophysics 449, 120-132*

Moore, D.M., Reynolds, R.C. (1989), X-ray diffraction and the identification and analysis of clay minerals. Oxford University Press, New York, 332 pp.

Morrow, C.A., Moore, D.E., Lockner, D.A. (2000), The effect of mineral bond strength and adsorbed water on fault gouge frictional strength, *Geophys. Res. Lett., 27*, 815– 818

Morrow, C., Radney, B., Byerlee, J. (1992), Frictional strength and the effective pressure law of montmorillonite and illite clays, *Fault Mechanisms and Transport Properties of Rocks*, edited by B. Evans and T-F. Wong, pp 69-88, Elsevier, New York.

Norrish, K. (1954), The swelling of montmorillonite, *Discussions of the Faraday Society 18*, pp. 120-134

Numelin, T.J., Marone, C., Kirby, E., 2007. Frictional properties of natural fault gouge from a low-angle normal fault, Panamit Valley, California**.** *Tectonics 26* (2), art. no. TC2004

Ormerod, E.C., Newman, A.C.D. (1983), Water sorption on Ca-saturated clays: ||. Internal and external surfaces of montmorillonite, *Clay Minerals 18,* 289-299

Paterson, M.S. ,1978. Experimental Rock Deformation – The Brittle Field, 254 pp., Springer, New York.

Poinsignon, C., Yvon, J., Mercier, R. (1982), Dehydration energy of the exchangeable cations in montmorillonite: a DTA study, *Israel Journal of Chemistry, 22*, 253-255

Prost, R., Koutit, T., Benchara, A., Huard, E. (1998), State and location of water adsorbed on clay minerals: consequences of the hydration and swelling-shrinkage phenomena, *Clays Clay Miner., 46, No.2*, 117-131

Renard, F., and Ortoleva, P. (1997), Water films at grain-grain contacts: Debye-Hückel, osmotic model of stress, salinity, and mineralogy dependence, *Geochim. Cosmochim. Acta 61*, 1963– 1970

Rice, J.R., Clearly, M.R. (1976), Some basic stress-diffusion solutions for fluid-saturated elastic porous media with compressible constituents, *Rev. Geophys., 14*, 227-241

Russell, J.D., Farmer, V.C. (1964), Infra-red spectroscopic study of the dehydration of montmorillonite and saponite, *Clay Min. Bull. 5*, 443-464

Rutter, E.H. (1983), Pressure solution in nature, theory, and experiment, *J. Geol. Soc. London, 140*, 725–740

Saffer, D.M., Frye, K.M., Marone, C., Mair, K. (2001), Laboratory results indicating complex and potentially unstable frictional behavior of smectite clay, *Geophys. Res. Lett., 28*, no. 12, 2297-2300

Saffer, D.M., Marone, C. (2003), Comparison of smectite- and illite-rich gouge frictional properties: Application to the updip limit of the seismogenic zone along subduction megathrusts, *Earth Planet. Sci. Lett., 215*, 219 – 235.

Sato, T., Watanabe, T., Otsuka, R. (1992), Effects of layer charge, charge location, and energy change on expansion properties of dioctahedral smectites, *Clays and Clay Minerals, 40*, 103-113

Schilling, M.R. (1990), Effects of sample size and packing in the thermogravimetric analysis of calcium montmorillonite STx-1, *Clays and Clay Minerals, Vol. 38*, No. 5, 556-558

Schleicher, A.M., Warr, L.N., van der Pluijm, B.A. (2009a), On the origin of mixed-layered clay minerals from the San Andreas Fault at 2.5–3 km vertical depth (SAFOD drillhole at Parkfield, California), *Contrib. Mineral Petrol 157*:173–187

Schleicher, A. M., S. N. Tourscher, B. A. van der Pluijm, L. N. Warr (2009b), Constraints on mineralization, fluid-rock interaction, and mass transfer during faulting at 2–3 km depth from the SAFOD drill hole, *J. Geophys. Res., 114*, B04202,doi:10.1029/2008JB006092

Scholz, C.H. (1990), The mechanics of earthquakes and faulting. Cambridge University Press, New York.

Schrader, M.E., Yariv, S. (1990), Wettability of Clay Minerals, *Journal of Colloid and Interface Science. Vol. 136*, No. 1

Sibson, R.H. (1977), Fault rocks and fault mechanisms, *Journal of the Geological Society of London 133*, 190-213

Skipper, N.T., Sposito, G., Chang, E.R.C. (1995), Monte Carlo simulation of interlayer molecular structure in swelling clay minerals. 2. Monolayer hydrates. *Clays and Clay Minerals, 43*, 294-303

Solum, J. G., S. H. Hickman, D. A. Lockner, D. E.Moore, B. A. van der Pluijm, A. M. Schleicher, and J. P. Evans (2006), Mineralogical characterization of protolith and fault rocks from the SAFOD Main Hole, *Geophys. Res. Lett., 33*, L21314, doi:10.1029/2006GL027285

Solum, J.G., van der Pluijm, B.A., (2009), Quantification of fabrics in clay gouge from the Carboneras fault, Spain and implications for fault behavior, *Tectonophysics 475*, 554–562

Sposito, G. (1984), The Surface Chemistry of Soils, 234 pp., Oxford Univ. Press, New York.

Sposito, G., Prost, R. (1982), Structure of water adsorbed on smectites, *Chemical Reviews 82* (6), pp. 553-573

Takahashi, M., Mizoguchi, K., Kitamura, K., Masuda, K. (2007), Effects of clay content on the frictional strength and fluid transport property of faults, *J. Geophys. Res. Vol. 112*, B08206, doi:10.1029/2006JB004678

Tambach, T.J., Bolhuis, P.G., Hensen, E.J.M., Smit, B. (2006), Hysteresis in Clay Swelling Induced by Hydrogen Bonding: Accurate Prediction of Swelling States, *Langmuir, Issue 22*, Pages 1223-1234

Tambach, T.J. (2005), Swelling of clay minerals : a molecular simulation study, PhD Thesis UvA, 118pp.

Tamura, K., Yamada, H., Nakazawa, H. (2000), Stepwise hydration of high quality synthetic smectite with various cations, *Clays and Clay Minerals, 48*, 400-404

Tenório, R.P., Alme, L.R., Engelsberg, M., Fossum, J.O., Hallwass, F. (2008), Geometry and Dynamics of Intercalated Water in Na-Fluorhectorite Clay Hydrates, *J. Phys. Chem. C, 112*, 575-580

Underwood, M.B. (2007), Sediment inputs to subduction zones: Why lithostatigraphy and clay mineralogy matter , in *The Seismogenic Zone of Subduction Thrust Faults*., edited by T.H. Dixon and J.C. Moore, Columbia Univ. Press, New York.

Van Olphen, H. and Fripiat, J.J. (1979), Data handbook for clay minerals and other non-metallic minerals, Pergamon Press, New York, 346 pp.

Venyaminov, S.Y, Prendergast, EG. (1997), Water (H_2O and D_2O) molar absorptivity in the 1000-4000 cm^{-1} range and quantitative infrared spectroscopy of aqueous solutions, *Analytical Biochemistry, 248*, 234-245

Vrolijk, P. (1990), On the mechanical role of smectite, *Geology, 18*, 703–707

Vrolijk, P., and B. A. van der Pluijm (1999), Clay gouge, *J. Struct. Geol.,21*, 1039– 1048

Wang, C.Y., Mao, N.H., Wu, F.T. (1980), Mechanical properties of clays at high pressure, *J. Geophys. Res., 85*, 1462-1468

Wilson, M.J. (1994), Clay Mineralogy: spectroscopic and chemical determinative methods. Chapman and Hall, London, 366 pp.

Wintsch, R.P., Christoffersen, R., Kronenberg, A.K. (1995), Fluid-rock reaction weakening of fault zones, *J. Geophys. Res 100*, pp. 13021-13032

Wu, F.T., Blatter, L., Roberson, H. (1975), Clay gouges in the San Andreas fault system and their possible implications, *Pure Appl. Geophys. 113*: 87-95

Wu, T., Bassett, W.A., Huang, W.L., Guggenheim, S., Koster Van Groos, A.F. (1997), Montmorillonite under high H_2O pressures: Stability of hydrate phases, rehydration hysteresis, and the effect of interlayer cations, *American Mineralogist, 82*,69-78

Xu, W., Johnston, C.T., Parker, P, Agnew, S.F. (2000), Infrared studies of water sorption on Na-, Li-, Ca-, and Mg-exchanged (SWy-1 and SAz-1) montmorillonite, *Clays and Clay Minerals, Vol.48, no. 1*, 120-131

Zabat, M., Van Damme, H. (2000), Evaluation of the energy barrier for dehydration of homoionic (Li, Na, Cs, Mg, Ca, Ba, $Al_x(OH)^{z+}_y$ and La)-montmorillonite by a differentiation method, *Clay Minerals, 35*, 357-363

Zhou, Z., Gunter, W.D. (1992), The nature of the surface charge of kaolinite, *Clays and Clay Minerals, 40*, 365-368